RECENT TRENDS IN CAD TOOLS

FOR MICROWAVE CIRCUIT DESIGN

EXPLOITING SPACE MAPPING TECHNOLOGY

To my parents

To my wife Dina

To my kids Abdulrhman and Abdullah

RECENT TRENDS IN CAD TOOLS FOR MICROWAVE CIRCUIT DESIGN EXPLOITING SPACE MAPPING TECHNOLOGY

By

AHMED SAYED MOHAMED, B.Sc., M.Sc. (Eng.)

A Thesis

Submitted to the School of Graduate Studies

in Partial Fulfillment of the Requirements

for the Degree

Doctor of Philosophy

McMaster University

DOCTOR OF PHILOSOPHY (2005) McMASTER UNIVERSITY

(Electrical and Computer Engineering) Hamilton, Ontario

TITLE: **Recent Trends in CAD Tools for Microwave Circuit Design Exploiting Space Mapping Technology**

AUTHOR: Ahmed Sayed Mohamed

B.Sc. (Eng) (Faculty of Engineering, Cairo University)

M.Sc. (Eng) (Faculty of Engineering, Cairo University)

SUPERVISORS: J.W. Bandler, Professor Emeritus,

Department of Electrical and Computer Engineering

B.Sc.(Eng), Ph.D., D.Sc.(Eng) (University of London)

D.I.C. (Imperial College)

P.Eng. (Province of Ontario)

C.Eng., FIEE (United Kingdom)

Fellow, IEEE

Fellow, Royal Society of Canada

Fellow, Engineering Institute of Canada

Fellow, Canadian Academy of Engineering

M.H. Bakr, Assistant Professor,

Department of Electrical and Computer Engineering

B.Sc.(Eng), M.Sc.(Eng) (Cairo University, Egypt)

Ph.D.(Eng) (McMaster University, Canada)

P.Eng. (Province of Ontario)

Member, IEEE

NUMBER OF PAGES: xxii, 205

ABSTRACT

This thesis contributes to the development of novel methods and techniques for computer-aided electromagnetics (EM)-based modeling and design of microwave circuits exploiting space mapping (SM) technology.

Novel aggressive space mapping (ASM) algorithms exploiting sensitivity information from the fine and the coarse models are developed. The modified algorithm enhances the parameter extraction (PE) process by not only matching the responses of both fine and coarse models but also corresponding gradients. We also used the gradients to continuously update a suitable mapping between the fine and coarse spaces. The coarse model combined with the established mapping is considered a "surrogate" of the fine model in the region of interest. It can be used in statistical analysis and yield optimization.

A comprehensive review of SM technology in engineering device modeling and optimization, with emphasis in Radio Frequency (RF) and microwave circuit optimization, is introduced in this thesis. Significant practical applications are reviewed.

We explore the SM methodology in the transmission-line modeling (TLM) simulation environment. We design a CPU intensive fine-grid TLM

structure utilizing a coarse-grid TLM model with relaxed boundary conditions. Such a coarse model may not faithfully represent the fine-grid TLM model and it may not even satisfy the original design specifications. Hence, SM techniques such as the aggressive SM will fail to reach a satisfactory solution. To overcome the aforementioned difficulty, we combine the implicit SM (ISM) and output SM (OSM) approaches. As a preliminary PE step, the coarse model's dielectric constant is first calibrated. If the response deviation between the two TLM models is still large, an output SM scheme absorbs this deviation to make the updated surrogate represent the fine model. The subsequent surrogate optimization step is governed by a trust region strategy. Because of the discrete nature of the TLM simulator, we employ an interpolation scheme to evaluate the responses, and possibly derivatives, at off-grid points with a dynamically updated database system to avoid repeatedly invoking the simulator.

ACKNOWLEDGMENTS

All praise and gratitude belong to God, the One Who gives me the strength and patience to finish this work and the One whose bounties are countless.

I wish to express my sincere appreciation to my supervisor Dr. John W. Bandler, Simulation Optimization Systems Research Laboratory, McMaster University and President, Bandler Corporation, for his expert guidance, constant encouragement and patience during the course of this work. Special thanks go to my co-supervisor Dr. Mohamed H. Bakr for his constant support, fruitful discussions and friendship. I also thank Dr. Natalia K. Nikolova and Dr. Tamás Terlaky, members of my supervisory committee, for their continuing interest and ideas.

I wish to express my gratitude to my former colleagues Dr. Mostafa Ismail, now with ComDev International Ltd., Cambridge, Ontario, Dr. José E. Rayas-Sánchez, now with ITESO, Tlaquepaque, Jalisco, Mexico, and Sameh A. Dakroury, now with Cairo University, Egypt, for useful discussions and friendship. I also thank my colleagues Dr. Qingsha S. Cheng, Daniel M. Hailu and Dr. Slawomir Koziel for productive collaboration and for their nice company and support during the tough times.

ACKNOWLEDGMENTS

I would like to thank Dr. Kaj Madsen, Dr. Jacob Søndergaard and Frank Pedersen, Informatics and Mathematical Modelling, Technical University of Denmark, for productive discussions and their continuing collaboration.

I wish to acknowledge Dr. Wolfgang J.R. Hoefer, Faustus Scientific Corporation, Victoria, BC, for making the MEFiSTo system available and for assisting in its use. Special thanks go to Dr. James C. Rautio, President, Sonnet Software, Inc., North Syracuse, NY, for making ***em*** available and to Agilent Technologies, Santa Rosa, CA, for making ADS, Momentum and HFSS available.

I gratefully acknowledge the financial assistance provided by the Natural Sciences and Engineering Research Council of Canada under Grants OGP0007239 and STGP269760, by the Micronet Network of Centres of Excellence, by the Department of Electrical and Computer Engineering, McMaster University, through a Teaching Assistantship, Research Assistantship and Scholarship and by an Ontario Graduate Scholarship (OGS).

I would like to grant this thesis to the soul of my father who raised me to the best of his ability. I wish he could share this moment with me. I extend my love and respect to my mother for her continuous encouragement and to my sister Eman for her care. I am deeply indebted to them for their endless support.

Finally, I would like to express my deep gratitude to my wife, Dina, for her understanding, encouragement, patience and care and to my little kids, Abdulrhman and Abdullah, for their lovely smiles.

CONTENTS

ABSTRACT iii

ACKNOWLEDGMENTS v

LIST OF FIGURES xiii

LIST OF TABLES xix

LIST OF ACRONYMS xxi

CHAPTER 1 INTRODUCTION 1

References…..…….. 9

CHAPTER 2 RECENT TRENDS IN SPACE MAPPING TECHNOLOGY 15

2.1 Introduction……..... 15

2.2 The Space Mapping Concept……..... 21

2.2.1 Original Design Problem……... 21
2.2.2 The Space Mapping Concept..…..…….. 21
2.2.3 Jacobian Relationships…….…….. 23
2.2.4 Interpretation of Space Mapping Optimization……... 23

2.3 The Original Space Mapping Technique……..... 24

2.4 The Aggressive Space Mapping Technique…..... 25

2.4.1 Theory…….……..... 25
2.4.2 A Five-pole Interdigital Filter…… 26

2.5 Trust Regions and Aggressive Space Mapping... 30
2.5.1 Trust Region Methods……..... 30
2.5.2 Trust Regions and Aggressive SM…..... 32
2.6 Hybrid Aggressive SM and Surrogate Model Based Optimization……...……..... 33
2.6.1 Hybrid Aggressive SM Algorithm……. 33
2.6.2 Surrogate Model-Based SM Algorithm. 34
2.7 Implicit Space Mapping….……...……..... 35
2.8 Space Mapping-Based Model Enhancement….. 37
2.8.1 Generalized Space Mapping (GSM) Tableau……..... 38
2.8.2 Space Derivative Mapping……. 39
2.8.3 SM-Based Neuromodeling..……... 40
2.9 Neural SM-Based Optimization Techniques….. 41
2.9.1 Neural Space Mapping (NSM)……..... 41
2.9.2 Neural Inverse Space Mapping (NISM) 42
2.10 Output Space Mapping……..... 42
2.10.1 Implicitly Mapped Coarse Model with an Output Mapping……..... 43
2.10.2 The Output SM-Based Interpolating Surrogate (SMIS)……...… 44
2.11 Space Mapping: Mathematical Motivation and Convergence Analysis……. 44
2.11.1 Mathematical Motivation of the SM Technique……... 45
2.11.2 Convergence Analysis of SM Algorithms……. 46
2.12 Surrogate Modeling and Space Mapping….…... 47
2.13 Implementation and Applications……... 49
2.13.1 RF and Microwave Implementation….. 49
2.13.2 Major Recent Contributions to Space Mapping…….…..... 50
2.14 Concluding Remarks……... 53
References……... 54

CHAPTER 3 EM-BASED OPTIMIZATION EXPLOITING PARTIAL SPACE MAPPING AND EXACT SENSITIVITIES 65

3.1 Introduction……..... 65

3.2 Basic Concepts…….....…….. 67

3.2.1 Parameter Extraction (PE)..... 67

3.2.1.1 Single Point PE (SPE)…..... 68
3.2.1.2 Multipoint PE (MPE)……..... 68
3.2.1.3 Statistical PE……... 70
3.2.1.4 Penalized PE……..... 70
3.2.1.5 PE involving Frequency Mapping……..... 71
3.2.1.6 Other Considerations..... 72

3.2.2 Aggressive Space Mapping Approach... 72

3.3 Sensitivity-Based Approach…...……..……... 74

3.3.1 PE Exploiting Sensitivities……. 74
3.3.2 Partial Space Mapping (PSM)…..... 76
3.3.3 Mapping Considerations…… 77

3.3.3.1 Unit Mapping…….. 78
3.3.3.2 Broyden-like Updates...…….. 78
3.3.3.3 Jacobian Based Updates…….. 78
3.3.3.4 Constrained Update..……... 79

3.3.4 Proposed Algorithms……..... 80

3.4 Examples……...……..... 83

3.4.1 Rosenbrock Banana Problem…..……... 83

3.4.1.1 Shifted Rosenbrock Problem.. 84
3.4.1.2 Transformed Rosenbrock Problem……... 86

3.4.2 Capacitively Loaded 10:1 Impedance Transformer…… 91

3.4.2.1 Case 1: [L_1 L_2]……. 93
3.4.2.2 Case 2: [L_1]…….. 96
3.4.2.3 Case 3: [L_2]…….. 96

3.4.3 Bandstop Microstrip Filter with Open Stubs……... 98
3.4.4 Comparison with Pervious Approaches. 107
3.5 Concluding Remarks……... 107
References……..... 109

CHAPTER 4 TLM-BASED MODELING AND DESIGN EXPLOITING SPACE MAPPING 113

4.1 Introduction……. 113
4.2 Basic Concepts...……..... 115
4.2.1 Transmission-Line Matrix (TLM) Method……... 115
4.2.2 Design Problem…….…..... 116
4.2.3 Implicit Space Mapping (ISM)…….. 116
4.2.4 Output Space Mapping (OSM)…….. 117
4.2.5 Trust Region (TR) Methods……... 117
4.3 Theory…….....…… 118
4.3.1 Parameter Extraction (Surrogate Calibration)……..…….. 119
4.3.2 Surrogate Optimization (Prediction)..... 121
4.3.3 Stopping Criteria……..... 121
4.4 Algorithm…….....……... 122
4.5 Examples…….....……..... 123
4.5.1 An Inductive Obstacle in a Parallel-Plate Waveguide……..…….. 123
4.5.2 Single-Resonator Filter…….. 133
4.5.3 Six-Section H-plane Waveguide Filter……... 140
4.5.3.1 Case 1: Empirical Coarse Model…….. 142
4.5.3.2 Case 2: Coarse-grid TLM Model…….. 147
4.6 Concluding Remarks…….....…….. 152
References…… 154

CHAPTER 5 CONCLUSIONS 159

APPENDIX A BROYDEN VERSUS BFGS UPDATE 163

A.1 Theoretical Discussion……. 163

A.1.1 The Broyden Method..…… 164
A.1.2 The BFGS Method…….. 166
A.1.3 Comment……. 168
A.1.4 A non-symmetric BFGS updating formula…… 169

A.2 Examples…….. 170

A.2.1 Seven-section Capacitively Loaded Impedance Transformer…….. 170

A.3 Concluding Remarks…… 179

References…… 180

APPENDIX B CONSTRAINED UPDATE FOR *B* 183

APPENDIX C *L*-MODEL AND *Q*-MODEL 185

References……... 189

BIBLIOGRAPHY 191

LIST OF FIGURES

Fig. 2.1	Linking companion coarse (empirical) and fine (EM) models through a mapping……....	16
Fig. 2.2	Illustration of the fundamental notation of space mapping..	22
Fig. 2.3	A five-pole interdigital filter……	28
Fig. 2.4	A coarse model of the five-pole interdigital filter using decomposition…….…….	28
Fig. 2.5	Optimal coarse model target response (— $\|S_{11}\|$ and $\|S_{21}\|$) and the fine model response at the starting point (• $\|S_{11}\|$ and o $\|S_{21}\|$) for the five-pole interdigital filter……..	29
Fig. 2.6	Optimal coarse model target response (— $\|S_{11}\|$ and $\|S_{21}\|$) and the fine model response at the final design (• $\|S_{11}\|$ and o $\|S_{21}\|$) for the five-pole interdigital filter……..	29
Fig. 2.7	The fine model response at the final design (— $\|S_{11}\|$ and $\|S_{21}\|$) using a fine frequency sweep for the five-pole interdigital filter…….…..	30
Fig. 2.8	Illustration of the implicit space mapping (ISM) concept...	37
Fig. 2.9	The frequency-SM super model concept…….……	38
Fig. 2.10	Error plot for a two-section capacitively loaded impedance transformer, comparing the quasi-global effectiveness of SM (light grid) versus a classical Taylor approximation (dark grid)…….……...	46
Fig. 3.1	Partial Space Mapping (PSM)…….	77

Fig. 3.2 Contour plot of the "coarse" original Rosenbrock banana function……..……... 83

Fig. 3.3 Contour plot of the "fine" shifted Rosenbrock banana function…….……... 85

Fig. 3.4 Contour plot of the "fine" transformed Rosenbrock banana function…….……... 87

Fig. 3.5 Nonuniqueness occurs when single-point PE is used to match the models in the "transformed" Rosenbrock problem 87

Fig. 3.6 A unique solution is obtained when gradient PE is used in the "transformed" Rosenbrock problem in the 1st iteration. 88

Fig. 3.7 The 6th (last) gradient PE iteration of the "transformed" Rosenbrock problem…….……... 88

Fig. 3.8 Reduction of R_f versus iteration count of the "transformed" Rosenbrock problem……..... 89

Fig. 3.9 Reduction of $\| \boldsymbol{f} \|$ versus iteration count of the "transformed" Rosenbrock problem……..... 89

Fig. 3.10 Two-section impedance transformer: "fine" model……. 92

Fig. 3.11 Two-section impedance transformer: "coarse" model……. 92

Fig. 3.12 Optimal coarse model target response (—) and the fine model response at the starting point (•) for the capacitively loaded 10:1 transformer with L_1 and L_2 as the PSM coarse model parameters…….…… 94

Fig. 3.13 Optimal coarse model target response (—) and the fine model response at the final design (•) for the capacitively loaded 10:1 transformer with L_1 and L_2 as the PSM coarse model parameters…….…… 94

Fig. 3.14 $\left\| \boldsymbol{x}_c - \boldsymbol{x}_c^* \right\|_2$ versus iteration for the capacitively loaded 10:1 transformer with L_1 and L_2 as the PSM coarse model parameters……..…….. 95

Fig. 3.15 U versus iteration for the capacitively loaded 10:1 transformer with L_1 and L_2 as the PSM coarse model parameters…… 95

Fig. 3.16 Bandstop microstrip filter with open stubs: "fine" model.… 99

Fig. 3.17 Bandstop microstrip filter with open stubs: "coarse" model. 99

Fig. 3.18 Optimal OSA90/hope coarse target response (—) and ***em*** fine model response at the starting point (•) for the bandstop microstrip filter using a fine frequency sweep (51 points) with L_1 and L_2 as the PSM coarse model parameters 102

Fig. 3.19 Optimal OSA90/hope coarse target response (—) and ***em*** fine model response at the final design (•) for the bandstop microstrip filter using a fine frequency sweep (51 points) with L_1 and L_2 as the PSM coarse model parameters…… 103

Fig. 3.20 $\left\| \boldsymbol{x}_c - \boldsymbol{x}_c^* \right\|_2$ versus iteration for the bandstop microstrip filter using L_1 and L_2 as the PSM coarse model parameters…….. 104

Fig. 3.21 $\left\| \boldsymbol{x}_c - \boldsymbol{x}_c^* \right\|_2$ versus iteration for the bandstop microstrip filter using a full mapping…….. 106

Fig. 4.1 The implicit and output space mapping concepts. We calibrate the surrogate against the fine model utilizing the preassigned parameters $\boldsymbol{x}$, e.g., dielectric constant, and the output response mapping parameters: the scaling matrix $\boldsymbol{\alpha}$ and the shifting vector $\boldsymbol{\beta}$…… 119

Fig. 4.2 An inductive post in a parallel-plate waveguide: (a) 3D plot, and (b) cross section with magnetic side walls.…… 124

Fig. 4.3 The progression of the optimization iterates for the inductive post on the fine modeling grid (D and W are in mm)……... 126

Fig. 4.4 Optimal target response (—), the fine model response (•) and the surrogate response (--) for the inductive post ($|S_{21}|$): (a) at the initial design, and (b) at the final design…… 128

Fig. 4.5 Optimal target response (—), the fine model response (•) and the surrogate response (--) for the inductive post ($|S_{11}|$): (a) at the initial design, and (b) at the final design…… 129

Fig. 4.6 The reduction of the objective function (U) for the fine model (—) and the surrogate (--) for the inductive post….. 130

Fig. 4.7 Statistical analysis for the real and imaginary of S_{21} of the inductive post with 2% relative tolerances: (a) using the fine model, and (b) using the surrogate at the final iteration of the optimization. 100 outcomes are used……. 131

Fig. 4.8 Statistical analysis for the real and imaginary of S_{11} of the inductive post with 2% relative tolerances: (a) using the fine model, and (b) using the surrogate at the final iteration of the optimization. 100 outcomes are used……. 132

Fig. 4.9 Topology of the single-resonator filter…….. 133

Fig. 4.10 The surrogate response (--•--) and the corresponding fine model response (–•–) at: (a) the initial design, and (b) the final design (using linear interpolation) for the single-resonator filter……... 137

Fig. 4.11 The reduction of the objective function (U) for the fine model (—) and the surrogate (--) for the single-resonator filter……... 138

Fig. 4.12 The progression of the optimization iterates for the single-resonator filter on the fine modeling grid (d and W are in mm)……... 138

Fig. 4.13 The final design reached by the algorithm (–•–) versus the simulation results using MEFiSTo 2D with the rubber cell feature (—) for the single-resonator filter: (a) $|S_{11}|$ and (b) $|S_{21}|$…… 139

Fig. 4.14 The six-section H-plane waveguide filter: (a) the 3D view, (b) one half of the 2D cross section, and (c) the equivalent empirical circuit model…….. 141

Fig. 4.15 The surrogate response (--•--) and the corresponding fine model response (–•–) at: (a) the initial design, and (b) the final design (using linear interpolation) for the six-section H-plane waveguide filter designed using the empirical coarse model……. 144

Fig. 4.16 The reduction of the objective function (*U*) of the fine model (—) and the surrogate (--) for the six-section H-plane waveguide filter designed using the empirical coarse model……. 145

Fig. 4.17 The final design reached by the algorithm (–•–) compared with MEFiSTo 2D simulation with the rubber cell feature (—) for the six-section H-plane waveguide filter designed using the empirical coarse model…….. 146

Fig. 4.18 The surrogate response (--•--) and the corresponding fine model response (–•–) at: (a) the initial design, and (b) the final design (using linear interpolation) for the six-section H-plane waveguide filter designed using the coarse-grid TLM model……... 149

Fig. 4.19 The reduction of the objective function (*U*) of the fine model (—) and the surrogate (--) for the six-section H-plane waveguide filter designed using the coarse-grid TLM model……. 150

Fig. 4.20 The final design reached by the algorithm (–•–) compared with MEFiSTo 2D simulation with the rubber cell feature (—) for the six-section H-plane waveguide filter designed using the coarse-grid TLM model……. 151

Fig. A.1 Seven-section capacitively-loaded impedance transformer: "fine" model…….. 171

Fig. A.2 Seven-section capacitively-loaded impedance transformer: "coarse" model…….. 171

Fig. A.3 Optimal coarse model response (--), optimal fine model response (–•–) and the fine model response (•) at the starting point for the seven-section transmission line capacitively loaded impedance transformer…….. 174

Fig. A.4 Optimal coarse model response (--), optimal fine model response (–•–) and the fine model response (•) at the final iteration for the seven-section transmission line capacitively loaded impedance transformer using the Broyden update……. 175

Fig. A.5 Optimal coarse model response (--), optimal fine model response (–•–) and the fine model response (•) at the final iteration for the seven-section transmission line capacitively loaded impedance transformer using the modified BFGS update…….. 175

Fig. A.6 $\|\boldsymbol{f}\|_2$ versus iteration for the seven-section transmission line capacitively loaded impedance transformer using the Broyden update……. 176

Fig. A.7 $\|\boldsymbol{f}\|_2$ versus iteration for the seven-section transmission line capacitively loaded impedance transformer using the modified BFGS update…….. 176

Fig. A.8 $U - U_{\text{opt}}$ versus iteration for the seven-section transmission line capacitively loaded impedance transformer using the Broyden update……. 177

Fig. A.9 $U - U_{\text{opt}}$ versus iteration for the seven-section transmission line capacitively loaded impedance transformer using the modified BFGS update…….. 177

Fig. A.10 $\|\boldsymbol{f}\|_2$ versus iteration for the seven-section transmission line capacitively loaded impedance transformer using the original BFGS update…… 178

Fig. A.11 $U - U_{\text{opt}}$ versus iteration for the seven-section transmission line capacitively loaded impedance transformer using the original BFGS update…… 178

Fig. C.1 Selection of base points in the $n = 2$ case: (a) for the L-model, and (b) for the Q-model……. 188

LIST OF TABLES

TABLE 3.1 "Shifted" Rosenbrock banana problem……. 85

TABLE 3.2 "Transformed" Rosenbrock banana problem…… 90

TABLE 3.3 Normalized coarse model sensitivities with respect to design parameters for the capacitively loaded impedance transformer 92

TABLE 3.4 Initial and final designs for the capacitively loaded impedance transformer……. 97

TABLE 3.5 Normalized coarse model sensitivities with respect to design parameters for the bandstop microstrip filter……..……..... 100

TABLE 3.6 Initial and final designs for the bandstop microstrip filter using L_1 and L_2…..……..……. 104

TABLE 3.7 Initial and final designs for the bandstop microstrip filter using a full mapping……...……... 106

TABLE 4.1 Optimization results for the inductive post…..……..... 127

TABLE 4.2 Optimization results for the single-resonator filter…… 136

TABLE 4.3 Initial and final designs for the six-section H-plane waveguide filter designed using the empirical coarse model……... 143

TABLE 4.4 Initial and final designs for the six-section H-plane waveguide filter designed using the coarse-grid TLM model…….. 148

TABLE 4.5 Our approach with/without database system versus direct optimization for the six-section H-plane waveguide filter designed using coarse-grid TLM model…...……. 152

TABLE A.1 The characteristic impedances for the seven-section capacitively loaded impedance transformer……..... 172

TABLE A.2 ASM algorithm using Broyden rank-1 versus BFGS rank-2 updating formulas for the seven-section capacitively loaded impedance transformer……...…… 174

LIST OF ACRONYMS

ANN	Artificial Neural Networks
ASM	Aggressive Space Mapping
CAD	Computer-Aided Design
EM	Electromagnetics
FAST	Feasible Adjoint Sensitivity Technique
FDTD	Finite Difference Time Domain
FEM	Finite Element Method
GPE	Gradient Parameter Extraction
HFSS	High Frequency Structure Simulator
HTS	High-Temperature Superconductor
ISM	Implicit Space Mapping
KAMG	Knowledge-based Automatic Model Generation
LTCC	Low-Temperature Cofired Ceramics
MM	Mode Matching
MoM	Method of Moment
MPE	Multi-point Parameter Extraction
NISM	Neural Inverse Space Mapping

NSM	Neural Space Mapping
OSM	Output Space Mapping
PCB	Printed Circuit Board
PE	Parameter Extraction
RF	Radio Frequency
SM	Space Mapping
SMF	Surrogate Management Framework
SMIS	Space Mapping-based Interpolating Surrogates
SMS	Straw Man Surrogate
SMT	Surface Mount Technology
SPE	Single-point Parameter Extraction
TLM	Transmission-Line Matrix (Modeling)
TR	Trust Regions

CHAPTER 1

INTRODUCTION

The development of computer-aided design (CAD) for RF, microwave and millimeter-wave circuits originated in the 1960s—roughly corresponding to the era of computer growth. For nearly half a century, CAD of electronic circuits have evolved from special-purpose to highly flexible and interactive general-purpose software systems with strong capabilities of automation and visualization.

Many of the important early developments in microwave engineering were made possible when the electromagnetic (EM) environment was represented in terms of circuit equivalents, lumped elements and transmission lines. Thus, capturing the relevant, usually complex, physical behavior of a microwave structure became available in a form that could lend itself to linear solution [1].

Four particular developments exemplify the modeling procedure of transforming a distributed structure into a lumped circuit [1]. The first is the modeling work by Marcuvitz showing how waveguide discontinuities can be modeled by lumped-element equivalents [2]. Barrett [3] documented a similar treatment for planar transmission-line circuits. The second development that had

a tremendous effect on a generation of microwave engineers was Collin's *Foundation of Microwave Engineering*, which presented a formalism for treating distributed structures as circuit elements [4]. The third significant development was the work of Eisenhart and Khan [5] that presented an approach to modeling waveguide-based structures as circuit elements. The final development in linear circuit modeling technology is the segmentation approach most recently reviewed by Gupta [6]. In this segmentation (or diakoptic) approach, a structure is partitioned into smaller parts and each part is characterized electromagnetically. These characterizations are then combined using network theory to yield the overall response of the circuit.

Engineers have been using optimization techniques for device, component and system modeling and CAD for decades. The target of component design is to determine a set of physical parameters to satisfy certain design specifications. Traditional optimization techniques [7], [8] directly utilize the simulated responses and possibly available derivatives to force the responses to satisfy the design specifications.

Bearing in mind the aforementioned RF and microwave circuits modeling developments, advances in the direction of automated design of high-frequency structures were made in the late 1960's and early 1970's. The classic paper by Temes and Calahan in 1967 [9] advocates the use of iterative optimization in circuit design. Since then, optimization techniques have evolved and have been applied to design and modeling in several major directions. Areas of application

include filter design [10], [11], linear array design [12], worst-case design [13], [14], design centering [15], [16], [17], and yield optimization [18], [19]. Comprehensive surveys by Calahan [20], Bandler and Rizk [21], Brayton *et al.* [22], and Bandler and Chen [7] are relevant to microwave circuit designers.

While developments in circuit modeling and design automation were taking place, numerical electromagnetic techniques were also emerging. The finite-difference time-domain (FDTD) approach is traceable to Yee [23]. The finite-element method (FEM) is traced back to Silvester [24]. Wexler, known for his novel mode-matching (MM) contribution [25], makes the case for numerical solutions of field equations and reviews solution techniques based on finite differences [26]. Foundations of the method of moments (MoM) for EM can be attributed to Harrington [27] and, for implementation in planar simulators, to Rautio and Harrington [28]. An overview of the transmission-line modeling (TLM) method, pioneered in the microwave arena by Johns in the 1970s, is presented by Hoefer [29].

Electromagnetic (EM) simulators, that emerged in the late 1980s, are considered effective tools in an automated design environment. The EM field solvers can simulate EM structures of arbitrary geometrical shapes and are accurate up to millimeter wave frequencies. Particularly, they offer excellent accuracy if critical areas are meshed with a sufficiently small grid. Jain and Onno [30] divided the EM simulators into two main categories: the so-called two-and-one-half dimensional (2.5D) and three-dimensional (3D) field solvers. The 2.5D

EM solver analyzes planar structures based on the MoM [27] analysis. Examples of commercial 2.5D simulators include Sonnet's ***em*** [31] and Agilent Momentum [32]. The 3D EM solvers use volume meshing based on the FEM [24], the FDTD [23] or the TLM [29] analysis. Examples of 3D commercial software include the FEM High Frequency Structure Simulator (HFSS) from Ansoft [33] and HP Agilent [34], FDTD XFDTD from Remcom [35] and TLM MEFiSTo from Faustus [36].

Circuit-theory based simulation and CAD tools using empirical device models are fast. Analytical solutions or available exact derivatives cut down optimization time. They are simple and efficient but may lack the necessary accuracy or have limited validity region. Examples of commercial circuit simulators with optimization capabilities include OSA90/hope [37] and Agilent ADS [38]. On the other hand, EM simulators, long used for design verification, can be exploited in the optimization process. However, the higher the fidelity (accuracy) of the simulation the more expensive direct optimization is expected to be. For complex problems, this cost may be prohibitive.

In the 1990s, advances in microwave CAD technology have been made as a result of the availability of powerful PCs, workstations and massively parallel systems. This suggested the feasibility of interfacing EM simulations into optimization systems or CAD frameworks for direct application of powerful optimizers. Bandler *et al.* [39], [40] introduced the geometry capture concept which made automated EM optimization realizable. This concept was

implemented in Empipe and Empipe3D [41] to perform 2.5D and 3D EM optimization, respectively [42], [43], [44].

Alternative design schemes combining the speed and maturity of circuit simulators with the accuracy of EM solvers are desirable. The recent exploitation of iteratively refined surrogates of fine, accurate or high-fidelity models, and the implementation of space mapping (SM) methodologies address this issue. Through the construction of a space mapping, a suitable surrogate is obtained. This surrogate is faster than the "fine" model and at least as accurate as the underlying "coarse" model. The SM approach updates the surrogate to better approximate the corresponding fine model. The SM concept was coined by Bandler in 1993 and the first SM algorithms were introduced in [45], [46].

The objective of this thesis is to introduce some new trends and developments in CAD and modeling of RF and microwave circuits exploiting SM technology. This includes the contribution to the recent comprehensive review of the SM concept and applications [47], [48], [49]. It also includes the development of a family of robust techniques exploiting sensitivities, [50], [51], [52], [53] and TLM-based modeling and design exploiting the implicit and the output SM with a trust region methodology [54]–[55].

Chapter 2 reviews the SM technique and the SM-based surrogate (modeling) concept and their applications in engineering design optimization [47]–[49]. The aim of SM is to achieve a satisfactory solution with a minimal number of computationally expensive "fine" model evaluations. SM procedures

iteratively update and optimize surrogates based on a fast physically-based "coarse" model. Proposed approaches to SM-based optimization include the original algorithm, the Broyden-based aggressive space mapping algorithm, various trust region approaches, neural space mapping and implicit space mapping. We discuss also a mathematical formulation of the SM with respect to classical optimization techniques and convergence issues of SM algorithms. Significant practical applications are reviewed.

In Chapter 3, we present a family of robust techniques for exploiting sensitivities in EM-based circuit optimization through SM [50]–[53]. We utilize derivative information for parameter extractions and mapping updates. We exploit a partial SM (PSM) concept, where a reduced set of parameters is sufficient for the parameter extraction (PE) step. This reflects the idea of tuning and results in reducing the execution time. Upfront gradients of both EM (fine) model and coarse surrogates initialize possible mapping approximations. We also introduce several effective approaches for updating the mapping during the optimization iterations. Examples include the classical Rosenbrock function, modified to illustrate the approach, a two-section transmission-line 10:1 impedance transformer and a microstrip bandstop filter with open stubs.

In Chapter 4, we study the use of SM techniques within the TLM method environment [54]–[55]. Previous work on SM relies on an "idealized" coarse model in the design process of a computationally expensive fine model. For the first time, we examine the case when the coarse model is not capable of providing

an ideal optimal response. We exploit a coarse-grid TLM solver with relaxed boundary conditions. Such a coarse model may be incapable of satisfying design specifications and traditional SM may fail. Our approach, which exploits implicit SM (ISM) and the novel output SM (OSM), overcomes this failure. Dielectric constant, an expedient preassigned parameter, is first calibrated to roughly align the coarse and fine TLM models. Our OSM scheme absorbs the remaining deviation between the "implicitly" mapped coarse-grid and fine-grid TLM responses. Because the TLM simulations are on a fixed grid, response interpolation is crucial. We also create a database system to avoid repeating simulations unnecessarily. Our optimization routine employs a trust region methodology. The TLM-based design of an inductive post, a single-resonator filter and a six-section H-plane waveguide filter illustrate our approach. In a few iterations, our coarse-grid TLM surrogate, with approximate boundary conditions, achieves a good design of the fine-grid TLM model in spite of poor initial responses. Our results are verified with MEFiSTo simulations.

The thesis is concluded in Chapter 5, providing suggestions for further research. For convenience, a bibliography is given at the end of the thesis collecting all the references used.

The author's original contributions presented in this thesis are:

(1) Development of a CAD algorithm exploiting response sensitivities.

(2) Development of an algorithm employing sensitivities for improving the parameter extraction process.

(3) Development and implementation of the partial SM concept.

(4) Introducing effective approaches for updating the mapping function along optimization iterates.

(5) Contribution to the comprehensive review of space mapping technology: theory and applications.

(6) Development and implementation of a CAD algorithm utilizing the implicit and output SM concepts along with the trust regions methodologies.

(7) Implementation of an algorithm for obtaining response interpolations and a dynamically-updated database to avoid repeating unnecessary simulations.

REFERENCES

[1] M.B. Steer, J.W. Bandler and C.M. Snowden, "Computer-aided design of RF and microwave circuits and systems," *IEEE Trans. Microwave Theory Tech.*, vol. 50, pp. 996–1005, Mar. 2002.

[2] N. Marcuvitz, *Waveguide Handbook*, 1st ed. New York, NY: McGraw Hill, 1951.

[3] R. M. Barrett, "Microwave printed circuits—A historical survey," *IEEE Trans. Microwave Theory Tech.*, vol. MTT-3, pp. 1–9, Mar. 1955.

[4] R. E. Collin, *Foundations for Microwave Engineering*. New York, NY: McGraw Hill, 1966.

[5] R. L. Eisenhart and P. J. Khan, "Theoretical and experimental analysis of a waveguide mounting structure," *IEEE Trans. Microwave Theory Tech.*, vol. MTT-19, pp. 706–19, Aug. 1971.

[6] K. C. Gupta, "Emerging trends in millimeter-wave CAD," *IEEE Trans. Microwave Theory Tech.*, vol. 46, pp. 475–483, Apr. 1998.

[7] J.W. Bandler and S.H. Chen, "Circuit optimization: the state of the art," *IEEE Trans. Microwave Theory Tech.*, vol. 36, pp. 424–443, Feb. 1988.

[8] J.W. Bandler, W. Kellermann and K. Madsen, "A superlinearly convergent minimax algorithm for microwave circuit design," *IEEE Trans. Microwave Theory Tech.*, vol. MTT-33, pp. 1519–1530, Dec. 1985.

[9] G.C. Temes and D.A. Calahan, "Computer-aided network optimization the state-of-the-art," *Proc. IEEE*, vol. 55, pp.1832–1863, 1967.

[10] L.S. Lasdon and A.D. Waren, "Optimal design of filters with bounded, lossy elements," *IEEE Trans. Circuit Theory*, vol. CT-13, pp. 175–187, June 1966.

[11] L.S. Lasdon, D.F. Suchman and A.D. Waren, "Nonlinear programming applied to linear array design," *J. Acoust. Soc. Amer.*, vol. 40, pp. 1197–1200, Nov. 1966.

[12] A.D. Waren, L.S. Lasdon and D.F. Suchman, “Optimization in engineering design,” *Proc. IEEE,* vol. 55, pp. 1885–1897, 1967.

[13] J.W. Bandler, P.C. Liu and J.H.K. Chen, “Worst case network tolerance optimization,” *IEEE Trans. Microwave Theory Tech.*, vol. MTT-23, pp. 630–641, Aug. 1975.

[14] J.W. Bandler, P.C. Liu and H. Tromp, “A nonlinear programming approach to optimal design centering, tolerancing and tuning,” *IEEE Trans. Circuits Syst*., vol. CAS-23 pp. 155-165, Mar. 1976.

[15] J. W. Bandler, P. C. Liu, and H. Tromp, “Integrated approach to microwave design,” *IEEE Trans. Microwave Theory Tech.,* vol. MTT-24, pp. 584–591, Sep. 1976.

[16] S.W. Director and G.D. Hachtel, “The simplicial approximation approach to design centering,” *IEEE Trans. Circuits Syst.*, vol. CAS-24, pp.363–372, July 1977.

[17] R.S. Soin and R. Spence, “Statistical exploration approach to design centering,” *Proc. Inst. Elec. Eng.*, vol. 127, pt. G., pp. 260–269, 1980.

[18] J.W. Bandler and H.L. Abdel-Malek, “Optimal centering, tolerancing and yield determination via updated approximations and cuts,” *IEEE Trans. Circuits Syst*., vol. CAS-25, pp. 853–871, Oct. 1978.

[19] J.W. Bandler, R.M. Biernacki, S.H. Chen, P.A. Grobelny and S. Ye, ”Yield-driven electromagnetic optimization via multilevel multidimensional models,” *IEEE Trans. Microwave Theory Tech.*, vol. 41, pp. 2269–2278, Dec. 1993.

[20] D.A. Calahan, *Computer-Aided Network Design*, rev. ed. New York, NY: McGraw Hill, 1972.

[21] J.W. Bandler and M.R.M. Rizk, “Optimization of electrical circuits,” *Math. Program. Study*, vol. 11, pp. 1–64, 1979.

[22] R.K. Brayton, G.D. Hachtel and A.L. Sangiovanni-Vincentelli, “A survey of optimization techniques for integrated-circuit design,” *Proc. IEEE,* vol. 69, pp. 1334–1362, 1981.

[23] K. S. Yee, "Numerical solution of initial boundary value problems involving Maxwell's equations in isotropic media," *IEEE Trans. Antennas Propagat.*, vol. AP-14, pp. 302–307, May 1966.

[24] P. Silvester, "A general high-order finite-element waveguide analysis program," *IEEE Trans. Microwave Theory Tech.*, vol. MTT-17, pp. 204–210, Apr. 1969.

[25] A. Wexler, "Solution of waveguide discontinuities by modal analysis," *IEEE Trans. Microwave Theory Tech.*, vol. MTT-15, pp. 508–517, Sep. 1967.

[26] A. Wexler, "Computation of electromagnetic fields," *IEEE Trans. Microwave Theory Tech.*, vol. MTT-17, pp. 416–439, Aug. 1969.

[27] R. F. Harrington, "Matrix methods for field problems," *Proc. IEEE*, vol. 55, pp. 136–149, Feb. 1967.

[28] J. C. Rautio and R. F. Harrington, "An electromagnetic time-harmonic analysis of shielded microstrip circuits," *IEEE Trans. Microwave Theory Tech.*, vol. MTT-35, pp. 726–730, Aug. 1987.

[29] W. J. R. Hoefer, "The transmission-line matrix method—Theory and applications," *IEEE Trans. Microwave Theory Tech.*, vol. MTT-33, pp. 882–893, Oct. 1985.

[30] N. Jain and P. Onno, "Methods of using commercial electromagnetic simulators for microwave and millimeter-wave circuit design and optimization," *IEEE Trans. Microwave Theory Tech.*, vol.45, pp. 724–746, May 1997.

[31] ***em***, Sonnet Software, Inc. 100 Elwood Davis Road, North Syracuse, NY 13212, USA.

[32] Agilent Momentum, Agilent Technologies, 1400 Fountaingrove Parkway, Santa Rosa, CA 95403-1799, USA.

[33] Ansoft HFSS, Ansoft Corporation, 225 West Station Square Drive, Suite 200, Pittsburgh, PA 15219, USA.

[34] Agilent HFSS, Agilent Technologies, 1400 Fountaingrove Parkway, Santa Rosa, CA 95403-1799, USA.

[35] XFDTD, Remcom Inc., 315 South Allen Street, Suite 222, State College, PA 16801, USA.

[36] MEFiSTo-3D, Faustus Scientific Corporation, 1256 Beach Drive, Victoria, BC, V8S 2N3, Canada.

[37] OSA90/hope Version 4.0, formerly Optimization Systems Associates Inc., P.O. Box 8083, Dundas, ON, Canada, L9H 5E7, 1997, now Agilent Technologies, 1400 Fountaingrove Parkway, Santa Rosa, CA 95403-1799, USA.

[38] Agilent ADS, Agilent Technologies, 1400 Fountaingrove Parkway, Santa Rosa, CA 95403-1799, USA.

[39] J.W. Bandler, R.M. Biernacki and S.H. Chen, "Parameterization of arbitrary geometrical structures for automated electromagnetic optimization," in *IEEE MTT-S Int. Microwave Symp. Dig.*, San Francisco, CA, 1996, pp. 1059–1062.

[40] J.W. Bandler, R.M. Biernacki and S.H. Chen, "Parameterization of arbitrary geometrical structures for automated electromagnetic optimization," *Int. J. RF and Microwave CAE*, vol. 9, pp. 73–85, 1999.

[41] Empipe and Empipe3D Version 4.0, formerly Optimization Systems Associates Inc., P.O. Box 8083, Dundas, Ontario, Canada L9H 5E7, 1997, now Agilent Technologies, 1400 Fountaingrove, Parkway, Santa Rosa, CA 95403-1799, USA.

[42] J.W. Bandler, R.M. Biernacki, S.H. Chen, D.G. Swanson, Jr. and S. Ye, "Microstrip filter design using direct EM field simulation," *IEEE Trans. Microwave Theory Tech.*, vol. 42, pp. 1353–1359, July 1994.

[43] J.W. Bandler, R.M. Biernacki, S.H. Chen, W.J. Getsinger, P.A. Grobelny, C. Moskowitz and S.H. Talisa, "Electromagnetic design of high-temperature superconducting microwave filters," *Int. J. RF and Microwave CAE*, vol. 5, pp. 331–343, 1995.

[44] D.G. Swanson, Jr., "Optimizing a microstrip bandpass filter using electromagnetics," *Int. J. Microwave and Millimeter-wave CAE*, vol. 5, pp. 344–351, 1995.

[45] J.W. Bandler, R.M. Biernacki, S.H. Chen, P.A. Grobelny and R.H. Hemmers, "Space mapping technique for electromagnetic optimization," *IEEE Trans. Microwave Theory Tech.*, vol. 42, pp. 2536–2544, Dec. 1994.

[46] J.W. Bandler, R.M. Biernacki, S.H. Chen, R.H. Hemmers and K. Madsen, "Electromagnetic optimization exploiting aggressive space mapping," *IEEE Trans. Microwave Theory Tech*., vol. 43, pp. 2874–2882, Dec. 1995.

[47] J.W. Bandler, Q.S. Cheng, S.A. Dakroury, A.S. Mohamed, M.H. Bakr, K. Madsen and J. Søndergaard, "Trends in space mapping technology for engineering optimization," *3rd Annual McMaster Optimization Conference: Theory and Applications, MOPTA03,* Hamilton, ON, Aug. 2003.

[48] J.W. Bandler, Q. Cheng, S.A. Dakroury, A.S. Mohamed, M.H. Bakr, K. Madsen, and J. Søndergaard, "Space mapping: the state of the art," in *SBMO/IEEE MTT-S International Microwave and Optoelectronics Conference* (IMOC 2003), Parana, Brazil, 2003, vol. 2, pp. 951–956.

[49] J.W. Bandler, Q. Cheng, S.A. Dakroury, A.S. Mohamed, M.H. Bakr, K. Madsen, and J. Søndergaard, "Space mapping: the state of the art," *IEEE Trans. Microwave Theory and Tech.*, vol. 52, pp. 337–361, Jan. 2004.

[50] J.W. Bandler and A.S. Mohamed, "Space mapping optimization exploiting adjoint sensitivities," *Micronet Annual Workshop,* Ottawa, ON, 2002, pp. 61–62.

[51] J.W. Bandler, A.S. Mohamed, M.H. Bakr, K. Madsen and J. Søndergaard, "EM–based optimization exploiting partial space mapping and exact sensitivities," in *IEEE MTT–S Int. Microwave Symp. Dig.*, Seattle, WA, 2002, pp. 2101–2104.

[52] J.W. Bandler and A.S. Mohamed, "Engineering space mapping optimization exploiting exact sensitivities," *2nd Annual McMaster Optimization Conference: Theory and Applications, MOPTA02,* Hamilton, ON, 2002.

[53] J.W. Bandler, A.S. Mohamed, M.H. Bakr, K. Madsen and J. Søndergaard, "EM-based optimization exploiting partial space mapping and exact sensitivities," *IEEE Trans. Microwave Theory Tech.*, vol. 50, pp. 2741–2750, Dec. 2002.

[54] J.W. Bandler, Q.S. Cheng, D.M. Hailu, A.S. Mohamed, M.H. Bakr, K. Madsen and F. Pedersen, "Recent trends in space mapping technology," in *Proc. 2004 Asia-Pacific Microwave Conf.* (APMC'04), New Delhi, India, Dec. 2004.

[55] J.W. Bandler, A.S. Mohamed and M.H. Bakr, "TLM modeling and design exploiting space mapping," *IEEE Trans. Microwave Theory Tech.*, vol. 53, 2005.

CHAPTER 2

RECENT TRENDS IN SPACE MAPPING TECHNOLOGY

2.1 INTRODUCTION

CAD procedures for RF and microwave circuits such as statistical analysis and yield optimization demand elegant optimization techniques and accurate, fast models so that the design solutions can be achieved feasibly and reliably [1]. Traditional optimization techniques for engineering design [2]–[3] exploit simulated responses and possible derivatives with respect to design parameters. Circuit-theory CAD tools using empirical device models are fast but less accurate. Electromagnetic (EM) simulators need to be exploited in the optimization process. However, the higher the fidelity (accuracy) of the simulation the more expensive direct optimization will be.

The space mapping (SM) approach, conceived by Bandler in 1993, involves a calibration of a physically-based “coarse” surrogate by a “fine” model to accelerate design optimization. This simple CAD methodology embodies the

learning process of a designer. It makes effective use of the surrogate's fast evaluation to sparingly manipulate the iterations of the fine model.

In this chapter, a review of the state of the art of SM is presented. Bandler *et al.* [4]–[5] demonstrated how SM intelligently links companion "coarse" (simplified, fast or low-fidelity) and "fine" (accurate, practical or high-fidelity) models of different complexities. For example, an EM simulator could serve as a fine model. A low fidelity EM simulator or an empirical circuit model could be a coarse model (see Fig. 2.1 [6]).

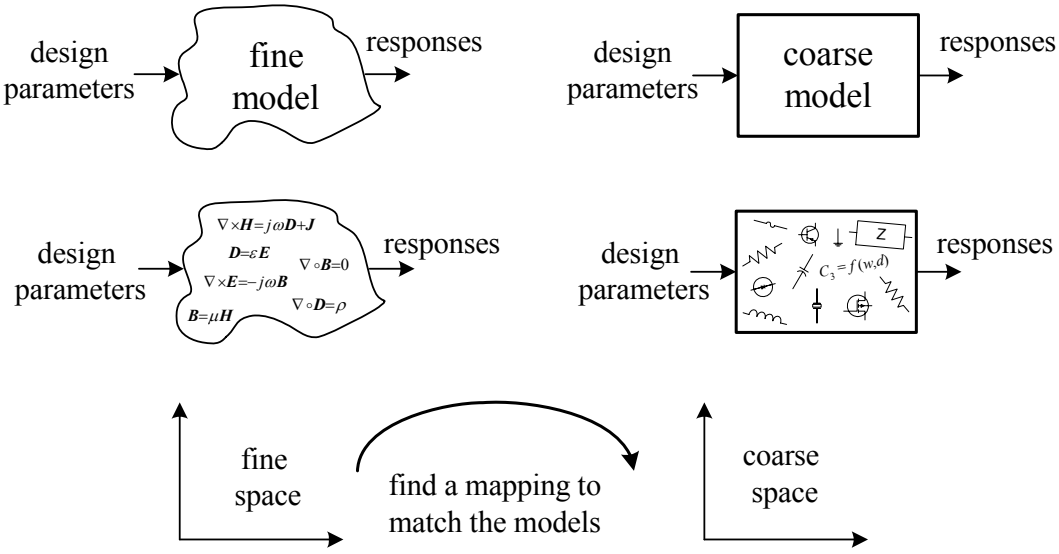

Fig. 2.1 Linking companion coarse (empirical) and fine (EM) models through a mapping [6].

The first algorithm was introduced in 1994 [4]. A linear mapping between the coarse and fine parameter spaces is evaluated by a least squares solution of the equations resulting from associating points (data) in the two spaces. The corresponding surrogate is a piecewise linearly mapped coarse model.

The aggressive SM (ASM) approach [5] exploits each fine model iterate immediately. This iterate, determined by a quasi-Newton step, in effect optimizes the corresponding surrogate model.

Parameter extraction (PE) is key to establishing mappings and updating surrogates. PE attempts to locally align a surrogate with a given fine model, but nonuniqueness may cause breakdown of the algorithm [7]. Multi-point PE [7], [8], a statistical PE [8], a penalty PE [9], aggressive PE [10] and a gradient PE approach [11] attempt to improve uniqueness (see Chapter 3 for details).

The trust region aggressive SM algorithm [12] exploits trust region (TR) strategies [13] to stabilize optimization iterations. The hybrid aggressive SM algorithm [14] alternates between optimization of a surrogate and direct response matching. The surrogate model based SM [15] algorithm combines a mapped coarse model with a linearized fine model and defaults to direct optimization of the fine model.

Neural space mapping approaches [16], [17], [18] utilize artificial neural networks (ANN) for EM-based modeling and design of microwave devices. A full review of ANN applications in microwave circuit design including the SM technology is found in [19].

The SMX [20] system was a first attempt to automate SM optimization through linking different simulators. A recent comprehensive microwave SM design framework and possible software implementations are given in [21].

Several SM-based model enhancement approaches have been proposed: the SM tableau approach [22], space derivative mapping [23], and SM-based neuromodeling [16]. Enhanced surrogate models for statistical analysis and yield-driven design exploiting SM technology are proposed in [24]. SM-based surrogate methodology for RF and microwave CAD library model creation is presented in [25].

Comprehensive reviews of SM techniques for modeling and design are presented in [6], [26].

In implicit SM (ISM) [27], an auxiliary set of preassigned parameters, e.g., dielectric constants or substrate heights, is extracted to match the surrogate with the fine model. The resulting calibrated coarse model is then reoptimized to predict the next fine model. ISM is effective for microwave circuit modeling and design using EM simulators and is more easily implemented than the expanded SM EM-based design framework described in [28].

Output SM (OSM) [29] was originally proposed to tune the residual response misalignment between the fine model and its surrogate. A highly accurate SM-based interpolating surrogate (SMIS) model is used in gradient-based optimization [30]. The SMIS surrogate is forced to match both the responses and derivatives of the fine model within a local region of interest.

SM technology has been recognized as a contribution to engineering design [31]–[37], especially in microwave and RF arena. Zhang and Gupta [31] have considered the integration of the SM concept into neural network modeling for RF and microwave design. Hong and Lancaster [32] describe the aggressive SM algorithm as an elegant approach to microstrip filter design. Conn, Gould and Toint [33] have stated that TR methods have been effective in the SM framework, especially in circuit design. Bakr [34] introduces advances in SM algorithms, Rayas-Sánchez [35] employs ANN, Ismail [36] studies SM-based model enhancement and Cheng [37] introduces advances in implicit and output SM.

In 2002, a workshop on microwave component design using SM methodologies was held [38]. This workshop brought together the foremost practitioners in microwave and RF arena including microwave component designers, software developers and academic innovators. They addressed designers' needs for effective tools for optimal designs, including yield optimization, exploiting accurate physically based device and component models.

Mathematicians are addressing mathematical interpretations of the formulation and convergence issues of SM algorithms [39]–[45]. Søndergaard gives a new definition of the original SM [39], combines the SM technique with the classical optimization methods [40] and places the SM in the context of the surrogate modeling and optimization techniques [41]. Pedersen [42] investigates how the transition from the SM technique to the classical methods could be done. Madsen and Søndergaard investigate convergence properties of SM algorithms

[43]. Vicente studies convergence properties of SM for design using the least squares formulation [44], and Hintermüller and Vicente introduce SM to solve optimal control problems [45]. Koziel *et al.* propose a rigorous formulation of the SM technique and discuss the convergence conditions for the OSM-based algorithm [46].

A workshop on surrogate modeling and SM was held in 2000 [47]. The focus was on techniques and practical applications suited to physically-based design optimization of computationally expensive engineering devices and systems through fast, inexpensive surrogate models and SM technology. Two minisymposia on SM methodologies were held in Sweden in May 2005 [48]. The event brought together mathematicians and engineers to present advances in algorithm convergence and new engineering implementations, including RF, wireless and microwave circuit design, integrating EM simulations (8 papers were presented).

Section 2.2 presents a formulation of the SM concept. Section 2.3 addresses the original SM optimization algorithm. The aggressive SM algorithm is described in Section 2.4. TR algorithms are discussed in Section 2.5, the hybrid and the surrogate model based optimization algorithms in Section 2.6, the implicit SM approach in Section 2.7, device model enhancement (quasi-global modeling) in Section 2.8, neural approaches in Section 2.9 and output SM techniques in Section 2.10. A mathematical motivation and convergence analysis for SM are presented in Section 2.11, a comparison between "the surrogate

management" approach with the SM technique in Section 2.12 and a review of various applications in Section 2.13. Conclusions are drawn in Section 2.14.

2.2 THE SPACE MAPPING CONCEPT

As depicted in Fig. 2.2, we denote the coarse and fine model design parameters $\boldsymbol{x}_c \in X_c$ and $\boldsymbol{x}_f \in X_f$, respectively where, $X_c, X_f \subseteq \mathbb{R}^n$. For simplicity, we assume that $X_c = X_f$. The corresponding response vectors are denoted by $\boldsymbol{R}_c$ and $\boldsymbol{R}_f : X_f \mapsto \mathbb{R}^m$, respectively, where $\boldsymbol{R}$ is a vector of m responses of the model, e.g., the magnitude of the microwave scattering parameter $|S_{11}|$ at m selected frequency points.

2.2.1 Original Design Problem

The design optimization problem to be solved is given by

$$\boldsymbol{x}_f^* \triangleq \arg \min_{\boldsymbol{x}_f} U(\boldsymbol{R}_f(\boldsymbol{x})) \tag{2.1}$$

where U is a suitable objective function. For example, U could be the minimax objective function with upper and lower specifications. $\boldsymbol{x}_f^*$ is the optimal solution to be determined.

2.2.2 The Space Mapping Concept

We obtain a mapping $\boldsymbol{P}$ relating the fine and coarse model parameters as

$$\boldsymbol{x}_c = \boldsymbol{P}(\boldsymbol{x}_f) \tag{2.2}$$

such that

$$\boldsymbol{R}_c(\boldsymbol{P}(\boldsymbol{x}_f)) \approx \boldsymbol{R}_f(\boldsymbol{x}_f) \tag{2.3}$$

in a region of interest.

Then we can avoid using direct optimization, i.e., solving (2.1) to find $\boldsymbol{x}_f^*$. Instead, we declare $\bar{\boldsymbol{x}}_f$, given by

$$\bar{\boldsymbol{x}}_f \triangleq \boldsymbol{P}^{-1}(\boldsymbol{x}_c^*) \tag{2.4}$$

as a good estimate of $\boldsymbol{x}_f^*$, where $\boldsymbol{x}_c^*$ is the result of coarse model optimization.

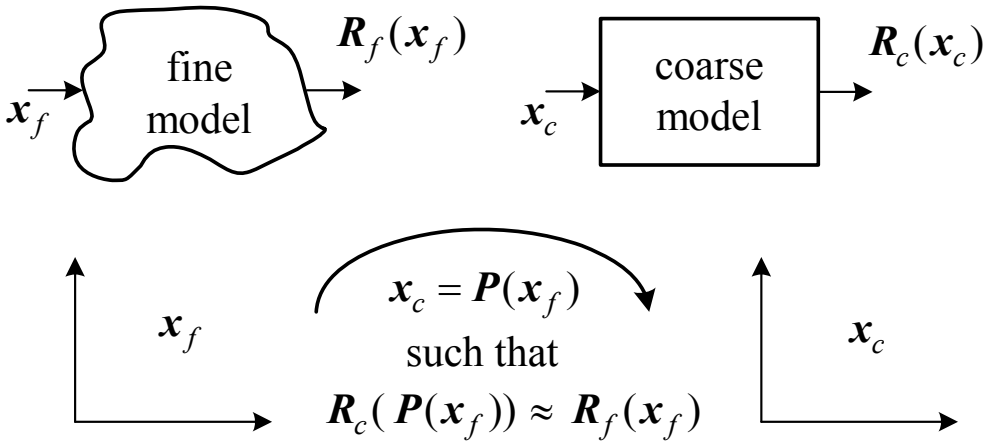

Fig. 2.2 Illustration of the fundamental notation of space mapping [6].

2.2.3 Jacobian Relationships

Using (2.2), the Jacobian of $\boldsymbol{P}$ is given by

$$\boldsymbol{J}_P \triangleq \boldsymbol{J}_P(\boldsymbol{x}_f) = \left(\frac{\partial \boldsymbol{P}^T}{\partial \boldsymbol{x}_f} \right)^T = \left(\frac{\partial (\boldsymbol{x}_c^T)}{\partial \boldsymbol{x}_f} \right)^T \tag{2.5}$$

An approximation to the mapping Jacobian is designated by the matrix $\boldsymbol{B} \in \mathbb{R}^{n \times n}$, i.e., $\boldsymbol{B} \approx \boldsymbol{J}_P(\boldsymbol{x}_f)$. Using (2.3) we obtain [14]

$$\boldsymbol{J}_f \approx \boldsymbol{J}_c \boldsymbol{B} \tag{2.6}$$

where $\boldsymbol{J}_f$ and $\boldsymbol{J}_c$ are the Jacobians of the fine and coarse models, respectively. This relation can be used to estimate the fine model Jacobian if the mapping is already established.

An expression for $\boldsymbol{B}$ which satisfies (2.6) can be derived as [14]

$$\boldsymbol{B} = (\boldsymbol{J}_c^T \boldsymbol{J}_c)^{-1} \boldsymbol{J}_c^T \boldsymbol{J}_f \tag{2.7}$$

If the coarse and fine model Jacobians are available, the mapping can be established through (2.7), provided that $\boldsymbol{J}_c$ has full rank and $m \geq n$.

2.2.4 Interpretation of Space Mapping Optimization

SM algorithms initially optimize the coarse model to obtain the optimal design $\boldsymbol{x}_c^*$, for instance in the minimax sense. Subsequently, a mapped solution is found through the PE process such that $\|\boldsymbol{g}\|_2^2$ is minimized, where $\boldsymbol{g}$ is defined by

$$\boldsymbol{g} = \boldsymbol{g}(\boldsymbol{x}_f) \triangleq \boldsymbol{R}_f(\boldsymbol{x}_f) - \boldsymbol{R}_c(\boldsymbol{x}_c^*) \tag{2.8}$$

Correspondingly, according to [40], $\boldsymbol{R}_c\left(\boldsymbol{P}(\boldsymbol{x}_f)\right)$ is optimized in the effort of finding a solution to (2.1). Here, $\boldsymbol{R}_c\left(\boldsymbol{P}(\boldsymbol{x}_f)\right)$ is an expression of an "enhanced" coarse model or "surrogate." Thus, the problem formulation can be rewritten as

$$\bar{\boldsymbol{x}}_f = \arg\min_{\boldsymbol{x}_f} U(\boldsymbol{R}_c(\boldsymbol{P}(\boldsymbol{x}_f)) \tag{2.9}$$

where $\bar{\boldsymbol{x}}_f$ may be close to $\boldsymbol{x}_f^*$ if $\boldsymbol{R}_c$ is close enough to $\boldsymbol{R}_f$. If $\boldsymbol{x}_c^*$ is unique then the solution of (2.9) is equivalent to driving the following residual vector $\boldsymbol{f}$ to zero

$$\boldsymbol{f} = \boldsymbol{f}(\boldsymbol{x}_f) \triangleq \boldsymbol{P}(\boldsymbol{x}_f) - \boldsymbol{x}_c^* \tag{2.10}$$

2.3 THE ORIGINAL SPACE MAPPING TECHNIQUE

In this technique [4], an initial approximation of the mapping, $\boldsymbol{P}^{(0)}$ is obtained by performing fine model analyses at a pre-selected set of at least m_0 base points, $m_0 \geq n+1$. One base point may be taken as the optimal coarse model solution, thus $\boldsymbol{x}_f^{(1)} = \boldsymbol{x}_c^*$. The remaining $m_0 - 1$ base points are chosen by perturbation. A corresponding set of coarse model points is then constructed through the parameter extraction (PE) process

$$\boldsymbol{x}_c^{(j)} \triangleq \arg\min_{\boldsymbol{x}_c} \left\| \boldsymbol{R}_f(\boldsymbol{x}_f^{(j)}) - \boldsymbol{R}_c(\boldsymbol{x}_c) \right\| \tag{2.11}$$

The additional $m_0 - 1$ points apart from $\boldsymbol{x}_f^{(1)}$ are required to establish full-rank conditions leading to the first mapping approximation $\boldsymbol{P}^{(0)}$. Bandler *et al*. [4] assumed a linear mapping between the two spaces.

This algorithm is simple but has pitfalls. First, m_0 upfront high-cost fine model analyses are needed. Second, a linear mapping may not be valid for significantly misaligned models. Third, nonuniqueness in the PE process may lead to an erroneous mapping estimation and algorithm breakdown.

2.4 THE AGGRESSIVE SPACE MAPPING TECHNIQUE

2.4.1 Theory

The aggressive SM technique iteratively solves the nonlinear system

$$\boldsymbol{f}(\boldsymbol{x}_f) = \boldsymbol{0} \tag{2.12}$$

for $\boldsymbol{x}_f$. Note, from (2.10), that at the *j*th iteration, the error vector $\boldsymbol{f}^{(j)}$ requires an evaluation of $\boldsymbol{P}^{(j)}\left(\boldsymbol{x}_f^{(j)}\right)$. This is executed indirectly through the PE (evaluation of $\boldsymbol{x}_c^{(j)}$). Coarse model optimization produces $\boldsymbol{x}_c^*$.

The quasi-Newton step in the fine space is given by

$$\boldsymbol{B}^{(j)}\boldsymbol{h}^{(j)} = -\boldsymbol{f}^{(j)} \tag{2.13}$$

where $\boldsymbol{B}^{(j)}$, the approximation of the mapping Jacobian $\boldsymbol{J}_p$ defined in (2.5), is updated using Broyden's rank one update [49]. Solving for $\boldsymbol{h}^{(j)}$ provides the next iterate $\boldsymbol{x}_f^{(j+1)}$

$$\boldsymbol{x}_f^{(j+1)} = \boldsymbol{x}_f^{(j)} + \boldsymbol{h}^{(j)} \tag{2.14}$$

The algorithm terminates if $\left\| \boldsymbol{f}^{(j)} \right\|$ becomes sufficiently small. The output of the algorithm is $\overline{\boldsymbol{x}}_f = \boldsymbol{P}^{-1}(\boldsymbol{x}_c^*)$ and the mapping matrix $\boldsymbol{B}$. The matrix $\boldsymbol{B}$ can be obtained in several ways (see Chapter 3, for more details).

2.4.2 A Five-pole Interdigital Filter [9]

Interdigital filters [50]–[51] have the advantage of compact size and adaptability to narrow- and wide-band applications. A five-pole interdigital filter is shown in Fig. 2.3. It consists of five quarter-wavelength resonators as well as input and output microstrip T-junctions within a shielded box. Each resonator is formed by one quarter-wavelength microstrip line section, shorted by a via at one end and opened at the other end. The arrows in Fig. 2.3 indicate the input and output reference planes, and the triangles symbolize the grounded vias.

Decomposition is used to construct a coarse model. As shown in Fig. 2.4, the coarse filter has a 12-port center piece, the vias, the microstrip line sections and the open ends. The vias are analyzed by Sonnet's ***em*** [52] with a fine grid. All the other parts are analyzed using coarse grid ***em*** or empirical models in OSA90/hope [53]. The results are then connected through circuit theory to obtain the responses of the overall filter.

The alumina substrate height is 15 mil (0.381 mm) with ε_r = 9.8. The width of each microstrip is chosen as 10 mil (0.254 mm). The optimization variables are chosen to be $x_1, x_2, \ldots, x_6$ as shown in Fig. 2.4.

The interdigital filter design specifications are

Passband ripple ≤ 0.1 dB for 4.9 GHz ≤ ω ≤ 5.3 GHz

Isolation: 30 dB,

Isolation bandwidth: 0.95 GHz

Sonnet's ***em*** [52] driven by Empipe [54] is employed as the fine model, using a high-resolution grid with a 1.0 mil ×1.0 mil (0.0254 mm × 0.0254 mm) cell size. With this grid size, the EM simulation time is about 1.5 CPU hour per frequency point on a Sun SPARCstation 10. The coarse model simulation takes less than 1.5 CPU min per frequency point on a Sun SPARCstation 10. The overall CPU time required for optimizing the coarse model is about 2 hours, which is the same order of magnitude as the fine-model EM simulation at a single frequency point.

The aggressive SM technique terminates in 2 iterations. The coarse and fine model responses at the optimal coarse model solution are shown in Fig. 2.5. The optimal coarse model response and the final fine model response are shown in Fig. 2.6. The final fine model response using a fine frequency sweep is shown in Fig. 2.7. The passband return loss is better than 18.5 dB and the insertion loss ripples are less than 0.1 dB.

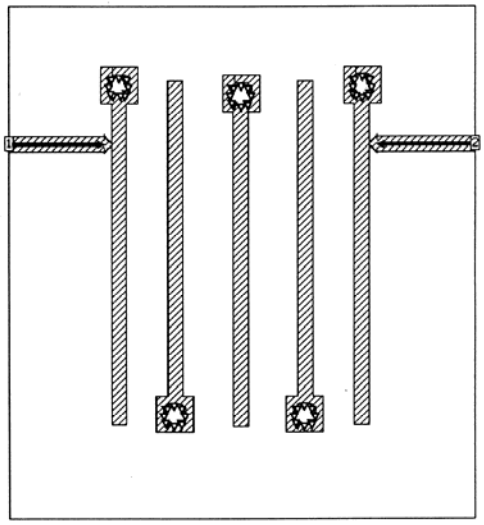

Fig. 2.3 A five-pole interdigital filter [9]

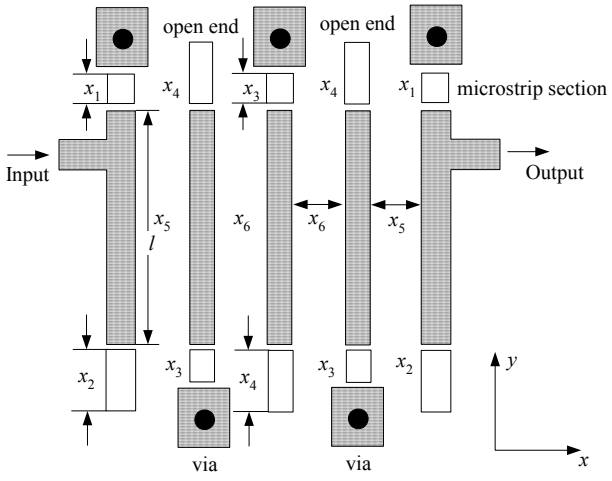

Fig. 2.4 A coarse model of the five-pole interdigital filter using decomposition [9].

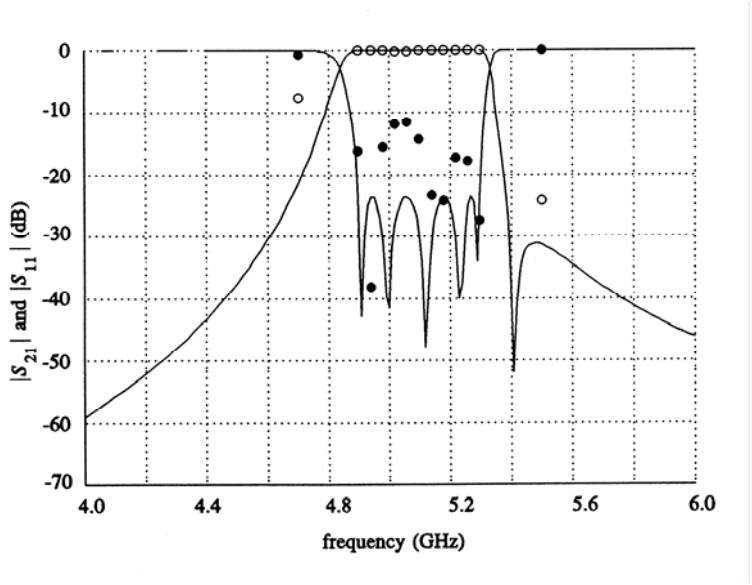

Fig. 2.5 Optimal coarse model target response (— $|S_{11}|$ and $|S_{21}|$) and the fine model response at the starting point (• $|S_{11}|$ and o $|S_{21}|$) for the five-pole interdigital filter [9].

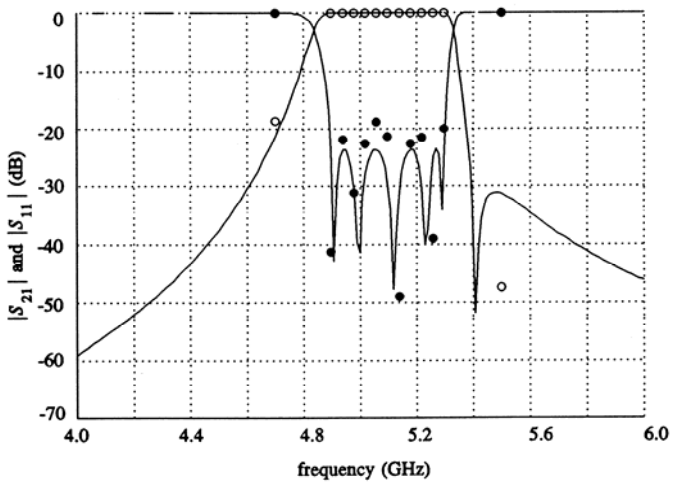

Fig. 2.6 Optimal coarse model target response (— $|S_{11}|$ and $|S_{21}|$) and the fine model response at the final design (• $|S_{11}|$ and o $|S_{21}|$) for the five-pole interdigital filter [9].

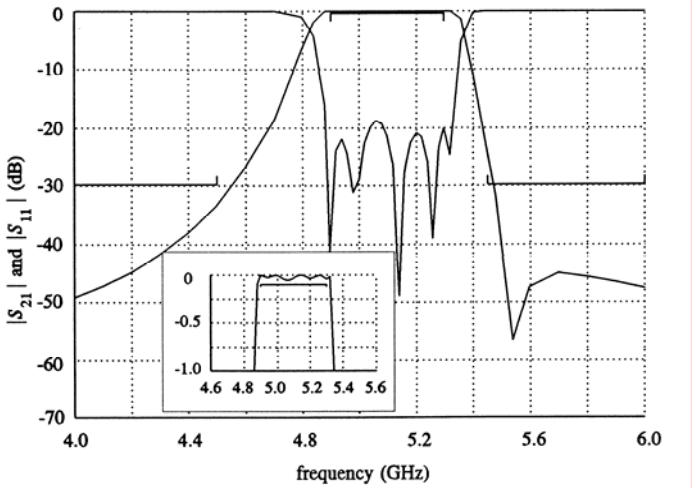

Fig. 2.7 The fine model response at the final design (— $|S_{11}|$ and $|S_{21}|$) using a fine frequency sweep for the five-pole interdigital filter [9].

2.5 TRUST REGIONS AND AGGRESSIVE SPACE MAPPING

A goal of modern nonlinear programming is robust global behavior of the algorithms. By robust global behavior we mean the mathematical assurance that the iterates produced by an optimization algorithm, started at an arbitrary initial iterate, will converge to a stationary point or local minimizer for the problem [13]. TR strategies can be used to achieve this property.

2.5.1 Trust Region Methods [33]

The idea of TR methods is to adjust the length of the step taken at each iteration based on how well an approximate linear or quadratic model predicts the objective function. The approximate model is trusted to represent the objective

function only within a region of specific radius around the current iteration. The local model minimum inside the TR is found by solving a TR subproblem. If the model minimum achieves sufficient actual reduction in the objective function, the TR size is increased. If insufficient reduction is achieved the TR is reduced. Otherwise the TR is kept unchanged.

Assume that the objective function is a scalar function $f(\boldsymbol{x})$. At the *j*th iterate $\boldsymbol{x}^{(j)}$, a local approximate model $L^{(j)}(\boldsymbol{x})$ is used to approximate $f(\boldsymbol{x})$. It is crucial that $L^{(j)}(\boldsymbol{x})$ is interpolating f at $\boldsymbol{x}^{(j)}$, i.e., it has the property

$$L^{(j)}(\boldsymbol{x}^{(j)}+\boldsymbol{h}^{(j)})-f(\boldsymbol{x}^{(j)})\to 0 \quad \text{as } \boldsymbol{h}^{(j)}\to 0 \tag{2.15}$$

The step $\boldsymbol{h}^{(j)}$ to the next tentative iterate is found by solving the TR subproblem

$$\underset{\boldsymbol{h}^{(j)}}{\text{minimize}}\, \boldsymbol{L}^{(j)}(\boldsymbol{x}^{(j)},\boldsymbol{h}^{(j)}), \quad \left\|\boldsymbol{h}^{(j)}\right\| \le \delta^{(j)} \tag{2.16}$$

where $\delta^{(j)}$ is the TR size. A quality measure of the next tentative step $\boldsymbol{h}^{(j)}$ is the ratio $\rho^{(j)}$:

$$\rho^{(j)}=\frac{f(\boldsymbol{x}^{(j)})-f(\boldsymbol{x}^{(j)}+\boldsymbol{h}^{(j)})}{L^{(j)}(\boldsymbol{x}^{(j)})-L^{(j)}(\boldsymbol{x}^{(j)}+\boldsymbol{h}^{(j)})} \tag{2.17}$$

where the numerator represents the actual reduction and the denominator is the reduction predicted by the local approximation. The TR size is adjusted at the end of each iteration based on $\rho^{(j)}$. The next iteration is accepted only if an

actual reduction is achieved in the objective function. A good survey of methods for updating the TR size is given in [55].

2.5.2 Trust Region and Aggressive SM [12]

The trust region aggressive SM algorithm integrates a TR methodology with the aggressive SM technique. Instead of using a quasi-Newton step in the aggressive SM to drive $\boldsymbol{f}$ to zero, a TR subproblem is solved within a certain TR to minimize $\left\| \boldsymbol{f}^{(j+1)} \right\|_2^2$. Consider the linearized function

$$\boldsymbol{L}^{(j)}(\boldsymbol{x}^{(j)}, \boldsymbol{h}^{(j)}) \triangleq \boldsymbol{f}^{(j)} + \boldsymbol{B}^{(j)}\boldsymbol{h}^{(j)} \tag{2.18}$$

The next step is obtained by solving the TR subproblem

$$\boldsymbol{h}^{(j)} = \arg\min_{\boldsymbol{h}} \left\| \boldsymbol{L}^{(j)}(\boldsymbol{x}^{(j)}, \boldsymbol{h}) \right\|_2^2, \quad \left\| \boldsymbol{h} \right\|_2 \le \delta^{(j)} \tag{2.19}$$

Thus the step taken is constrained by a suitable TR $\delta^{(j)}$. Solving (2.19) is equivalent to solving

$$(\boldsymbol{B}^{(j)T}\boldsymbol{B}^{(j)} + \lambda\, \boldsymbol{I})\boldsymbol{h}^{(j)} = -\boldsymbol{B}^{(j)T}\boldsymbol{f}^{(j)} \tag{2.20}$$

where $\boldsymbol{B}^{(j)}$ is an approximation to the Jacobian of the mapping $\boldsymbol{P}$ at the jth iteration. The parameter λ can be selected such that the step is identical to that of (2.19). As in aggressive SM, $\boldsymbol{B}^{(j)}$ is updated by Broyden's formula [49].

The trust region aggressive SM algorithm also uses recursive multipoint PE (see Chapter 3). Through the set of points used in the multi-point parameter extraction (MPE), the algorithm estimates the Jacobian of the fine model.

2.6 HYBRID AGGRESSIVE SM AND SURROGATE MODEL BASED OPTIMIZATION

2.6.1 Hybrid Aggressive SM Algorithm [14]

Hybrid aggressive SM starts with an SM optimization phase and defaults to a response matching phase when SM fails. The algorithm exploits (2.6) and (2.7) to enable switching between the two phases.

In the SM phase, trust region aggressive SM optimization is carried out using the objective function $\|\boldsymbol{f}\|_2^2$ for $\boldsymbol{f}$ defined by (2.10). While in the response matching phase, the objective function is $\|\boldsymbol{g}\|_2^2$ where $\boldsymbol{g}$ is defined by (2.8).

At the *j*th iteration $\boldsymbol{x}_f^{(j+1)}$ is evaluated. If an actual reduction is achieved in $\|\boldsymbol{f}\|_2^2$ and $\|\boldsymbol{g}\|_2^2$, then the SM iteration is accepted, the matrix $\boldsymbol{B}$ is updated and the SM optimization phase continues. Whenever no reduction is achieved in $\|\boldsymbol{g}\|_2^2$, the point $\boldsymbol{x}_f^{(j+1)}$ is rejected, the Jacobian of the fine model response $\boldsymbol{J}_f^{(j)}$ is evaluated at the point $\boldsymbol{x}_f^{(j)}$ using (2.6) and response matching starts.

If $\boldsymbol{x}_f^{(j+1)}$ achieves reduction in $\|\boldsymbol{g}\|_2^2$ but does not achieve any reduction in $\|\boldsymbol{f}\|_2^2$, mainly because of PE nonuniqueness, the point $\boldsymbol{x}_f^{(j+1)}$ is accepted and recursive MPE is used to find another vector $\boldsymbol{f}^{(j+1)}$. If the new $\boldsymbol{f}^{(j+1)}$ still does

not achieve improvement in $\|\boldsymbol{f}\|_2^2$, $\boldsymbol{J}_f^{(j+1)}$ is approximated using the n+1 MPE fine model points, then $\boldsymbol{x}_f^{(j+1)}$ and $\boldsymbol{J}_f^{(j+1)}$ are supplied to the response matching phase.

2.6.2 Surrogate Model-Based SM Algorithm [15]

Surrogate model-based SM optimization exploits a surrogate in the form of a convex combination of a mapped coarse model and a linearized fine model. The algorithm employs the TR method in which the surrogate replaces the formal approximation to a linear or quadratic model.

At the jth iteration, the surrogate model response $\boldsymbol{R}_s^{(j)} \in \mathbb{R}^m$ is given by

$$\boldsymbol{R}_s^{(j)}(\boldsymbol{x}_f) \triangleq \lambda^{(j)} \boldsymbol{R}_m^{(j)}(\boldsymbol{x}_f) + (1-\lambda^{(j)})(\boldsymbol{R}_f(\boldsymbol{x}_f^{(j)}) + \boldsymbol{J}_f^{(j)} \Delta \boldsymbol{x}_f) \tag{2.21}$$

where $\boldsymbol{R}_m^{(j)}(\boldsymbol{x}_f)$ is the mapped coarse model response, $\boldsymbol{R}_f^{(j)} + \boldsymbol{J}_f^{(j)} \Delta \boldsymbol{x}_f$ is the linearized fine model response and $\lambda^{(j)}$ is a parameter to determine how each model is favored. If $\lambda^{(j)} = 1$, the surrogate becomes a mapped coarse model. If $\lambda^{(j)} = 0$, then the surrogate becomes a linearized fine model. Initially, $\lambda^{(0)} = 1$. Its update at each iteration depends on the predicted errors produced by the mapped coarse model and the linearized fine model with respect to the fine model [15].

The step suggested is given by

$$\boldsymbol{h}^{(j)} = \arg \min_{\boldsymbol{h}} U(\boldsymbol{R}_s^{(j)}(\boldsymbol{x}_f^{(j)} + \boldsymbol{h})), \quad \|\boldsymbol{h}\| \le \delta^{(j)} \tag{2.22}$$

where $\delta^{(j)}$ is the TR size at the *j*th iteration. The mapped coarse model utilizes a frequency-sensitive mapping.

Two approaches based on (2.21) are described in [40] and [42]. In [40], the value of $\lambda^{(j)}$ is monotonically decreased from 1 to 0 during the iterations. In [15], the value of $\lambda^{(j)}$ is only decreased if unsuccessful steps are produced. In [42], $\lambda^{(j)} = 1$ until at least n linearly independent steps have been tried. Thereafter, $\lambda^{(j)}$ remains 1 until an unsuccessful step is produced, then $\lambda^{(j)}$ is set to 0 for the remaining iterations.

2.7 IMPLICIT SPACE MAPPING

Implicit SM (ISM) [27] is a recent development. Selected preassigned parameters are extracted to match the coarse and fine models. Examples of preassigned parameters are dielectric constant and substrate height. With these parameters fixed, the calibrated coarse model (the surrogate) is reoptimized. The optimized parameters are assigned to the fine model. This process repeats until the fine model response is sufficiently close to the target response.

The idea of using preassigned parameters was introduced in [28] within an expanded SM design framework. This method selects certain key preassigned parameters based on sensitivity analysis of the coarse model. These parameters are extracted to match corresponding coarse and fine models. A mapping from optimization parameters to preassigned parameters is then established.

As indicated in Fig. 2.8, ISM aims at establishing an implicit mapping $\boldsymbol{Q}$ between the spaces $\boldsymbol{x}_f$, $\boldsymbol{x}_c$ and $\boldsymbol{x}$

$$\boldsymbol{Q}(\boldsymbol{x}_f, \boldsymbol{x}_c, \boldsymbol{x}) = \boldsymbol{0} \tag{2.23}$$

where $\boldsymbol{x}$ is a set of auxiliary parameters, e.g., preassigned, to be varied in the coarse model only. Thus, the corresponding calibrated coarse model (surrogate) response is $\boldsymbol{R}_c(\boldsymbol{x}_c, \boldsymbol{x})$.

ISM optimization obtains a space-mapped design $\bar{\boldsymbol{x}}_f$ whose response approximates an optimized target response. It is a solution of the nonlinear system (2.23), obtained through a PE with respect to $\boldsymbol{x}$ and (re)optimization of the surrogate with respect to $\boldsymbol{x}_c$ to give $\bar{\boldsymbol{x}}_f = \boldsymbol{x}_c^*(\boldsymbol{x})$, the prediction of the fine model. The corresponding response is denoted by $\boldsymbol{R}_c^*$.

Implicit SM is effective for microwave circuit modeling and design using full-wave EM simulators. Since explicit mapping is not involved, this "space mapping" technique is more easily implemented than the expanded SM algorithm described in [28]. The HTS filter design is entirely done by Agilent ADS [56] and Momentum [57] or Sonnet's ***em*** [52], with no matrices to keep track of [27].

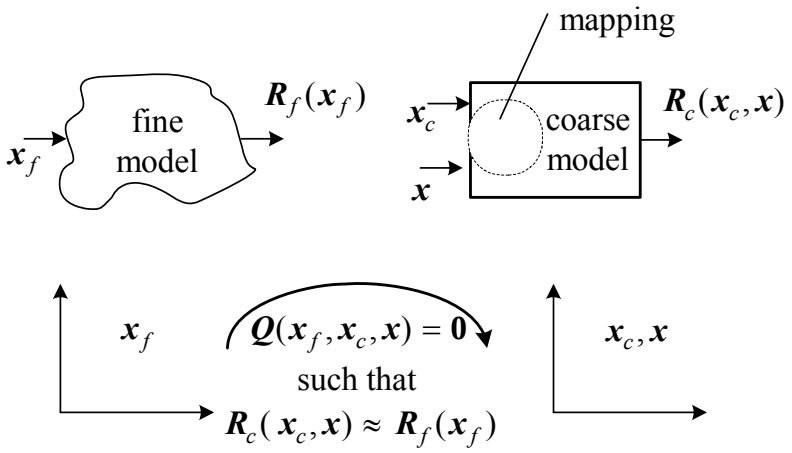

Fig. 2.8 Illustration of the implicit space mapping (ISM) concept [27].

2.8 SPACE MAPPING-BASED MODEL ENHANCEMENT

The development of fast, accurate models for components that can be utilized for CAD over wide ranges of the parameter space is crucial [16], [22], [23], [58]. Consider

$$\boldsymbol{R}_f(\boldsymbol{x}_f, \omega) \approx \boldsymbol{R}_c(\boldsymbol{P}(\boldsymbol{x}_f, \omega)) \tag{2.24}$$

This formulation offers the possibility of enhancing a pre-existing coarse model through a mapping. Approaches to SM-based model enhancement differ in the way in which the mapping is established, the nature of the mapping and the region of validity. The generalized SM tableau approach, the space derivative mapping approach and the SM-based neuromodeling have been proposed.

2.8.1 Generalized Space Mapping (GSM) Tableau [22]

This engineering device modeling framework exploits the SM [4], the frequency SM [5] and multiple SM [59] concepts.

The frequency-SM super model (Fig. 2.9) maps both the designable device parameters and the frequency. The SM super model is a special case where it maps only designable device parameters and keeps the frequency unchanged. In multiple SM, either the device responses or the frequency intervals are divided into a number of subsets and a separate mapping is established for each.

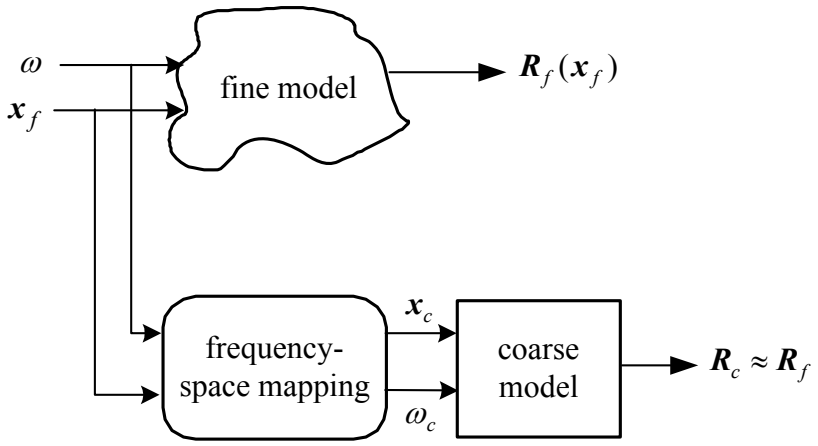

Fig. 2.9 The frequency-SM super model concept [22].

The mapping relating fine model parameters and frequency to coarse model parameters and frequency is given by

$$(\boldsymbol{x}_c, \omega_c) = \boldsymbol{P}(\boldsymbol{x}_f, \omega) \tag{2.25}$$

or, in matrix form, assuming a linear mapping,

$$\begin{bmatrix} \boldsymbol{x}_c \\ \omega_c^{-1} \end{bmatrix} = \begin{bmatrix} \boldsymbol{c} \\ \delta \end{bmatrix} + \begin{bmatrix} \boldsymbol{B} & \boldsymbol{s} \\ \boldsymbol{t}^T & \sigma \end{bmatrix} \begin{bmatrix} \boldsymbol{x}_f \\ \omega^{-1} \end{bmatrix} \tag{2.26}$$

The inverse of the frequency variable (proportional to wavelength) used in (2.26) shows good results [22].

The parameters $\{\boldsymbol{c}, \boldsymbol{B}, \boldsymbol{s}, \delta, \boldsymbol{t}, \sigma\}$ can be evaluated by solving the optimization problem

$$\min_{\boldsymbol{c},\boldsymbol{B},\boldsymbol{s},\delta,\boldsymbol{t},\sigma} \left\| [\boldsymbol{e}_1^T \quad \boldsymbol{e}_2^T \quad \cdots \quad \boldsymbol{e}_N^T]^T \right\| \tag{2.27}$$

where N is the number of base points and the kth error vector $\boldsymbol{e}_k$ is given by

$$\boldsymbol{e}_k = \boldsymbol{R}_f(\boldsymbol{x}_{f,k}, \omega) - \boldsymbol{R}_c(\boldsymbol{x}_c, \omega_c); \quad k = 1, ..., N \tag{2.28}$$

The total number of fine model simulations is $N \times m$, where m is the number of frequency points per frequency sweep.

2.8.2 Space Derivative Mapping [23]

This algorithm develops a locally valid approximation of the fine model in the vicinity of a particular point $\tilde{\boldsymbol{x}}_f$. We denote by $\tilde{\boldsymbol{J}}_f$ the Jacobian of the fine model responses at $\tilde{\boldsymbol{x}}_f$. The first step obtains the point $\tilde{\boldsymbol{x}}_c$ corresponding to $\tilde{\boldsymbol{x}}_f$ through the single point PE problem (2.11). The Jacobian $\tilde{\boldsymbol{J}}_c$ at $\tilde{\boldsymbol{x}}_c$ may be estimated by finite differences. Both (2.11) and the evaluation of $\tilde{\boldsymbol{J}}_c$ should add no significant overhead. The mapping matrix $\boldsymbol{B}$ is then calculated by applying (2.7) as

$$\boldsymbol{B} = (\tilde{\boldsymbol{J}}_c^T \tilde{\boldsymbol{J}}_c)^{-1} \tilde{\boldsymbol{J}}_c^T \tilde{\boldsymbol{J}}_f \tag{2.29}$$

Once $\boldsymbol{B}$ is available the linear mapping is given by

$$\boldsymbol{x}_c = \boldsymbol{P}(\boldsymbol{x}_f) \triangleq \tilde{\boldsymbol{x}}_c + \boldsymbol{B}(\boldsymbol{x}_f - \tilde{\boldsymbol{x}}_f) \tag{2.30}$$

The space derivative mapping model is given by (2.24) with $\boldsymbol{P}$ given by (2.30).

The space derivative mapping technique was applied to statistical analysis of a two-section waveguide impedance transformer and a six-section H-plane waveguide filter [23]. For these examples, the design parameters are assumed to be uniformly distributed with a given relative tolerance.

2.8.3 SM-Based Neuromodeling [16]

Using artificial neural networks (ANN), a mapping $\boldsymbol{P}$ from the fine to the coarse input space is constructed. The implicit "expert" knowledge in the coarse model permits a reduced number of learning points and reduces complexity of the ANN.

Here, the optimization problem

$$\min_{\boldsymbol{w}} \left\| [\boldsymbol{e}_1^T \quad \boldsymbol{e}_2^T \quad \cdots \quad \boldsymbol{e}_N^T]^T \right\| \tag{2.31}$$

is solved, where the vector $\boldsymbol{w}$ contains the internal parameters of the ANN (weights, bias, etc.), N is the total number of learning base points, and $\boldsymbol{e}_k$ is the error vector given by

$$\begin{aligned} \boldsymbol{e}_k(\boldsymbol{w}) &\triangleq \boldsymbol{R}_f(\boldsymbol{x}_{f,k},\ \omega) \ -\ \boldsymbol{R}_c(\boldsymbol{P}(\boldsymbol{x}_{f,k}, \omega, \boldsymbol{w})), \\ \boldsymbol{P}(\boldsymbol{x}_{f,k}, \omega, \boldsymbol{w}) &= (\boldsymbol{x}_c, \omega_c), \qquad k = 1, \ldots, N \end{aligned} \tag{2.32}$$

A "star set" for the base learning points is considered. A Huber norm is used in (2.31), exploiting its robust characteristics for data fitting [60]. Frequency-sensitive mappings from the fine to the coarse spaces can be realized by making frequency an additional input variable of the ANN that implements the mapping [17].

2.9 NEURAL SM-BASED OPTIMIZATION TECHNIQUES

ANNs are suitable for modeling high-dimensional and highly nonlinear devices due to their ability to learn and generalize from data, their nonlinear processing nature and their massively parallel structure [31]. Rayas-Sánchez reviews the state of the art in EM-based design and optimization of microwave circuits using ANNs [19].

2.9.1 Neural Space Mapping (NSM) [17]

A strategy is proposed to exploit the SM-based neuromodeling techniques [16] in an optimization algorithm, including frequency mapping. A coarse model is used to select the initial learning base points through sensitivity analysis. The proposed procedure does not require PE to predict the next point. Huber optimization is used to train the SM-based neuromodels at each iteration. These neuromodels are developed without using testing points: their generalization performance is controlled by gradually increasing their complexity starting with a 2-layer perceptron. Five neuromapping variations have been presented [17].

The SM-based neuromodels, obtained through modeling [16] or optimization [17] processes, have been used in statistical simulation and yield optimization [61]. This technique has increased the yield of an HTS filter from 14% to 69%. In addition, excellent agreement is achieved between the SM-based neuromodel and the EM responses at the optimal yield solution [61].

2.9.2 Neural Inverse Space Mapping (NISM) [18]

Neural inverse SM (NISM) follows the aggressive approach [5] by not requiring a number of up-front fine model evaluations to start building the mapping. A statistical procedure for PE is used to overcome poor local minima. At each iteration a neural network whose generalization performance is controlled through a network growing strategy approximates the inverse of the mapping. The NISM step simply evaluates the current neural network at the optimal coarse solution. This step is equivalent to a quasi-Newton step while the inverse mapping remains essentially linear.

2.10 OUTPUT SPACE MAPPING

The output SM-based approach addresses the deviation between the coarse and fine models in the response space [21], [29]–[30]. A sequence of surrogates $\boldsymbol{R}_s^{(j)}; j = 1, 2, ...$ of the fine model is generated iteratively, through the PE process.

2.10.1 Implicitly Mapped Coarse Model with an Output Mapping

The implicitly mapped surrogate that involves an output or response residual is defined as [21], [29]

$$\boldsymbol{R}_s \triangleq \boldsymbol{R}_c(\boldsymbol{x}_c, \boldsymbol{x}) + \text{diag}\{\lambda_1, \lambda_2, ..., \lambda_m\}\,\Delta\boldsymbol{R} \tag{2.33}$$

where, $\Delta\boldsymbol{R}$ is the residual between the implicitly mapped coarse model response after PE and the fine model response at each sample point. The output mapping ($\boldsymbol{O}$) is characterized by a diagonal matrix $\boldsymbol{\Lambda} \triangleq diag\{\lambda_1, \lambda_2, ..., \lambda_m\}$.

In [29] only the implicitly mapped coarse model $\boldsymbol{R}_c(\boldsymbol{x}_c, \boldsymbol{x})$ is utilized in the PE step while the output-mapped surrogate defined in (2.33) is employed in the surrogate optimization with $\lambda_i = 0.5; \forall i = 1, 2, ..., m$.

In a more comprehensive approach, the output-mapped surrogate (2.33) could be utilized in both PE and surrogate optimization in an iterative way. In this approach a full residual step is employed, i.e., $\lambda_i = 1; \forall i = 1, 2, ..., m$. Moreover, the frequency transformation parameters are employed as preassigned parameters $\boldsymbol{x} = \begin{bmatrix} \sigma & \delta \end{bmatrix}^T$.

The response residual SM (RRSM) [21] employs a hybrid approach. Initially, an implicit SM iteration is executed to obtain a near-optimum design. Then, an implicit SM and RRSM iteration, using the output-mapped surrogate (2.33), are employed with $\lambda_i = 0.5; \forall i = 1, 2, ..., m$ followed by iterations with a full residual added.

2.10.2 The Output SM-Based Interpolating Surrogate (SMIS)

A recently explored surrogate that involves an output SM (***O***) and an explicit parameter mapping ***P*** is defined to satisfy interpolating conditions (response match, response Jacobian match at the current point and global match at a set of points) [30]. Here, the *j*th surrogate of the *i*th response is given by

$$\begin{aligned} R_{s,i}^{(j)} &= O_i^{(j)} \circ R_{c,i}^{(j)} \\ R_{s,i}^{(j)} &\triangleq \alpha_i^{(j)} \left(R_{c,i}\left(\boldsymbol{P}_i^{(j)}(\boldsymbol{x}_f) \right) - R_{c,i}\left(\boldsymbol{P}_i^{(j)}(\boldsymbol{x}_f^{(j)}) \right) \right) + R_i^{(j)} \\ \boldsymbol{P}_i^{(j)}(\boldsymbol{x}_f) &= \boldsymbol{B}_i^{(j)} \boldsymbol{x}_f + \boldsymbol{c}_i^{(j)}; i = 1, 2, ..., m \end{aligned} \tag{2.34}$$

where $\boldsymbol{B}_i^{(j)} \in \mathbb{R}^{n \times n}$ and $\boldsymbol{c}_i^{(j)} \in \mathbb{R}^n$ are the input mapping parameters of the *i*th response and $\alpha_i^{(j)} \in \mathbb{R}$ is the corresponding *i*th output mapping parameter. It is suggested in [30] to use $R_i^{(0)} = R_{c,i}(\boldsymbol{x}_f^{(0)})$ initially, and to set $R_i^{(j)} = R_{f,i}(\boldsymbol{x}_f^{(j)})$ for *j* > 0. The surrogate is built iteratively around the current point $\boldsymbol{x}_f^{(j)}$. The SMIS algorithm delivers the accuracy expected from classical direct optimization using sequential linear programming [30].

2.11 SPACE MAPPING: MATHEMATICAL MOTIVATION AND CONVERGENCE ANALYSIS

The space mapping technique is appealing to the mathematical community for its applicability in different fields. Therefore, mathematicians have started to study the formulation and convergence issues of SM algorithms.

2.11.1 Mathematical Motivation of the SM Technique

In [6], [40], a mathematical motivation of SM in the context of classical optimization based on local Taylor approximations is presented. If the nonlinearity of the fine model is reflected by the coarse model then the space mapping is expected to involve less curvature (less nonlinearity) than the two physical models. The SM model is then expected to yield a good approximation over a large region, i.e., it generates large descent iteration steps. Close to the solution, however, only small steps are needed, in which case the classical optimization strategy based on local Taylor models is better. A combination of the two strategies gives the highest solution accuracy and fast convergence.

Fig. 2.10 depicts model effectiveness plots for a two-section capacitively loaded impedance transformer [40], at the final iterate $\boldsymbol{x}_f^{(j)}$, approximately [74.23 79.27]^T. Centered at $\boldsymbol{h} = \boldsymbol{0}$, the light grid shows $\left\| \boldsymbol{R}_f(\boldsymbol{x}_f^{(j)} + \boldsymbol{h}) - \boldsymbol{R}_c(\boldsymbol{L}_p(\boldsymbol{x}_f^{(j)} + \boldsymbol{h})) \right\|$. This represents the deviation of the mapped coarse model (using the Taylor approximation to the mapping, i.e., a linearized mapping $\boldsymbol{L}_p : \mathbb{R}^n \mapsto \mathbb{R}^n$) from the fine model. The dark grid shows $\left\| \boldsymbol{R}_f(\boldsymbol{x}_f^{(j)} + \boldsymbol{h}) - \boldsymbol{L}_f(\boldsymbol{x}_f^{(j)} + \boldsymbol{h}) \right\|$. This is the deviation of the fine model from its classical first-order Taylor approximation $\boldsymbol{L}_f : \mathbb{R}^n \mapsto \mathbb{R}^m$. It is seen that the Taylor approximation is most accurate close to $\boldsymbol{x}_f^{(j)}$ whereas the mapped coarse model is best over a large region.

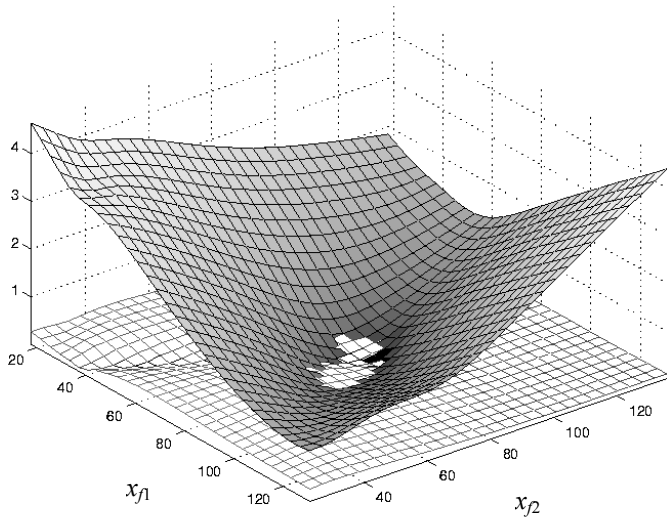

Fig. 2.10 Error plot for a two-section capacitively loaded impedance transformer [40], comparing the quasi-global effectiveness of SM (light grid) versus a classical Taylor approximation (dark grid).

2.11.2 Convergence Analysis of SM Algorithms

Convergence studies of SM algorithms originally considered hybrid algorithms where the surrogate model is a convex combination of the mapped coarse model and the linearized fine model [15], [40]. Those algorithms employ minimization subject to a trust region [43]–[44]. For example, Vicente [44] has shown convergence of a hybrid algorithm assuming the objective function to be the square of l_2 norm and Madsen *et al.* in [43] have dealt with the case of non-differentiable objective functions. In [43]–[44], the authors utilized the general methodology of trust regions, made possible by their formulation of the response vector as a convex combination of the mapped coarse model and fine model response vectors. However, the convergence theories in these papers heavily rely

on the combination with a classical Taylor based method. Therefore, classical principles of convergence proofs are feasible. Unfortunately, it is not possible to prove convergence of true SM algorithms in this way because in these algorithms we do not necessarily have local model interpolation at the current iterate. Furthermore, tentative iterates may be accepted regardless of the improvement of the objective function of the fine model.

A Convergence theory for true SM algorithms is being developed. Convergence properties of the output SM algorithm are discussed in [46]. Convergence proofs for the original SM and output SM have been proposed in [62] and [63], respectively. In these studies, convergence is demonstrated under conditions concerning SM and the engineering optimization problem itself (i.e., the fidelity of the coarse model with respect to the fine model). It follows that the SM algorithms may or may not be convergent depending on the quality of the match between the coarse and fine models. The convergence rate is also subject to the same considerations.

2.12 SURROGATE MODELING AND SPACE MAPPING

Dennis *et al*. in 1999 [64] developed a rigorous optimization framework using "surrogates" to apply to engineering design problems in which the original objective function is so expensive that traditional optimization techniques become impractical. This research is driven by the design of a low-vibration helicopter

rotor blade from Boeing [64]. The evaluation of the objective function requires running expensive analysis code(s).

Dennis defines the surrogate as a relatively inexpensive approximation of the expensive function f [65]. Dennis uses the SM terminology "coarse" and "fine" to denote the inexpensive and the expensive models, respectively. Dennis observes that the coarse model might act as a surrogate, but it may also be a step in building a surrogate. Dennis proposes the straw man surrogate (SMS) approach within the surrogate management framework (SMF) for solving the original design problem. The SMS involves three steps [66].

1. Choose the surrogate based on either a simplified physical model of f or approximation of f obtained by evaluating f at selected design sites and interpolating the function values.
2. Solve the surrogate optimization problem to obtain tentative designs.
3. Compute f at the tentative new designs to determine if any improvement has been made over the pervious design sites.

Dennis suggests the following strategy to construct the surrogate [65].

1. Choose the fine model data sites by using: statistical approaches based on the underlying functional forms and domain of interest, by judiciously scattering the points to fill the space or by enforcing poisedness conditions on the geometry of the points.
2. Surfaces that directly approximate the fine model and act as an autonomous surrogate could be either: some polynomial models and

response surfaces using experimental designs, kriging, ANN, least degree polynomial using space filling design, or Hermite surfaces using data on the fine model and its gradient.

3. Surfaces that are designed to correct the coarse model and combined with the coarse model to act as a surrogate.
    - The "difference" between the fine and coarse surfaces (responses) is "added" to the coarse model to construct the surrogate (output SM).
    - The "quotient" of the fine and coarse surfaces is "multiplied" to the coarse model to construct a surrogate.
    - SM surface from the fine model parameters to the coarse model parameters. The surrogate is defined by the coarse model applied to the image of the fine model parameters under the SM surface (the regular input-based SM approach).

2.13 IMPLEMENTATION AND APPLICATIONS

2.13.1 RF and Microwave Implementation

The required interaction between coarse model, fine model and optimization tools makes SM difficult to automate within existing simulators. A set of design or preassigned parameters and frequencies have to be sent to the different simulators and corresponding responses retrieved. Software packages such as OSA90 or Matlab can provide coarse model analyses as well as

optimization tools. Empipe [54] and Momentum driver [36] have been designed to drive and communicate with Sonnet's ***em*** [52] and Agilent Momentum [57] as fine models, respectively. Aggressive SM optimization of 3D structures [7] has been automated using a two-level Datapipe [53] architecture of OSA90. The Datapipe technique allows the algorithm to carry out nested optimization loops in two separate processes while maintaining a functional link between their results (e.g., the next increment to $\boldsymbol{x}_f$ is a function of the result of parameter extraction).

Agilent ADS circuit models can be used as coarse models. ADS has a suite of built-in optimization tools. The ADS component *S*-parameter file enables *S*-parameters to be imported in Touchstone file format from different EM simulators (fine model) such as Sonnet's ***em*** and Agilent Momentum. Imported *S*-parameters can be matched with the ADS circuit model (coarse model) responses. This PE procedure can be done simply by proper setup of the ADS optimization components (optimization algorithm and goals). These major steps of SM are friendly for engineers to apply.

2.13.2 Major Recent Contributions to Space Mapping

Leary *et al.* apply the SM technique in civil engineering structural design [67]. Jansson *et al.* [68] and Redhe *et al.* [69] apply the SM technique and surrogate models together with response surfaces in structural optimization and vehicle crashworthiness problems. Devabhaktuni *et al.* [70] propose a technique for generating microwave neural models of high accuracy using less accurate

data. The proposed Knowledge-based Automatic Model Generation (KAMG) technique integrates automatic model generation, knowledge neural networks and SM. Swanson and Wenzel [71] introduce a design approach based on the SM concept and commercial FEM solvers to Combline-type microwave filters which have found extensive applications as a result of their compact size, low cost, wide tuning range and high performance. Harscher *et al*. [72] propose a technique combines EM simulations with a minimum prototype filter network (surrogate). They execute optimization in the surrogate model space with n+1 EM simulations (in the best case), where n is the number of geometrical parameters. Draxler [73] introduces a methodology for CAD of integrated passive elements on Printed Circuit Board (PCB) incorporating Surface Mount Technology (SMT). The proposed methodology uses the SM concept to exploit the benefits of both domains. Ye and Mansour [74] apply SM steps to reduce the simulation overhead required in microstrip filter design. They use a coarse model of cascaded microstrip circuit sections simulated individually by their EM simulator. Snel [75] proposed the SM technique in RF filter design for power amplifier circuits. He suggests building a library of fast, space-mapped RF filter components used in the design of ceramic multilayer filters. Pavio *et al.* [76] apply typical SM techniques (with unity mapping, $\boldsymbol{B} = \boldsymbol{I}$) in optimization of high-density multilayer LTCC RF and microwave circuits. Lobeek [77] demonstrates the design of a DCS/PCS output match of a cellular power amplifier using SM. Lobeek also applies the SM model to monitor the statistical behavior of the

design with respect to parameter values. Safavi-Naeini *et al.* [78] consider a 3-level design methodology for complex RF/microwave structure using an SM concept. Pelz [79] applies SM in realization of narrowband coupled resonator filter structures. A realization of such a filter involves the determination of dimensions of the apertures between the resonators. Wu *et al.* [80], [81] apply the aggressive SM approach to LTCC RF passive circuit design. Steyn *et al.* [82] consider the design of irises in multi-mode coupled cavity filters. They combine a reduced generalized scattering matrix with aggressive SM. Soto *et al.* [83], [84] apply the aggressive SM procedure to build a fully automated design of inductively coupled rectangular waveguide filters. The magnetic equivalent circuit (MEC) method and the FEM have been widely used for simulation of EM systems. Choi *et al.* [85] utilize SM to design magnetic systems. Ismail *et. al* [86] exploit SM-optimization in the design of dielectric-resonator filters and multiplexers. Ismail *et al.* also [87] exploit the multiple SM for RF T-switch design. Zhang *et al*. [88] introduce a new Neuro-SM approach for nonlinear device modeling and large signal circuit simulation. Feng *et al.* [89] employ the ASM technique for the design of antireflection coatings for photonic devices, such as the semiconductor optical amplifiers. Feng *et al.* also [90] utilize a generalized SM for modeling of photonic devices such as an optical waveguide facet. Gentili *et al.* [91] utilize SM for the design of microwave comb filters. Rayas-Sánchez *et al.* [92] introduce an inverse SM optimization algorithm for

linear and non-linear microwave circuit design in the frequency and/or transient-time domains.

2.14 CONCLUDING REMARKS

The SM technique and the SM-oriented surrogate (modeling) concept and their applications in engineering design optimization are reviewed. Proposed approaches to SM-based optimization include the original SM algorithm, the Broyden-based aggressive space mapping, trust region aggressive space mapping, hybrid aggressive space mapping, neural space mapping and implicit space mapping. Parameter extraction is an essential subproblem of any SM optimization algorithm. It is used to align the surrogate with the fine model at each iteration. A mathematical motivation and convergence analysis for the SM algorithms are briefly discussed. Interesting SM and surrogate applications are reviewed. They indicate that exploitation of properly managed "space mapped" surrogates promises significant efficiency in all branches of engineering design.

REFERENCES

[1] M.B. Steer, J.W. Bandler and C.M. Snowden, "Computer-aided design of RF and microwave circuits and systems," *IEEE Trans. Microwave Theory Tech.,* vol. 50, pp. 996–1005, Mar. 2002.

[2] J.W. Bandler and S.H. Chen, "Circuit optimization: the state of the art," *IEEE Trans. Microwave Theory Tech.*, vol. 36, pp. 424–443, Feb. 1988.

[3] J.W. Bandler, W. Kellermann and K. Madsen, "A superlinearly convergent minimax algorithm for microwave circuit design," *IEEE Trans. Microwave Theory Tech.,* vol. MTT-33, pp. 1519–1530, Dec. 1985.

[4] J.W. Bandler, R.M. Biernacki, S.H. Chen, P.A. Grobelny and R.H. Hemmers, "Space mapping technique for electromagnetic optimization," *IEEE Trans. Microwave Theory Tech.*, vol. 42, pp. 2536–2544, Dec. 1994.

[5] J.W. Bandler, R.M. Biernacki, S.H. Chen, R.H. Hemmers and K. Madsen, "Electromagnetic optimization exploiting aggressive space mapping," *IEEE Trans. Microwave Theory Tech*., vol. 43, pp. 2874–2882, Dec. 1995.

[6] J.W. Bandler, Q. Cheng, S.A. Dakroury, A.S. Mohamed, M.H. Bakr, K. Madsen and J. Søndergaard, "Space mapping: the state of the art," *IEEE Trans. Microwave Theory Tech.*, vol. 52 pp. 337–361, Jan. 2004.

[7] J.W. Bandler, R.M. Biernacki and S.H. Chen, "Fully automated space mapping optimization of 3D structures," in *IEEE MTT-S Int. Microwave Symp. Dig.*, San Francisco, CA, 1996, pp. 753–756.

[8] J.W. Bandler, R.M. Biernacki, S.H. Chen and D. Omeragic, "Space mapping optimization of waveguide filters using finite element and mode-matching electromagnetic simulators," *Int. J. RF and Microwave CAE*, vol. 9, pp. 54–70, 1999.

[9] J.W. Bandler, R.M. Biernacki, S.H. Chen and Y.F. Huang, "Design optimization of interdigital filters using aggressive space mapping and decomposition," *IEEE Trans. Microwave Theory Tech.*, vol. 45, pp. 761–769, May 1997.

[10] M.H. Bakr, J.W. Bandler and N. Georgieva, "An aggressive approach to parameter extraction," *IEEE Trans. Microwave Theory Tech.*, vol. 47, pp. 2428–2439, Dec. 1999.

[11] J.W. Bandler, A.S. Mohamed, M.H. Bakr, K. Madsen and J. Søndergaard, "EM-based optimization exploiting partial space mapping and exact sensitivities," *IEEE Trans. Microwave Theory Tech.*, vol. 50. pp. 2741–2750, Dec. 2002.

[12] M.H. Bakr, J.W. Bandler, R.M. Biernacki, S.H. Chen and K. Madsen, "A trust region aggressive space mapping algorithm for EM optimization," *IEEE Trans. Microwave Theory Tech.*, vol. 46, pp. 2412–2425, Dec. 1998.

[13] N. Alexandrov, J.E. Dennis, Jr., R.M. Lewis and V. Torczon, "A trust region framework for managing the use of approximation models in optimization," *Structural Optimization*, vol. 15, pp. 16–23, 1998.

[14] M.H. Bakr, J.W. Bandler, N.K. Georgieva and K. Madsen, "A hybrid aggressive space-mapping algorithm for EM optimization," *IEEE Trans. Microwave Theory Tech*., vol. 47, pp. 2440–2449, Dec. 1999.

[15] M.H. Bakr, J.W. Bandler, K. Madsen, J.E. Rayas-Sánchez and J. Søndergaard, "Space mapping optimization of microwave circuits exploiting surrogate models," *IEEE Trans. Microwave Theory Tech*., vol. 48, pp. 2297–2306, Dec. 2000.

[16] J.W. Bandler, M.A. Ismail, J.E. Rayas-Sánchez and Q.J. Zhang, "Neuromodeling of microwave circuits exploiting space mapping technology," *IEEE Trans. Microwave Theory Tech.*, vol. 47, pp. 2417–2427, Dec. 1999.

[17] M.H. Bakr, J.W. Bandler, M.A. Ismail, J.E. Rayas-Sánchez and Q.J. Zhang, "Neural space-mapping optimization for EM-based design," *IEEE Trans. Microwave Theory Tech*., vol. 48, pp. 2307–2315, Dec. 2000.

[18] J.W. Bandler, M.A. Ismail, J.E. Rayas-Sánchez and Q.J. Zhang, "Neural inverse space mapping (NISM) optimization for EM-based microwave design," *Int. J. RF and Microwave CAE*, vol. 13, pp. 136–147, 2003.

[19] J.E. Rayas-Sánchez, "EM-Based optimization of microwave circuits using artificial neural networks: the state-of-the-art," *IEEE Trans. Microwave Theory Tech.*, vol. 52, pp. 420–435, Jan. 2004.

[20] M.H. Bakr, J.W. Bandler, Q.S. Cheng, M.A. Ismail and J.E. Rayas-Sánchez, "SMX–A novel object-oriented optimization system," in *IEEE MTT-S Int. Microwave Symp. Dig.*, Phoenix, AZ, 2001, pp. 2083–2086.

[21] J.W. Bandler, Q.S. Cheng, D.M. Hailu, and N.K. Nikolova, "A space-mapping design framework," *IEEE Trans. Microwave Theory and Tech.*, vol. 52, pp. 2601–2610, Nov. 2004.

[22] J.W. Bandler, N. Georgieva, M.A. Ismail, J.E. Rayas-Sánchez and Q. J. Zhang, "A generalized space mapping tableau approach to device modeling," *IEEE Trans. Microwave Theory Tech*., vol. 49, pp. 67–79, Jan. 2001.

[23] M.H. Bakr, J.W. Bandler and N. Georgieva, "Modeling of microwave circuits exploiting space derivative mapping," in *IEEE MTT-S Int. Microwave Symp. Dig.*, Anaheim, CA, 1999, pp. 715–718.

[24] S. Koziel, J.W. Bandler, A.S. Mohamed and K. Madsen, "Enhanced surrogate models for statistical design exploiting space mapping technology," in *IEEE MTT-S Int. Microwave Symp. Dig.,* Long Beach, CA, 2005, (accepted).

[25] J.W. Bandler, Q.S. Cheng and S. Koziel, "Implementable space mapping approach to enhancement of microwave device models," in *IEEE MTT-S Int. Microwave Symp. Dig.,* Long Beach, CA, 2005, (accepted).

[26] M.H. Bakr, J.W. Bandler, K. Madsen and J. Søndergaard, "Review of the space mapping approach to engineering optimization and modeling," *Optimization and Engineering*, vol. 1, pp. 241–276, 2000.

[27] J.W. Bandler, Q.S. Cheng, N.K. Nikolova and M.A. Ismail, "Implicit space mapping optimization exploiting preassigned parameters," *IEEE Trans. Microwave Theory Tech.*, vol. 52, pp. 378–385, Jan. 2004.

[28] J.W. Bandler, M.A. Ismail and J.E. Rayas-Sánchez, "Expanded space mapping EM-based design framework exploiting preassigned parameters," *IEEE Trans. Circuits Syst.—I*, vol. 49, pp. 1833–1838, Dec. 2002.

[29] J.W. Bandler, Q.S. Cheng, D. Gebre-Mariam, K. Madsen, F. Pedersen and J. Søndergaard, "EM-based surrogate modeling and design exploiting implicit, frequency and output space mappings," in *IEEE MTT-S Int. Microwave Symp. Dig.,* Philadelphia, PA, 2003, pp. 1003–1006.

[30] J.W. Bandler, D.M. Hailu, K. Madsen, and F. Pedersen, "A space-mapping interpolating surrogate algorithm for highly optimized EM-based design of microwave devices," *IEEE Trans. Microwave Theory and Tech.*, vol. 52, pp. 2593–2600, Nov. 2004.

[31] Q.J. Zhang and K.C. Gupta, *Neural Networks for RF and Microwave Design*. Norwood, MA: Artech House Publishers, 2000, Chapter 9.

[32] J.-S. Hong and M.J. Lancaster, *Microstrip Filters for RF/Microwave Applications*. New York, NY: Wiley, 2001, pp. 295–299.

[33] A.R. Conn, N.I.M. Gould and P.L. Toint, *Trust-Region Methods*. Philadelphia, PA: SIAM and MPS, 2000, pp. 11.

[34] M.H. Bakr, *Advances in Space Mapping Optimization of Microwave Circuits*, Ph.D. Thesis, Department of Electrical and Computer Engineering, McMaster University, Hamilton, ON, Canada, 2000.

[35] J.E. Rayas-Sánchez, *Neural Space Mapping Methods for Modeling and Design of Microwave Circuits*, Ph.D. Thesis, Department of Electrical and Computer Engineering, McMaster University, Hamilton, ON, Canada, 2001.

[36] M.A. Ismail, *Space Mapping Framework for Modeling and Design of Microwave Circuits*, Ph.D. Thesis, Department of Electrical and Computer Engineering, McMaster University, Hamilton, ON, Canada, 2001.

[37] Q. Cheng, *Advances in Space Mapping Technology Exploiting Implicit Space Mapping and Output Space Mapping*, Ph.D. Thesis, Department of Electrical and Computer Engineering, McMaster University, Hamilton, ON, Canada, 2004.

[38] *Workshop on Microwave Component Design Using Space Mapping Methodologies, IEEE MTT-S Int. Microwave Symp*., Seattle, WA, 2002.

[39] J. Søndergaard, *Non-linear Optimization Using Space Mapping*, Masters Thesis, Informatics and Mathematical Modelling (IMM), Technical University of Denmark (DTU), Lyngby, Denmark, 1999.

[40] M.H. Bakr, J.W. Bandler, K. Madsen and J. Søndergaard, "An introduction to the space mapping technique," *Optimization and Engineering*, vol. 2, pp. 369–384, 2001.

[41] J. Søndergaard, *Optimization Using Surrogate Models—by the Space Mapping Technique*, Ph.D. Thesis, Informatics and Mathematical Modelling (IMM), Technical University of Denmark (DTU), Lyngby, Denmark, 2003.

[42] F. Pedersen, *Advances on the Space Mapping Optimization Method*, Masters Thesis, Informatics and Mathematical Modelling (IMM), Technical University of Denmark (DTU), Lyngby, Denmark, 2001.

[43] K. Madsen and J. Søndergaard, "Convergence of hybrid space mapping algorithms," *Optimization and Engineering*, vol. 5, pp. 145–156, 2004.

[44] L.N. Vicente, "Space mapping: models, sensitivities, and trust-regions methods," *Optimization and Engineering*, vol. 4, pp. 159–175, 2003.

[45] M. Hintermüller and L.N. Vicente, "Space mapping for optimal control of partial differential equations," to appear in SIAM Journal on Optimization, 2005.

[46] S. Koziel, J.W. Bandler and K. Madsen, "Towards a rigorous formulation of the space mapping technique for engineering design," *Proc. Int. Symp. Circuits Syst., ISCAS*, 2005, pp. 5605–5608.

[47] *First International Workshop on Surrogate Modeling and Space Mapping for Engineering Optimization*, Informatics and Mathematical Modeling (IMM), Technical University of Denmark (DTU), Lyngby, Denmark, 2000, http://www.imm.dtu.dk/~km/smsmeo/.

[48] *Space Mapping: A Knowledge-Based Engineering Modeling and Optimization Methodology Exploiting Surrogates, Minisymposia, SIAM Conference on Optimization*, Stockholm, Sweden, May 2005.

[49] C.G. Broyden, "A class of methods for solving nonlinear simultaneous equations," *Math. Comp.,* vol. 19, pp. 577–593, 1965.

[50] G. L. Matthaei, "Interdigital band-pass filters," *IEEE Trans. Microwave Theory Tech.,* vol. MTT-10, pp. 479–491, Nov. 1962.

[51] R.J. Wenzel, "Exact theory of interdigital band–pass filters and related coupled structures," *IEEE Trans. Microwave Theory Tech.,* vol. MTT-13, pp. 559–575, Sep. 1965.

[52] ***em***, Sonnet Software, Inc. 100 Elwood Davis Road, North Syracuse, NY 13212, USA.

[53] OSA90/hope Version 4.0, formerly Optimization Systems Associates Inc., P.O. Box 8083, Dundas, Ontario, Canada L9H 5E7, 1997, now Agilent Technologies, 1400 Fountaingrove Parkway, Santa Rosa, CA 95403–1799. USA.

[54] Empipe Version 4.0, formerly Optimization Systems Associates Inc., P.O. Box 8083, Dundas, Ontario, Canada L9H 5E7, 1997, now Agilent Technologies, 1400 Fountaingrove Parkway, Santa Rosa, CA 95403–1799, USA.

[55] J.J. Moré and D.C. Sorenson, "Computing a trust region step," *SIAM J. Sci. Stat. Comp*., vol. 4, pp. 553–572, 1983.

[56] Agilent ADS, Agilent Technologies, 1400 Fountaingrove Parkway, Santa Rosa, CA 95403–1799, USA.

[57] Agilent Momentum, Agilent Technologies, 1400 Fountaingrove Parkway, Santa Rosa, CA 95403-1799, USA.

[58] J.W. Bandler, M.A. Ismail and J.E. Rayas-Sánchez, "Broadband physics-based modeling of microwave passive devices through frequency mapping," *Int. J. RF and Microwave CAE*, vol. 11, pp. 156–170, 2001.

[59] J.W. Bandler, R.M. Biernacki, S.H. Chen and Q.H. Wang, "Multiple space mapping EM optimization of signal integrity in high-speed digital circuits," *Proc. 5th Int. Workshop on Integrated Nonlinear Microwave and Millimeterwave Circuits*, Duisburg, Germany, 1998, pp. 138–140.

[60] J.W. Bandler, S.H. Chen, R.M. Biernacki, L. Gao, K. Madsen and H. Yu, "Huber optimization of circuits: a robust approach," *IEEE Trans. Microwave Theory Tech.*, vol. 41, pp. 2279–2287, Dec. 1993.

[61] J.W. Bandler, J.E. Rayas-Sánchez and Q.J. Zhang, "Yield-driven electromagnetic optimization via space mapping-based neuromodels," *Int. J. RF and Microwave CAE*, vol. 12, pp. 79–89, 2002.

[62] S. Koziel, J.W. Bandler and K. Madsen, "On the convergence of a space mapping optimization algorithm," *SIAM Journal on Optimization*, (submitted).

[63] S. Koziel, J.W. Bandler and K. Madsen, "An output space mapping framework for engineering optimization," *Math. Programming*, (submitted).

[64] A.J. Booker, J.E. Dennis, Jr., P.D. Frank, D.B. Serafini, V. Torczon and M.W. Trosset, "A rigorous framework for optimization of expensive functions by surrogates," *Structural Optimization*, vol.17, pp.1–13, 1999.

[65] J.E. Dennis, Jr., "A summary of the Danish technical university November 2000 workshop," Dept. Computational and Applied Mathematics, Rice University, Houston, Texas, 77005-1892, USA.

[66] J.E. Dennis, Jr., "Optimization using surrogates for engineering design," *IMA short course: Industrial Strength Optimization*, Institute for Mathematics and its Applications (IMA), University of Minnesota, Minneapolis, MN, Jan. 2003.

[67] S.J. Leary, A. Bhaskar and A.J. Keane, "A constraint mapping approach to the structural optimization of an expensive model using surrogates," *Optimization and Engineering*, vol. 2, pp. 385–398, 2001.

[68] T. Jansson, L. Nilsson and M. Redhe, "Using surrogate models and response surfaces in structural optimization—with application to crashworthiness design and sheet metal forming," *Struct. Multidis. Optim.*, vol. 25, pp 129–140, 2003.

[69] M. Redhe and L. Nilsson, "Optimization of the new Saab 9-3 exposed to impact load using a space mapping technique," *Struct. Multidis. Optim.*, vol. 27, pp 411–420, 2004.

[70] V. Devabhaktuni, B. Chattaraj, M.C.E. Yagoub and Q.J. Zhang, "Advanced microwave modeling framework exploiting automatic model generation, knowledge neural networks and space mapping," *IEEE Trans. Microwave Theory Tech.*, vol. 51, pp. 1822–1833, July 2003.

[71] D. G. Swanson, Jr., and R. J. Wenzel, "Fast analysis and optimization of combline filters using FEM," in *IEEE MTT-S Int. Microwave Symp. Dig.*, Phoenix, AZ, 2001, pp. 1159–1162.

[72] P. Harscher, E. Ofli, R. Vahldieck and S. Amari, "EM-simulator based parameter extraction and optimization technique for microwave and millimeter wave filters," in *IEEE MTT-S Int. Microwave Symp. Dig.*, Seattle, WA, 2002, pp. 1113–1116.

[73] P. Draxler, "CAD of integrated passives on printed circuit boards through utilization of multiple material domains," in *IEEE MTT-S Int. Microwave Symp. Dig.*, Seattle, WA, 2002, pp. 2097–2100.

[74] S. Ye and R.R. Mansour, "An innovative CAD technique for microstrip filter design," *IEEE Trans. Microwave Theory Tech.*, vol. 45, pp. 780–786, May 1997.

[75] J. Snel, "Space mapping models for RF components," *Workshop on Statistical Design and Modeling Techniques For Microwave CAD*, *IEEE MTT-S Int. Microwave Symp. Dig.,* Phoenix, AZ, 2001.

[76] A.M. Pavio, J. Estes and L. Zhao, "The optimization of complex multi-layer microwave circuits using companion models and space mapping techniques," *Workshop on Microwave Component Design Using Space Mapping Methodologies*, *IEEE MTT-S Int. Microwave Symp. Dig.,* Seattle, WA, 2002.

[77] J.-W. Lobeek, "Space mapping in the design of cellular PA output matching circuits," *Workshop on Microwave Component Design Using Space Mapping Methodologies*, *IEEE MTT-S Int. Microwave Symp. Dig.*, Seattle, WA, 2002.

[78] S. Safavi-Naeini, S.K. Chaudhuri, N. Damavandi and A. Borji, "A multi-level design optimization strategy for complex RF/microwave structures," *Workshop on Microwave Component Design Using Space Mapping Methodologies*, *IEEE MTT-S Int. Microwave Symp. Dig.,* Seattle, WA, 2002.

[79] D. Pelz, "Coupled resonator filter realization by 3D-EM analysis and space mapping," *Workshop on Microwave Component Design Using Space Mapping Methodologies*, *IEEE MTT-S Int. Microwave Symp. Dig.,* Seattle, WA, 2002.

[80] K.-L. Wu, R. Zhang, M. Ehlert, and D.-G. Fang, "An explicit knowledge-embedded space mapping technique and its application to optimization of LTCC RF passive circuits," *IEEE Components and Packaging Technologies*, vol. 26, pp. 399–406, June 2003.

[81] K.-L. Wu, Y.-J. Zhao, J. Wang, and M.K.K. Cheng, "An effective dynamic coarse model for optimization design of LTCC RF circuits with aggressive space mapping," *IEEE Trans. Microwave Theory Tech.*, vol. 52, pp. 393–402, Jan. 2004.

[82] W. Steyn, R. Lehmensiek and P. Meyer, "Integrated CAD procedure for IRIS design in a multi-mode waveguide environment," in *IEEE MTT-S Int. Microwave Symp. Dig.*, Phoenix, AZ, 2001, pp. 1163–1166.

[83] J.V. Morro Ros, P. Soto Pacheco, H. Esteban Gonzalez, V.E. Boria Esbert, C. Bachiller Martin, M. Taroncher Calduch, S. Cogollos Borras and B. Gimeno Martinez, "Fast automated design of waveguide filters using aggressive space mapping with a new segmentation strategy and a hybrid optimization algorithm," *IEEE Trans. Microwave Theory Tech.*, vol. 53, pp.1130–1142, Apr. 2005.

[84] J.V. Morro, H. Esteban, P. Soto, V.E. Boria, C. Bachiller, S. Cogollos and B. Gimeno, "Automated design of waveguide filters using aggressive space mapping with a segmentation strategy and hybrid optimization techniques," in *IEEE MTT-S Int. Microwave Symp. Dig.*, Philadelphia, PA, 2003, pp. 1215–1218.

[85] H.-S. Choi, D.H. Kim, I.H. Park and S.Y. Hahn, "A new design technique of magnetic systems using space mapping algorithm," *IEEE Trans. Magnetics*, vol. 37, pp. 3627–3630, Sep. 2001.

[86] M.A. Ismail, D. Smith, A. Panariello, Y. Wang and M. Yu, "EM-based design of large-scale dielectric-resonator filters and multiplexers by space mapping," *IEEE Trans. Microwave Theory Tech.*, vol. 52, pp. 386–392, Jan. 2004.

[87] M. A. Ismail, K. G. Engel and M. Yu, "Multiple space mapping for RF T-switch design," in *IEEE MTT-S Int. Microwave Symp. Dig.*, Fort Worth, TX, 2004, pp. 1569–1572.

[88] L. Zhang, J.J. Xu, M.C.E. Yagoub, R.T. Ding and Q.J. Zhang, "Neuro-space mapping technique for nonlinear device modeling and large signal simulation," in *IEEE MTT-S Int. Microwave Symp. Dig.*, Philadelphia, PA, 2003, pp. 173–176.

[89] N.-N. Feng, G.-R. Zhou, and W.-P. Huang, "Space mapping technique for design optimization of antireflection coatings in photonic devices," *J. Lightwave Technol.*, vol. 21, pp. 281–285, Jan. 2003.

[90] N.-N. Feng and W.-P. Huang, "Modeling and simulation of photonic devices by generalized space mapping technique," *J. Lightwave Technol.*, vol. 21, pp. 1562–1567, June 2003.

[91] G. Gentili, G. Macchiarella and M. Politi, "A space-mapping technique for the design of comb filters," *33th European Microwave Conference*, Munich, 2003, pp. 171–173.

[92] J. E. Rayas-Sánchez, F. Lara-Rojo and E. Martínez-Guerrero, "A linear inverse space mapping algorithm for microwave design in the frequency and transient domains," in *IEEE MTT-S Int. Microwave Symp. Dig.*, Fort Worth, TX, 2004, pp. 1847–1850.

CHAPTER 3

EM-BASED OPTIMIZATION EXPLOITING PARTIAL SPACE MAPPING AND EXACT SENSITIVITIES

3.1 INTRODUCTION

Using an EM simulator ("fine" model) inside an optimization loop for the design process of microwave circuits can be prohibitive. Designers can overcome this problem by simplifying the circuit through circuit theory or by using the EM simulator with a coarser mesh. The SM approach [1]–[2] involves a suitable calibration of a physically–based "coarse" surrogate by a fine model. The fine model may be time intensive, field theoretic and accurate, while the surrogate is a faster, circuit based but less accurate representation. SM introduces an efficient way to describe the relationship between the fine model and its surrogate. It makes effective use of the fast computation ability of the surrogate on the one hand and the accuracy of the fine model on the other.

SM optimization involves the following steps. The "surrogate" is optimized to satisfy design specifications [3], thus providing the target response. A mapping is proposed between the parameter spaces of the fine model and its surrogate using a Parameter Extraction (PE) process. Then, an inverse mapping estimates the fine model parameters corresponding to the (target) optimal surrogate parameters.

We present new techniques to exploit exact sensitivities in EM–based circuit design in the context of SM technology [4]. If the EM simulator is capable of providing gradient information, these gradients can be exploited to enhance a coarse surrogate. New approaches for utilizing derivatives in the parameter extraction process and mapping update are presented [4].

We introduce also a new SM approach exploiting the concept of partial SM (PSM) [4]. Partial mappings were previously suggested in the context of neural SM [5]. Here, an efficient procedure exploiting a PSM concept is proposed. Several approaches for utilizing response sensitivities and PSM are suggested.

Exact sensitivity formulations have been developed for nonlinear, harmonic balance analyses [6] as well as implementable approximations such as the feasible adjoint sensitivity technique (FAST) [7]. In the 90s Alessandri *et al.* spurred the application of the adjoint network method using a mode matching orientation [8]. Feasible adjoint-based sensitivity implementations are proposed with the method of moments (MoM) in [9]. These techniques can be used for

efficient gradient-based optimization. Our proposed CAD approach for full-wave EM-based optimization complements these efforts of gradient estimation using EM simulations. An excellent review of adjoint techniques for sensitivity analysis in RF and microwave circuits CAD is introduced in [10].

3.2 BASIC CONCEPTS

In this section, we review different parameter extraction approaches suggested in the SM literature [11]. We also discuss the traditional aggressive SM technique [4].

3.2.1 Parameter Extraction (PE)

PE is a crucial step in any SM algorithm. In the PE, an optimization step is performed to extract a coarse model point $\boldsymbol{x}_c$ corresponding to the fine model point $\boldsymbol{x}_f$ that yields the best match between the fine model and its surrogate. The information stored in the design responses may not be sufficient to describe the system under consideration properly. Thus, using only the design response in the PE may lead to nonuniqueness problems. Therefore, we need to obtain more information about the system and exploit it to extract the "best" coarse point and avoid nonuniqueness. For example, we may use responses such as real and imaginary parts of *S*–parameters in the PE even though we need only the magnitude of S_{11} to satisfy a certain design criterion.

3.2.1.1 Single Point PE (SPE) [1]

The traditional SPE is described by the optimization problem given in (2.11), it is repeated here for convenience. It is simple and works in many cases.

$$\boldsymbol{x}_c^{(j)} = \arg\min_{\boldsymbol{x}_c} \left\| \boldsymbol{R}_f(\boldsymbol{x}_f^{(j)}) - \boldsymbol{R}_c(\boldsymbol{x}_c) \right\| \tag{3.1}$$

3.2.1.2 Multipoint PE (MPE) [12]–[13]

The MPE approach simultaneously matches the responses at a number of corresponding points in the coarse and fine model spaces. A set $V = \left\{ \boldsymbol{x}_f^{(j+1)} \right\} \cup \left\{ \boldsymbol{x}_f^{(j+1)} + \Delta\boldsymbol{x}_f^{(i)} \,\middle|\, i = 1, 2, ..., N_p \right\}$ of fine model points is constructed by selecting N_p perturbations around $\boldsymbol{x}_f^{(j+1)}$. The corresponding $\boldsymbol{x}_c^{(j+1)}$ is found by solving

$$\boldsymbol{x}_c^{(j+1)} = \arg\min_{\boldsymbol{x}_c} \left\| \left[\boldsymbol{e}_0^T \quad \boldsymbol{e}_1^T \quad \cdots \quad \boldsymbol{e}_{N_p}^T \right]^T \right\| \tag{3.2}$$

where

$$\boldsymbol{e}_0 = \boldsymbol{R}_c(\boldsymbol{x}_c) - \boldsymbol{R}_f(\boldsymbol{x}_f^{(j+1)}) \tag{3.3}$$

and

$$\boldsymbol{e}_i = \boldsymbol{R}_c(\boldsymbol{x}_c + \Delta\boldsymbol{x}_c^{(i)}) - \boldsymbol{R}_f(\boldsymbol{x}_f^{(j+1)} + \Delta\boldsymbol{x}_f^{(i)}),\ i = 1, 2, ..., N_p \tag{3.4}$$

The perturbations $\Delta\boldsymbol{x}_c^{(i)}$ in (3.4) are related to $\Delta\boldsymbol{x}_f^{(i)}$. The basic MPE [12] assumes the relation is given by

$$\Delta\boldsymbol{x}_c^{(i)} = \Delta\boldsymbol{x}_f^{(i)},\ i = 1, 2, ..., N_p \tag{3.5}$$

This MPE approach does not provide guidelines on the selection of fine model points.

A more reliable algorithm [14] considers the relation between the perturbations to be determined through the mapping matrix $\boldsymbol{B}$. Such a relation is given by

$$\Delta \boldsymbol{x}_c^{(i)} = \boldsymbol{B}\Delta \boldsymbol{x}_f^{(i)},\ i = 1,2,...,N_p \tag{3.6}$$

The algorithm proposed in [14] also automates the selection of the set of fine model points by recursively augmenting the set V until a unique parameter extraction is achieved.

Another improvement in the selection of V is suggested by the aggressive PE algorithm [15], which aims at minimizing the number of points used in MPE. It exploits the gradients and Hessians of the coarse model responses at the extracted point $\boldsymbol{x}_c^{(j+1)}$ to construct new points to be added to V. A perturbation $\Delta \boldsymbol{x}_c^{new}$ is found by solving the eigenvalue problem

$$\left(\boldsymbol{J}_c(\boldsymbol{x}_c^{(j+1)})^T \boldsymbol{J}_c(\boldsymbol{x}_c^{(j+1)}) + \boldsymbol{I}\right)\Delta \boldsymbol{x}_c^{new} = \lambda \Delta \boldsymbol{x}_c^{new} \tag{3.7}$$

The corresponding perturbation $\Delta \boldsymbol{x}_f^{new}$ is found consistent with (3.6) and the set V is augmented by

$$\boldsymbol{x}_f^{new} = \boldsymbol{x}_f^{(j+1)} + \Delta \boldsymbol{x}_f^{new} \tag{3.8}$$

3.2.1.3 Statistical PE [13]

Bandler *et al.* [13] suggest a statistical approach to PE. The SPE process is initiated from several starting points and is declared unique if consistent extracted parameters are obtained. Otherwise, the best solution is selected.

A set of N_s starting points are randomly selected in a region $D \subset \mathbb{R}^n$ where the solution $\boldsymbol{x}_c^{(j+1)}$ is expected. For the *j*th iteration, *D* is implied by

$$x_{c,i} \in \left[x_{c,i}^* - 2\left| f_i^{(j)} \right|, x_{c,i}^* + 2\left| f_i^{(j)} \right| \right], \; i = 1, 2, ..., n \tag{3.9}$$

where $x_{c,i}$ is the *i*th component of $\boldsymbol{x}_c$ and f_i the *i*th component of $\boldsymbol{f} = \boldsymbol{x}_c - \boldsymbol{x}_c^*$.

3.2.1.4 Penalized PE [16]

Another approach is suggested in [16]. Here, the point $\boldsymbol{x}_c^{(j+1)}$ is obtained by solving the penalized SPE process

$$\boldsymbol{x}_c^{(j+1)} = \arg\min_{\boldsymbol{x}_c} \; \left\| \boldsymbol{R}_c(\boldsymbol{x}_c) - \boldsymbol{R}_f(\boldsymbol{x}_f^{(j+1)}) \right\| + w \left\| \boldsymbol{x}_c - \boldsymbol{x}_c^* \right\| \tag{3.10}$$

where *w* is a user-assigned weighting factor. If the PE problem is not unique (3.10) is favored over (3.1) as the solution is biased towards $\boldsymbol{x}_c^*$. The process is designed to push the error vector $\boldsymbol{f} = \boldsymbol{x}_c - \boldsymbol{x}_c^*$ to zero. If *w* is too large the matching between the responses is poor. On the other hand, too small a value of *w* makes the penalty term ineffective, in which case, the uniqueness of the extraction step may not be enhanced.

3.2.1.5 PE Involving Frequency Mapping

Alignment of the models might be achieved by simulating the coarse model at a transformed set of frequencies [17]. For example, an electromagnetic model of a microwave structure usually exhibits a frequency shift with respect to an idealized representation. Also, available quasi-static empirical models exhibit good accuracy over a limited range of frequencies, which can be alleviated by frequency transformation.

The PE optimization process (3.1), which extracts $\boldsymbol{x}_c$ to correspond to a given $\boldsymbol{x}_f$, may fail if the responses $\boldsymbol{R}_f$ and $\boldsymbol{R}_c$ are disjoint. But, the responses might be aligned if a frequency transformation $\omega_c = P_\omega(\omega)$ is applied, relating frequency ω to the coarse model frequency ω_c. Frequency mapping introduces new degrees of freedom [18].

A suitable mapping can be as frequency shift and scaling given by [2]

$$\omega_c = P_\omega(\omega) \triangleq \sigma\omega + \delta \tag{3.11}$$

where σ represents a scaling factor and δ is an offset (shift).

The approach can be divided into two phases [2]. In *Phase* 1, we determine σ_0 and δ_0 that align $\boldsymbol{R}_f$ and $\boldsymbol{R}_c$ in the frequency domain. This is done by finding

$$\arg\min_{\sigma_0,\delta_0} \left\| \boldsymbol{R}_c(\boldsymbol{x}_c, \sigma_0\omega_i + \delta_0)) - \boldsymbol{R}_f(\boldsymbol{x}_f) \right\|,\ i = 1,2,...,k \tag{3.12}$$

In *Phase* 2, the coarse model point $\boldsymbol{x}_c$ is extracted to match $\boldsymbol{R}_c$ with $\boldsymbol{R}_f$, starting with $\sigma = \sigma_0$ and $\delta = \delta_0$. Three algorithms [2] can implement this phase: a sequential algorithm and two exact-penalty function algorithms, one using the l_1 norm and the other is suitable for minimax optimization [2].

3.2.1.6 Other Considerations

We can broaden the scope of parameters that are varied in an effort to match the coarse (surrogate) and fine models. We already discussed the scaling factor and shift parameters in the frequency mapping. We can also consider neural weights in neural SM [5], preassigned parameters in implicit SM [19], mapping coefficients $\boldsymbol{B}$, etc., as in the generalized SM tableau approach [20] and surrogate model-based SM [18].

3.2.2 Aggressive Space Mapping Approach

The aggressive SM (ASM) was presented in Chapter 2 in the context of reviewing the SM techniques. Here we consider another approach to obtain the same result, which should add insight to the method. Aggressive SM solves the nonlinear system

$$\begin{aligned} \boldsymbol{f} &\triangleq \boldsymbol{P}(\boldsymbol{x}_f) - \boldsymbol{x}_c^* \\ &= \boldsymbol{x}_c - \boldsymbol{x}_c^* \\ &= \boldsymbol{0} \end{aligned} \tag{3.13}$$

for $\boldsymbol{x}_f$, where $\boldsymbol{P}$ is a mapping defined between the two model spaces and $\boldsymbol{x}_c$ is the corresponding point in the coarse space, $\boldsymbol{x}_c = \boldsymbol{P}(\boldsymbol{x}_f)$. First-order Taylor approximations are given by

$$\boldsymbol{P}(\boldsymbol{x}_f) \approx \boldsymbol{P}(\boldsymbol{x}_f^{(j)}) + \boldsymbol{J}_P(\boldsymbol{x}_f^{(j)})(\boldsymbol{x}_f - \boldsymbol{x}_f^{(j)}) \tag{3.14}$$

This can be described as

$$\boldsymbol{x}_c \approx \boldsymbol{x}_c^{(j)} + \boldsymbol{J}_P(\boldsymbol{x}_f^{(j)})(\boldsymbol{x}_f - \boldsymbol{x}_f^{(j)})\Big|_{\text{Through PE}} \tag{3.15}$$

where the Jacobian of $\boldsymbol{P}$ at the jth iteration is expressed by

$$\boldsymbol{J}_P(\boldsymbol{x}_f^{(j)}) = \left(\frac{\partial \boldsymbol{P}^T}{\partial \boldsymbol{x}_f}\right)^T_{\boldsymbol{x}_f = \boldsymbol{x}_f^{(j)}} \tag{3.16}$$

Equation (3.15) illustrates the nonlinearity of the mapping, where $\boldsymbol{x}_c^{(j)}$ is related to $\boldsymbol{x}_f^{(j)}$ through the PE process which is a nonlinear optimization problem. Recalling (3.14) and (3.15) we state a useful definition of the mapping Jacobian at the jth iteration

$$\boldsymbol{J}_P^{(j)} \triangleq \left(\frac{\partial (\boldsymbol{x}_c^{(j)T})}{\partial \boldsymbol{x}_f}\right)^T\Bigg|_{\text{PE}} \tag{3.17}$$

We designate an approximation to this Jacobian by the square matrix $\boldsymbol{B} \in \mathbb{R}^{n \times n}$, i.e., $\boldsymbol{B} \approx \boldsymbol{J}_P(\boldsymbol{x}_f)$.

From (3.13) and (3.15) we can formulate the system

$$(\boldsymbol{x}_c^{(j)} - \boldsymbol{x}_c^*) + \boldsymbol{B}^{(j)}(\boldsymbol{x}_f^{(j+1)} - \boldsymbol{x}_f^{(j)}) = \boldsymbol{0} \tag{3.18}$$

which can be simplified in the useful form given in (2.13), and rewritten here for relevance,

$$\boldsymbol{B}^{(j)}\boldsymbol{h}^{(j)} = -\boldsymbol{f}^{(j)} \tag{3.19}$$

Solving (3.19) for $\boldsymbol{h}^{(j)}$, the quasi-Newton step in the fine space, provides the next tentative iterate $\boldsymbol{x}_f^{(j+1)}$ given in (2.14)

3.3 SENSITIVITY-BASED APPROACH

Here, an approach exploiting response sensitivities is presented to enhance the PE performance. We also introduce the partial SM concept where a reduced set is utilized in the PE process. Mapping schemes existing in the SM literature are also discussed.

3.3.1 PE Exploiting Sensitivity

We exploit the availability of the gradients of the fine model and surrogate responses to enhance the PE process. The Jacobian of the fine model responses $\boldsymbol{J}_f$ at $\boldsymbol{x}_f$ and the corresponding Jacobian of the surrogate responses $\boldsymbol{J}_c$ at $\boldsymbol{x}_c$ can be obtained. Adjoint sensitivity analysis could be used to provide the exact derivatives, while finite differences are employed to estimate the derivatives if the exact derivatives are not available. Here, we present a new technique to formulate the PE to take into account not only the responses of the fine and its surrogate, but the corresponding gradients as well.

Through the traditional PE process as in (3.1) we can obtain the point $\boldsymbol{x}_c$ that corresponds to $\boldsymbol{x}_f$ such that

$$\boldsymbol{R}_f \approx \boldsymbol{R}_c \tag{3.20}$$

Differentiating both sides of (3.20) with respect to $\boldsymbol{x}_f$, we obtain [4]

$$\left(\frac{\partial \boldsymbol{R}_f^T}{\partial \boldsymbol{x}_f}\right)^T \approx \left(\frac{\partial \boldsymbol{R}_c^T}{\partial \boldsymbol{x}_c}\right)^T \left(\frac{\partial \boldsymbol{x}_c^T}{\partial \boldsymbol{x}_f}\right)^T \tag{3.21}$$

Using (3.17) the relation (3.21) can be simplified to [21]

$$\boldsymbol{J}_f \approx \boldsymbol{J}_c \boldsymbol{B} \tag{3.22}$$

where $\boldsymbol{J}_f$ and $\boldsymbol{J}_c \in \mathbb{R}^{m\times n}$. Relation (3.22) assumes that $\boldsymbol{J}_c$ is full rank and $m \geq n$, where m is the dimensionality of both $\boldsymbol{R}_f$ and $\boldsymbol{R}_c$. Solving (3.22) for $\boldsymbol{B}$ yields a least squares solution [21]

$$\boldsymbol{B} = (\boldsymbol{J}_c^T \boldsymbol{J}_c)^{-1} \boldsymbol{J}_c^T \boldsymbol{J}_f \tag{3.23}$$

At the jth iteration we obtain $\boldsymbol{x}_c^{(j)}$ through a Gradient Parameter Extraction (GPE) process [4]. In GPE, we match not only the responses but also the derivatives of both models through the optimization problem

$$\boldsymbol{x}_c^{(j)} = \arg\min_{\boldsymbol{x}_c} \left\| [\boldsymbol{e}_0^T \quad \lambda \boldsymbol{e}_1^T \quad \cdots \quad \lambda \boldsymbol{e}_n^T]^T \right\|, \ \lambda \geq 0 \tag{3.24}$$

where λ is a weighting factor, $\boldsymbol{E} = [\boldsymbol{e}_1\ \boldsymbol{e}_2\ \ldots\ \boldsymbol{e}_n]$ and

$$\begin{aligned} \boldsymbol{e}_0 &= \boldsymbol{R}_f(\boldsymbol{x}_f^{(j)}) - \boldsymbol{R}_c(\boldsymbol{x}_c) \\ \boldsymbol{E} &= \boldsymbol{J}_f(\boldsymbol{x}_f^{(j)}) - \boldsymbol{J}_c(\boldsymbol{x}_c)\boldsymbol{B} \end{aligned} \tag{3.25}$$

The nonuniqueness in the PE step in (3.1) may lead to divergence or oscillatory behavior. Exploiting available gradient information enhances the uniqueness of the PE process. GPE reflects the idea of Multi-Point Extraction (MPE) [12]–[14] but, permits the use of exact and implementable sensitivity techniques [6]–[10]. Finite differences can be employed to estimate derivatives if exact ones are unavailable.

3.3.2 Partial Space Mapping (PSM)

Utilizing a reduced set of the physical parameters of the coarse space might be sufficient to obtain an adequate surrogate for the fine model. A selected set of the design parameters are mapped onto the coarse space and the rest of them, $\boldsymbol{x}_f^s \subset \boldsymbol{x}_f$, are directly passed. The mapped coarse parameters are denoted by $\boldsymbol{x}_c^{PSM} \in \mathbb{R}^k$, $k \le n$, where n is the number of design parameters. PSM is illustrated in Fig. 3.1. It can be represented in the matrix form by [4]

$$\boldsymbol{x}_c = \begin{bmatrix} \boldsymbol{x}_c^{PSM} \\ \boldsymbol{x}_f^s \end{bmatrix} = \begin{bmatrix} \boldsymbol{P}_{PSM}(\boldsymbol{x}_f) \\ \boldsymbol{x}_f^s \end{bmatrix} \tag{3.26}$$

In this context (3.22) becomes

$$\boldsymbol{J}_f \approx \boldsymbol{J}_c^{PSM} \boldsymbol{B}^{PSM} \tag{3.27}$$

where $\boldsymbol{B}^{PSM} \in \mathbb{R}^{k \times n}$ and $\boldsymbol{J}_c^{PSM} \in \mathbb{R}^{m \times k}$ is the Jacobian of the coarse model at $\boldsymbol{x}_c^{PSM}$. Solving (3.27) for $\boldsymbol{B}^{PSM}$ yields the least squares solution at the jth iteration [4]

$$\boldsymbol{B}^{PSM(j)} = (\boldsymbol{J}_c^{PSM(j)T} \boldsymbol{J}_c^{PSM(j)})^{-1} \boldsymbol{J}_c^{PSM(j)T} \boldsymbol{J}_f^{(j)} \tag{3.28}$$

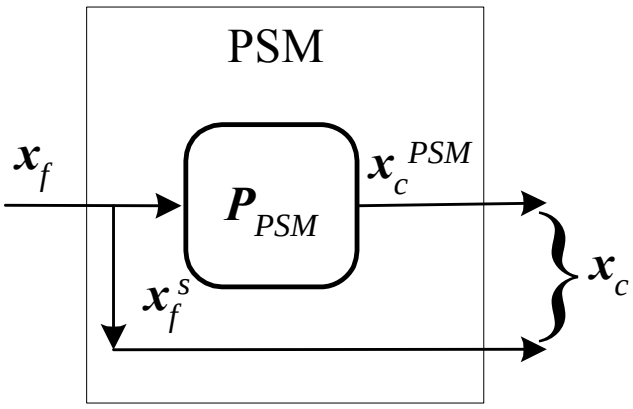

Fig. 3.1 Partial Space Mapping (PSM).

Relation (3.19) becomes underdetermined since $\boldsymbol{B}^{PSM}$ is a fat rectangular matrix, i.e., the number of columns is greater than the number of rows. The minimum norm solution for $\boldsymbol{h}^{(j)}$ is given by

$$\boldsymbol{h}^{(j)}_{\min\text{ norm}} = \boldsymbol{B}^{PSM(j)T}(\boldsymbol{B}^{PSM(j)}\boldsymbol{B}^{PSM(j)T})^{-1}(-\boldsymbol{f}^{(j)}) \tag{3.29}$$

The coarse model parameters $\boldsymbol{x}_c^{PSM}$ used in the PE can be determined by the sensitivity analysis proposed by Bandler *et al.* [22]. It chooses the parameters that the coarse model response is more sensitive to.

3.3.3 Mapping Considerations

Different mapping approaches existed in the SM literature are discussed [11]. Here, we review these updating techniques which include: unit mapping, Broyden-based updates, Jacobian-based updates [4] and constrained update.

3.3.3.1 Unit Mapping

A "steepest-descent" approach may succeed if the mapping between the two spaces is essentially represented by a shift. In this case Broyden's updating formula [23] is not utilized. We can solve (3.19) keeping the matrix $\boldsymbol{B}^{(j)}$ fixed at $\boldsymbol{B}^{(j)} = \boldsymbol{I}$. Bila *et al*. [24] and Pavio [25] utilized this special case.

3.3.3.2 Broyden-like Updates

An initial approximation to $\boldsymbol{B}$ can be taken as $\boldsymbol{B}^{(0)} = \boldsymbol{I}$, the identity matrix. $\boldsymbol{B}^{(j)}$ can be updated using Broyden's rank one formula [23]

$$\boldsymbol{B}^{(j+1)} = \boldsymbol{B}^{(j)} + \frac{\boldsymbol{f}^{(j+1)} - \boldsymbol{f}^{(j)} - \boldsymbol{B}^{(j)}\boldsymbol{h}^{(j)}}{\boldsymbol{h}^{(j)T}\boldsymbol{h}^{(j)}}\boldsymbol{h}^{(j)T} \tag{3.30}$$

When $\boldsymbol{h}^{(j)}$ is the quasi-Newton step, (3.30) can be simplified using (3.19) to

$$\boldsymbol{B}^{(j+1)} = \boldsymbol{B}^{(j)} + \frac{\boldsymbol{f}^{(j+1)}}{\boldsymbol{h}^{(j)T}\boldsymbol{h}^{(j)}}\boldsymbol{h}^{(j)T} \tag{3.31}$$

A comparison between the BFGS rank-2 updating formula versus the Broyden rank-1 formula for ASM techniques is given in Appendix A.

3.3.3.3 Jacobian Based Updates [4]

If we have exact Jacobians with respect to $\boldsymbol{x}_f$ and $\boldsymbol{x}_c$ at corresponding points we can use them to obtain $\boldsymbol{B}$ at each iteration through a least squares solution [4], [21] as given in (3.23). We can also use (3.28) to update $\boldsymbol{B}^{PSM}$.

Note that $\boldsymbol{B}$ can be fed back into the PE process and iteratively refined before making a step in the fine model space.

Hybrid schemes can be developed following the integrated gradient approximation approach to optimization [26]. One approach incorporates finite difference approximations and the Broyden formula [23]. Finite difference approximations could provide initial estimates of $\boldsymbol{J}_f$ and $\boldsymbol{J}_c$. These are then used to obtain a good approximation to $\boldsymbol{B}^{(0)}$. The Broyden formula is subsequently used to update $\boldsymbol{B}$. The same approach can be used for $\boldsymbol{B}^{PSM}$.

3.3.3.4 Constrained Update [27]

On the assumption that the fine and coarse models share the same physical background, Bakr *et al*. [27] suggested that $\boldsymbol{B}$ could be better conditioned in the PE process if it is constrained to be close to the identity matrix $\boldsymbol{I}$ by letting

$$\boldsymbol{B} = \arg\min_{\boldsymbol{B}} \left\| \left[\boldsymbol{e}_1^T \cdots \boldsymbol{e}_n^T \quad \eta\Delta\boldsymbol{b}_1^T \cdots \eta\Delta\boldsymbol{b}_n^T\right]^T \right\|_2^2 \tag{3.32}$$

where η is a user-assigned weighting factor, $\boldsymbol{e}_i$ and $\Delta\boldsymbol{b}_i$ are the ith columns of $\boldsymbol{E}$ and $\Delta\boldsymbol{B}$, respectively, defined as

$$\begin{aligned} \boldsymbol{E} &= \boldsymbol{J}_f - \boldsymbol{J}_c\boldsymbol{B} \\ \Delta\boldsymbol{B} &= \boldsymbol{B} - \boldsymbol{I} \end{aligned} \tag{3.33}$$

The analytical solution of (3.32) is given by

$$\boldsymbol{B} = (\boldsymbol{J}_c^T\boldsymbol{J}_c + \eta^2\boldsymbol{I})^{-1}(\boldsymbol{J}_c^T\boldsymbol{J}_f + \eta^2\boldsymbol{I}) \tag{3.34}$$

A mathematical proof for (3.34) is given in Appendix B.

3.3.4 Proposed Algorithms

Algorithm 1 Full Mapping/GPE/Jacobian update

Step 1 Set $j = 0$. Initialize $\boldsymbol{B} = \boldsymbol{I}$ for the PE process. Obtain the optimal coarse model design $\boldsymbol{x}_c^*$ and use it as the initial fine model point

$$\boldsymbol{x}_f^{(0)} = \boldsymbol{x}_c^* = \arg\min_{\boldsymbol{x}_c} U(\boldsymbol{R}_c(\boldsymbol{x}_c)) \tag{3.35}$$

Comment Minimax optimization is used to obtain the optimal coarse solution.

Step 2 Execute a preliminary GPE step as in (3.24).

Comment Match the responses and the corresponding gradients.

Step 3 Refine the mapping matrix $\boldsymbol{B}$ using Jacobians (3.23).

Comment A least squares solution is used to refine a square matrix $\boldsymbol{B}$ using Jacobians.

Step 4 Stop if

$$\left\| \boldsymbol{f}^{(j)} \right\| \le \varepsilon_1 \text{ or } \left\| \boldsymbol{R}_f^{(j)} - \boldsymbol{R}_c^* \right\| \le \varepsilon_2 \tag{3.36}$$

Comment Loop until the stopping conditions are satisfied.

Step 5 Solve (3.19) for $\boldsymbol{h}^{(j)}$.

Step 6 Find the next $\boldsymbol{x}_f^{(j+1)}$ using $\boldsymbol{x}_f^{(j+1)} = \boldsymbol{x}_f^{(j)} + \boldsymbol{h}^{(j)}$.

Step 7 Perform GPE as in (3.24).

Step 8 Update $\boldsymbol{B}^{(j)}$ using (3.23).

Comment A least squares solution is used to update $\boldsymbol{B}$ at each iteration exploiting Jacobians.

Step 9 Set $j = j + 1$ and go to Step 4.

Algorithm 2 Partial SM/GPE/Jacobian update

Step 1 Set $j = 0$. Initialize $\boldsymbol{B}^{PSM} = \left[\boldsymbol{I}^{PSM} \quad \boldsymbol{0} \right]$ for the PE process. Obtain the optimal coarse model design $\boldsymbol{x}_c^*$ and use it as the initial fine model point as in (3.35).

Step 2 Execute a preliminary GPE step as in (3.24).

Step 3 Refine the mapping matrix $\boldsymbol{B}^{PSM}$ using (3.28).

Comment A least squares solution is used to refine a rectangular matrix $\boldsymbol{B}^{PSM}$ using Jacobians.

Step 4 Stop if (3.36) holds.

Comment Loop until the stopping conditions are satisfied.

Step 5 Evaluate $\boldsymbol{h}^{(j)}$ using (3.29).

Comment A minimum norm solution for a quasi-Newton step $\boldsymbol{h}^{(j)}$ in the fine space is used.

Step 6 Find the next $\boldsymbol{x}_f^{(j+1)}$ using $\boldsymbol{x}_f^{(j+1)} = \boldsymbol{x}_f^{(j)} + \boldsymbol{h}^{(j)}$.

Step 7 Perform GPE as in (3.24).

Step 8 Use (3.28) to update $\boldsymbol{B}^{PSM(j)}$.

Comment A least squares solution is used to update $\boldsymbol{B}^{PSM}$ at each iteration.

Step 9 Set $j = j + 1$ and go to Step 4.

Algorithm 3 Partial SM/PE/Hybrid approach for mapping update

Step 1 Set $j = 0$. Initialize $\boldsymbol{B}^{PSM} = \left[\boldsymbol{I}^{PSM} \quad \boldsymbol{0} \right]$ for the PE process. Obtain the optimal coarse model design $\boldsymbol{x}_c^*$ and use it as the initial fine model point as in (3.35).

Step 2 Execute a preliminary traditional PE step as in (3.1).

Step 3 Refine the mapping matrix $\boldsymbol{B}^{PSM}$ using (3.28).

Comment A least squares solution is used to refine a rectangular matrix $\boldsymbol{B}^{PSM}$ using Jacobians.

Step 4 Stop if (3.36) holds.

Comment Loop until the stopping conditions are satisfied.

Step 5 Evaluate $\boldsymbol{h}^{(j)}$ using (3.29).

Step 6 Find the next $\boldsymbol{x}_f^{(j+1)}$ using $\boldsymbol{x}_f^{(j+1)} = \boldsymbol{x}_f^{(j)} + \boldsymbol{h}^{(j)}$.

Step 7 Perform traditional PE as in (3.1).

Step 8 Update $\boldsymbol{B}^{PSM(j)}$ using a Broyden formula.

Comment A hybrid approach is used to update $\boldsymbol{B}^{PSM}$.

Step 9 Set $j = j + 1$ and go to Step 4.

The output of the algorithms is the fine space mapped optimal design $\bar{\boldsymbol{x}}_f$ and the mapping matrix $\boldsymbol{B}$ (Algorithm 1) or $\boldsymbol{B}^{PSM}$ (Algorithms 2 and 3).

3.4 EXAMPLES

3.4.1 Rosenbrock Banana Problem [21], [28]

Test problems based on the classical Rosenbrock banana function are first studied. We let the original Rosenbrock function

$$R_c = 100(x_2 - x_1^2)^2 + (1 - x_1)^2 \tag{3.37}$$

be a "coarse" model. The optimal solution is $\boldsymbol{x}_c^* = \begin{bmatrix} 1.0 & 1.0 \end{bmatrix}^T$. A contour plot is shown in Fig. 3.2.

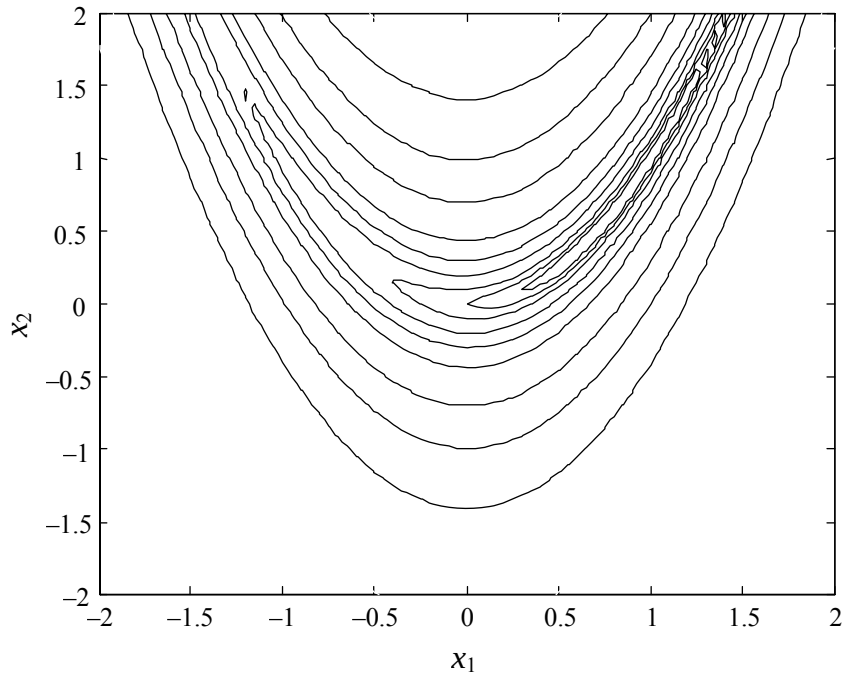

Fig. 3.2 Contour plot of the "coarse" original Rosenbrock banana function.

3.4.1.1 Shifted Rosenbrock Problem

We propose a "fine" model as a shifted Rosenbrock function

$$R_f = 100\left((x_2 + \alpha_2) - (x_1 + \alpha_1)^2\right)^2 + \left(1 - (x_1 + \alpha_1)\right)^2 \tag{3.38}$$

where

$$\boldsymbol{\alpha} = \begin{bmatrix} \alpha_1 \\ \alpha_2 \end{bmatrix} = \begin{bmatrix} -0.2 \\ 0.2 \end{bmatrix} \tag{3.39}$$

The optimal fine model solution is $\boldsymbol{x}_f^* = \boldsymbol{x}_c^* - \boldsymbol{\alpha} = \begin{bmatrix} 1.2 & 0.8 \end{bmatrix}^T$. See Fig. 3.3 for a contour plot.

We apply Algorithm 1. Exact "Jacobians" $\boldsymbol{J}_f$ and $\boldsymbol{J}_c$ are used in the GPE process and in mapping update. The algorithm converges in one iteration to the exact solution. See Table 3.1.

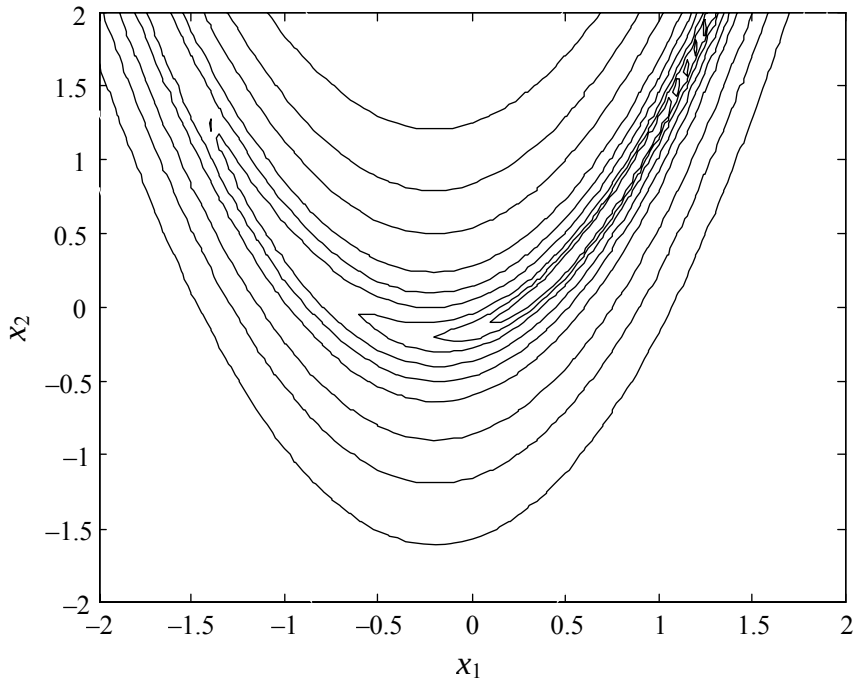

Fig. 3.3 Contour plot of the "fine" shifted Rosenbrock banana function.

TABLE 3.1

"SHIFTED" ROSENBROCK BANANA PROBLEM

j	$\boldsymbol{x}_c^{(j)}$	$\boldsymbol{f}^{(j)}$	$\boldsymbol{B}^{(j)}$	$\boldsymbol{h}^{(j)}$	$\boldsymbol{x}_f^{(j)}$	$R_f^{(j)}$
0	$\begin{bmatrix}1.0\\1.0\end{bmatrix}$	-----	------	------	$\begin{bmatrix}1.0\\1.0\end{bmatrix}$	31.4
1	$\begin{bmatrix}0.8\\1.2\end{bmatrix}$	$\begin{bmatrix}-0.2\\0.2\end{bmatrix}$	$\begin{bmatrix}1.0 & 0.0\\0.0 & 1.0\end{bmatrix}$	$\begin{bmatrix}0.2\\-0.2\end{bmatrix}$	$\begin{bmatrix}1.2\\0.8\end{bmatrix}$	0
	$\begin{bmatrix}1.0\\1.0\end{bmatrix}$	$\begin{bmatrix}0\\0\end{bmatrix}$				

3.4.1.2 Transformed Rosenbrock Problem

A "fine" model is described by the transformed Rosenbrock function

$$R_f = 100(u_2 - u_1^2)^2 + (1 - u_1)^2 \tag{3.40}$$

Where

$$\boldsymbol{u} = \begin{bmatrix} 1.1 & -0.2 \\ 0.2 & 0.9 \end{bmatrix} \boldsymbol{x} + \begin{bmatrix} -0.3 \\ 0.3 \end{bmatrix} \tag{3.41}$$

The exact solution evaluated by the inverse transformation is $\boldsymbol{x}_f^* = \begin{bmatrix} 1.2718447 & 0.4951456 \end{bmatrix}^T$ to seven decimals. A contour plot is shown in Fig. 3.4.

A simple SPE process involving only function values produces a nonunique solution (Fig. 3.5). The enhanced PE process such as GPE or MPE leads to improved results. The first and last GPE iterations are shown in Fig. 3.6 and Fig. 3.7, respectively.

Applying Algorithm 1, we get a solution, to a very high accuracy, in six iterations. The corresponding function value is 9×10^{-29}. At the final GPE step, the contour plot is similar to that of the coarse model (See Fig. 3.7). The SM optimization results for $\boldsymbol{R}_f$ and $\|\boldsymbol{f}\|$ are shown in Fig. 3.8 and Fig. 3.9, respectively. See Table 3.2 for details.

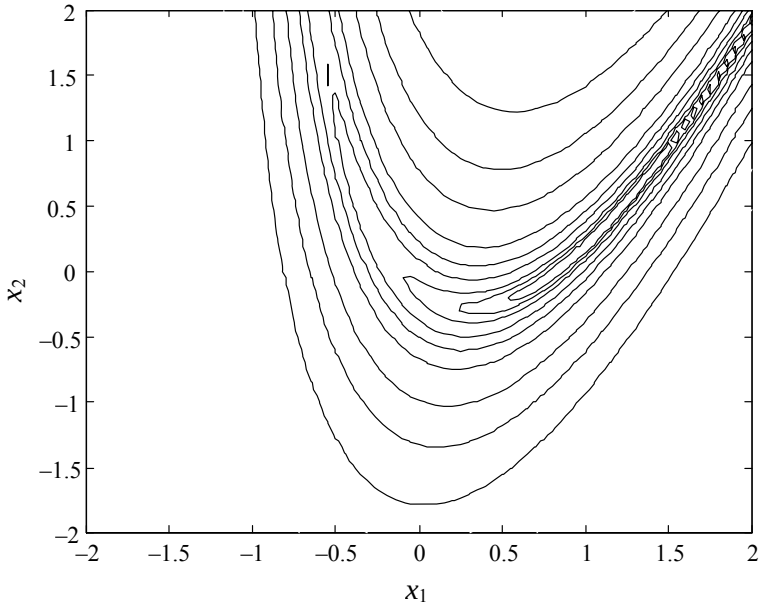

Fig. 3.4 Contour plot of the "fine" transformed Rosenbrock banana function.

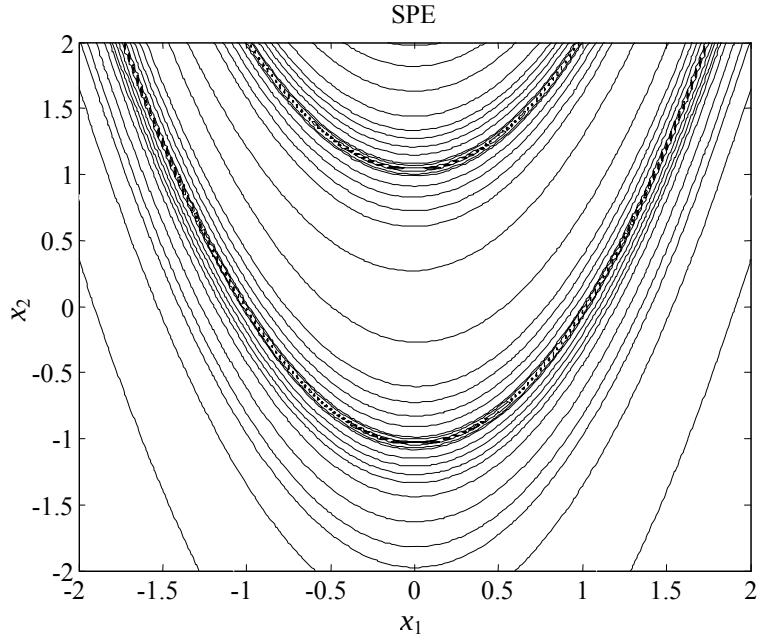

Fig. 3.5 Nonuniqueness occurs when single-point PE is used to match the models in the "transformed" Rosenbrock problem.

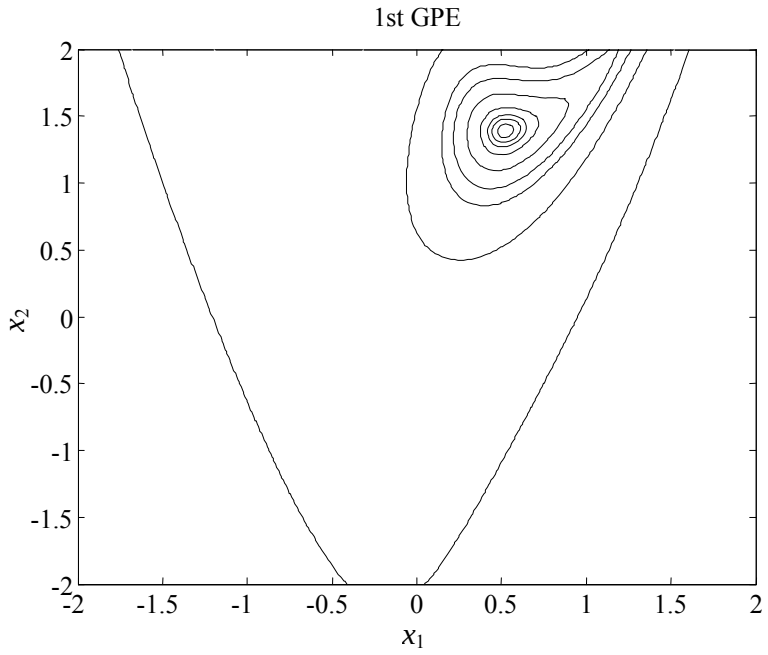

Fig. 3.6 A unique solution is obtained when gradient PE is used in the "transformed" Rosenbrock problem in the 1st iteration.

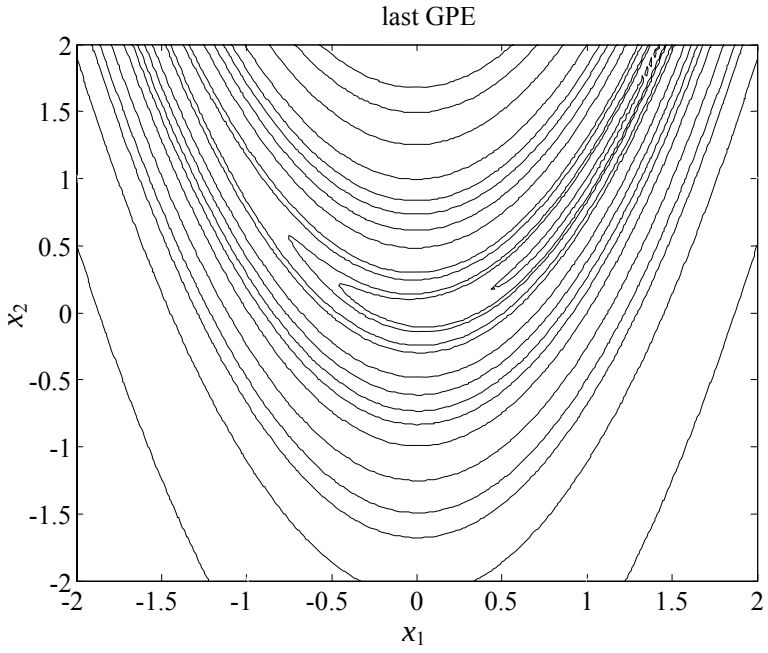

Fig. 3.7 The 6th (last) gradient PE iteration of the "transformed" Rosenbrock problem.

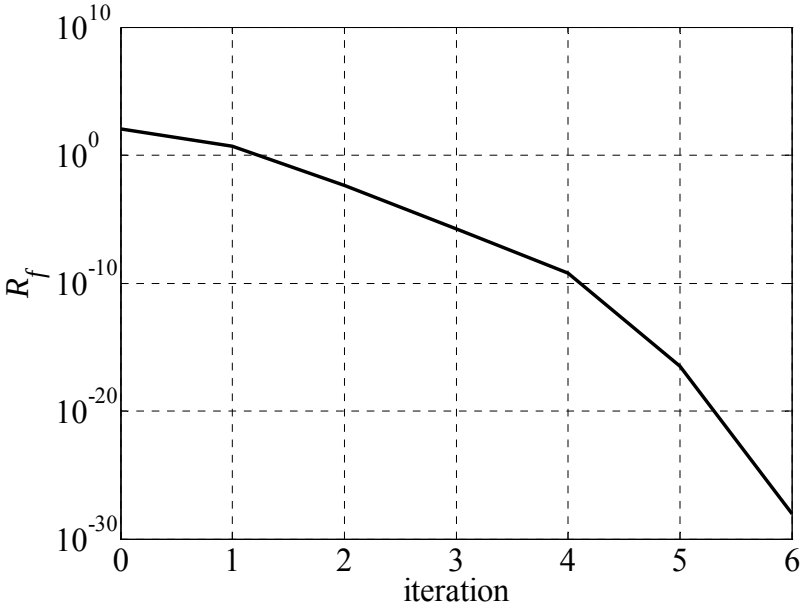

Fig. 3.8 Reduction of R_f versus iteration count of the "transformed" Rosenbrock problem.

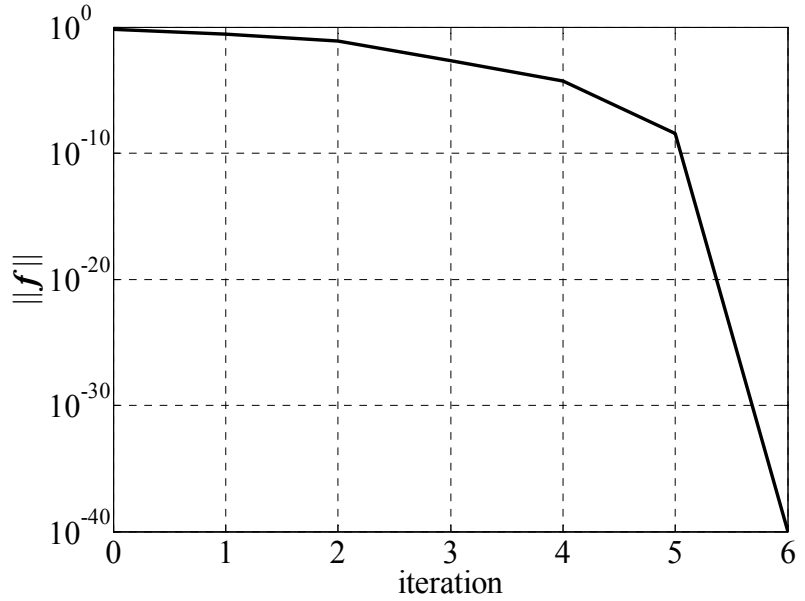

Fig. 3.9 Reduction of $\| \boldsymbol{f} \|$ versus iteration count of the "transformed" Rosenbrock problem.

TABLE 3.2

"TRANSFORMED" ROSENBROCK BANANA PROBLEM

j	$\boldsymbol{x}_c^{(j)}$	$\boldsymbol{f}^{(j)}$	$\boldsymbol{B}^{(j)}$	$\boldsymbol{h}^{(j)}$	$\boldsymbol{x}_f^{(j)}$	$R_f^{(j)}$
0	$\begin{bmatrix}1.0\\1.0\end{bmatrix}$	------	----------	------	$\begin{bmatrix}1.0\\1.0\end{bmatrix}$	108.3
1	$\begin{bmatrix}0.526\\1.384\end{bmatrix}$	$\begin{bmatrix}-0.474\\0.384\end{bmatrix}$	$\begin{bmatrix}1.01 & -0.05\\0.01 & 1.01\end{bmatrix}$	$\begin{bmatrix}0.447\\-0.385\end{bmatrix}$	$\begin{bmatrix}1.447\\0.615\end{bmatrix}$	5.119
2	$\begin{bmatrix}1.185\\1.178\end{bmatrix}$	$\begin{bmatrix}0.185\\0.178\end{bmatrix}$	$\begin{bmatrix}0.96 & -0.13\\-0.096 & 1.06\end{bmatrix}$	$\begin{bmatrix}-0.218\\-0.187\end{bmatrix}$	$\begin{bmatrix}1.23\\0.427\end{bmatrix}$	4e–3
3	$\begin{bmatrix}0.967\\0.929\end{bmatrix}$	$\begin{bmatrix}-0.033\\-0.071\end{bmatrix}$	$\begin{bmatrix}1.09 & -0.19\\0.168 & 0.92\end{bmatrix}$	$\begin{bmatrix}0.0429\\0.0697\end{bmatrix}$	$\begin{bmatrix}1.273\\0.497\end{bmatrix}$	1e–6
4	$\begin{bmatrix}1.001\\1.001\end{bmatrix}$	$\begin{bmatrix}0.001\\0.001\end{bmatrix}$	$\begin{bmatrix}1.10001 & -0.1999\\0.1999 & 0.9001\end{bmatrix}$	$\begin{bmatrix}-0.001\\-0.002\end{bmatrix}$	$\begin{bmatrix}1.2719\\0.4952\end{bmatrix}$	5e–10
5	$\begin{bmatrix}1.00002\\1.00004\end{bmatrix}$	$\begin{bmatrix}0.2\text{E}-4\\0.4\text{E}-4\end{bmatrix}$	$\begin{bmatrix}1.1 & -0.2\\0.2 & 0.9\end{bmatrix}$	$\begin{bmatrix}0.3\text{E}-4\\0.5\text{E}-4\end{bmatrix}$	$\begin{bmatrix}1.2718\\0.4951\end{bmatrix}$	3e–17
6	$\begin{bmatrix}1.0\\1.0\end{bmatrix}$	$\begin{bmatrix}0.1\text{E}-8\\0.3\text{E}-8\end{bmatrix}$	$\begin{bmatrix}1.1 & -0.2\\0.2 & 0.9\end{bmatrix}$	$\begin{bmatrix}0.2\text{E}-8\\0.3\text{E}-8\end{bmatrix}$	$\boldsymbol{x}_f^*$	9e–29

3.4.2 Capacitively Loaded 10:1 Impedance Transformer [18]

We apply Algorithm 2 to a two–section transmission–line 10:1 impedance transformer. We consider a "coarse" model as an ideal two–section transmission line (TL), where the "fine" model is a capacitively loaded TL with capacitors $C_1 = C_2 = C_3 = 10$ pF. The fine and coarse models are shown in Fig. 3.10 and Fig. 3.11, respectively. Design parameters are normalized lengths L_1 and L_2, with respect to the quarter–wave length L_q at the center frequency 1 GHz, and characteristic impedances Z_1 and Z_2. Normalization makes the problem well posed. Thus, $\boldsymbol{x}_f = \begin{bmatrix} L_1 & L_2 & Z_1 & Z_2 \end{bmatrix}^T$. Design specifications are

$$\left|S_{11}\right| \le 0.5, \quad \text{for } 0.5\,\text{GHz} \le \omega \le 1.5\,\text{GHz}$$

with eleven points per frequency sweep. We utilize the real and imaginary parts of S_{11} in the GPE (3.24). The fine and surrogate responses can be easily computed as a function of the design parameters using circuit theory [29]. We solve (3.24) using the Levenberg-Marquardt algorithm for nonlinear least squares optimization available in the Matlab Optimization Toolbox [30].

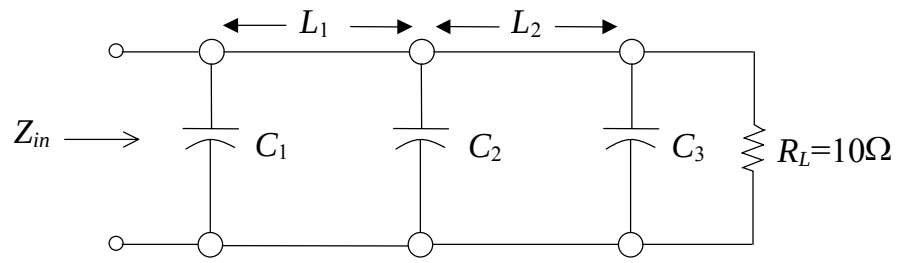

Fig. 3.10 Two-section impedance transformer: "fine" model [18].

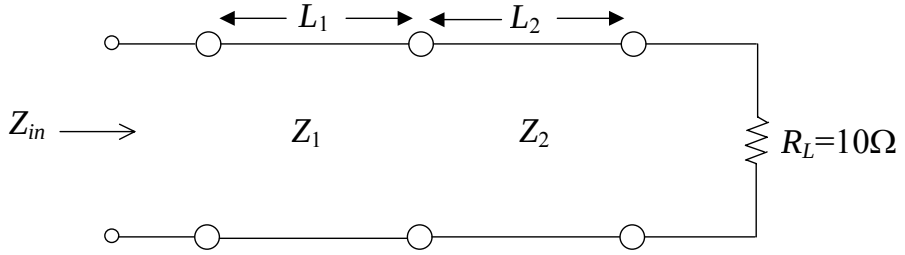

Fig. 3.11 Two-section impedance transformer: "coarse" model [18].

TABLE 3.3

NORMALIZED COARSE MODEL SENSITIVITIES WITH RESPECT TO THE DESIGN PARAMETERS FOR THE CAPACITIVELY LOADED IMPEDANCE TRANSFORMER

Parameter	$\hat{S}_i$
L_1	0.98
L_2	1.00
Z_1	0.048
Z_2	0.048

3.4.2.1 Case 1: [L_1 L_2]

Based on a normalized sensitivity analysis, proposed in [22], for the design parameters of the coarse model shown in Table 3.3, we note that the normalized lengths [L_1 L_2] are the key parameters. Thus, we consider $\boldsymbol{x}_c^{PSM} = \begin{bmatrix} L_1 & L_2 \end{bmatrix}^T$ while $\boldsymbol{x}_f^s = \begin{bmatrix} Z_1 & Z_2 \end{bmatrix}^T$ are kept fixed at the optimal values, i.e., Z_1 = 2.23615 Ω and Z_2 = 4.47230 Ω. We employ adjoint sensitivity analysis techniques [31] to obtain the exact Jacobians of the fine and coarse models. We initialize $\boldsymbol{B}^{PSM}$ by using the Jacobian information of both models at the starting point as in (3.28). The algorithm converges in a single iteration (2 fine model evaluations). The corresponding responses are illustrated in Fig. 3.12 and Fig. 3.13, respectively. The final mapping is

$$\boldsymbol{B}^{PSM} = \begin{bmatrix} 1.075 & 0.087 & 0.006 & 0.002 \\ 0.049 & 1.139 & -0.008 & 0.006 \end{bmatrix}$$

This result confirms the sensitivity analysis presented in Table 3.3. It supports our decision of taking into account only [L_1 L_2], represented by the first and the second columns in $\boldsymbol{B}^{PSM}$, as design parameters. As is well–known, the effect of the capacitance in the fine model can only be substantially compensated by a change of the length of a TL. Therefore, changes of $\begin{bmatrix} Z_1 & Z_2 \end{bmatrix}^T$ hardly affect the final response. The reduction of $\left\| \boldsymbol{x}_c - \boldsymbol{x}_c^* \right\|_2$ versus iteration is shown in Fig. 3.14. The reduction of the objective function U in Fig. 3.15 also illustrates convergence (two iterations).

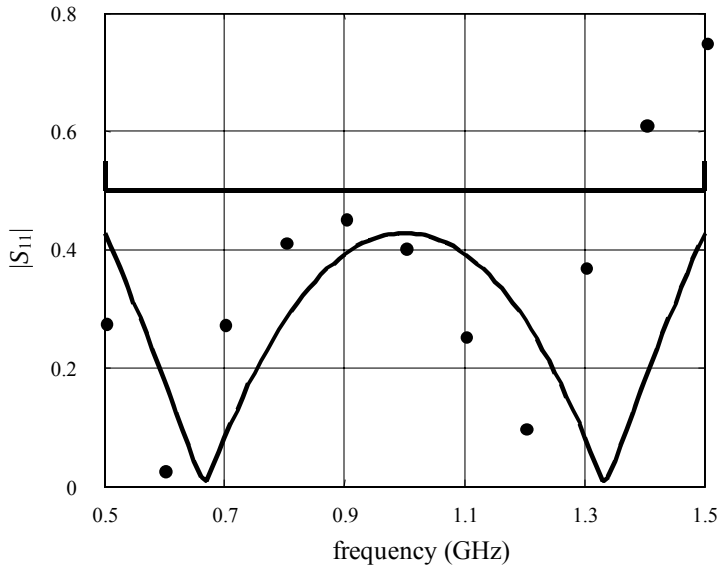

Fig. 3.12 Optimal coarse model target response (—) and the fine model response at the starting point (•) for the capacitively loaded 10:1 transformer with L_1 and L_2 as the PSM coarse model parameters.

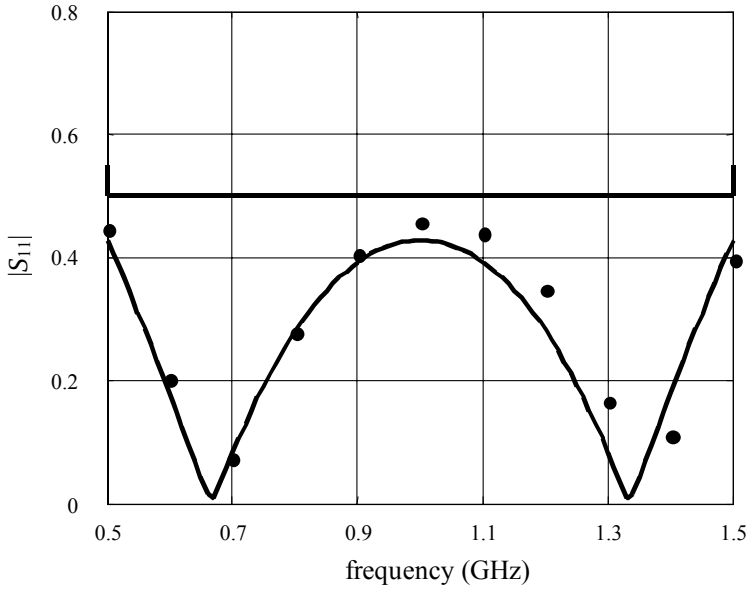

Fig. 3.13 Optimal coarse model target response (—) and the fine model response at the final design (•) for the capacitively loaded 10:1 transformer with L_1 and L_2 as the PSM coarse model parameters.

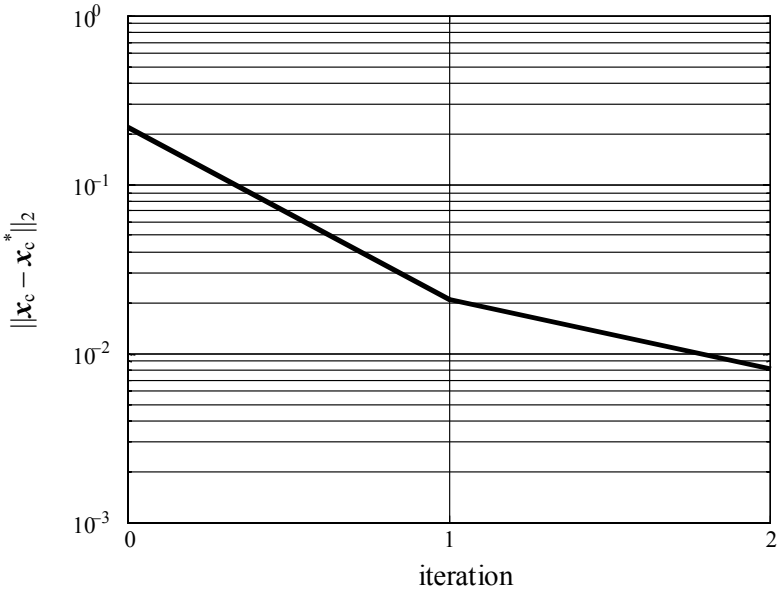

Fig. 3.14 $\left\|\boldsymbol{x}_c - \boldsymbol{x}_c^*\right\|_2$ versus iteration for the capacitively loaded 10:1 transformer with L_1 and L_2 as the PSM coarse model parameters.

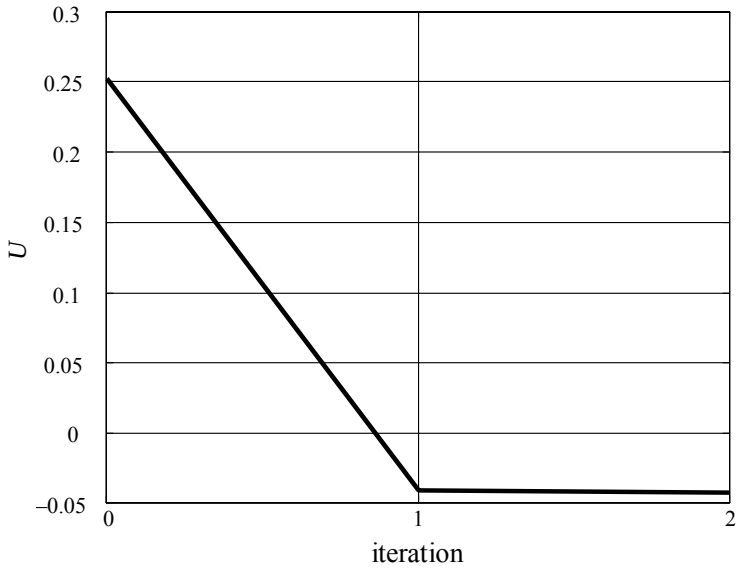

Fig. 3.15 U versus iteration for the capacitively loaded 10:1 transformer with L_1 and L_2 as the PSM coarse model parameters.

3.4.2.2 Case 2: [L_1]

We apply Algorithm 2 for $\boldsymbol{x}_c^{PSM} = [L_1]$. The result is similar to Fig. 3.13. Convergence is in a single iteration (2 fine model evaluations). The final mapping is

$$\boldsymbol{B}^{PSM} = [1.371 \quad 0.909 \quad 0.0033 \quad 0.0055]$$

As we see changes in [L_1], represented by the first element in $\boldsymbol{B}^{PSM}$, are significant. However, the second parameter [L_2] is affected also. This arises from the fact that [L_1 L_2] have the same physical effect, namely, that of length in a TL.

3.4.2.3 Case 3: [L_2]

We apply Algorithm 2 for $\boldsymbol{x}_c^{PSM} = [L_2]$. The result is similar to Fig. 3.13 and it converges in a single iteration (2 fine model evaluations). The final mapping is

$$\boldsymbol{B}^{PSM} = [0.8989 \quad 1.186 \quad -0.0043 \quad 0.0087]$$

As in case 2, changes in one parameter, [L_2] in this case, have the dominant role. This affects [L_1], the parameter which shares the same physical nature.

The initial and final designs for all three cases are shown in Table 3.4. We realize that the algorithm aims to rescale the TL lengths to match the responses in the PE process (see Fig. 3.12). In all cases both [L_1 L_2] are reduced by similar overall amounts, as expected.

By carefully choosing a reduced set of design parameters we can affect other "redundant" parameters and the overall circuit response as well, which implies the idea of tuning. Nevertheless, the use of the entire set of design parameters should give the best result.

TABLE 3.4

INITIAL AND FINAL DESIGNS FOR
THE CAPACITIVELY LOADED IMPEDANCE TRANSFORMER

Parameter	$\boldsymbol{x}_f^{(0)}$	$\boldsymbol{x}_f^{(1)}$ (L_1 and L_2)	$\boldsymbol{x}_f^{(1)}$ (L_1)	$\boldsymbol{x}_f^{(1)}$ (L_2)
L_1	1.0	0.8995	0.8631	0.8521
L_2	1.0	0.8228	0.9126	0.8259
Z_1	2.23615	2.2369	2.2352	2.2365
Z_2	4.47230	4.4708	4.4716	4.4707

L_1 and L_2 are normalized lengths

Z_1 and Z_2 are in ohm

3.4.3 Bandstop Microstrip Filter with Open Stubs [5]

Algorithm 3 is applied to a symmetrical bandstop microstrip filter with three open stubs. The open stub lengths are L_1, L_2, L_1 and W_1, W_2, W_1 are the corresponding stub widths. An alumina substrate with thickness H = 25 mil, width W_0 = 25 mil, dielectric constant ε_r = 9.4 and loss tangent = 0.001 is used for a 50 Ω feeding line. The design parameters are $\boldsymbol{x}_f = \begin{bmatrix} W_1 & W_2 & L_0 & L_1 & L_2 \end{bmatrix}^T$. The design specifications are

$$\begin{aligned} &|S_{21}| \le 0.05 \quad \text{for } 9.3\,\text{GHz} \le \omega \le 10.7\,\text{GHz} \text{ and,} \\ &|S_{21}| \ge 0.9 \quad \text{for } 12\,\text{GHz} \le \omega \text{ and } \omega \le 8\,\text{GHz} \end{aligned}$$

Sonnet's ***em*** [32] driven by Empipe [33] is employed as the fine model, using a high-resolution grid with a 1.0 mil × 1.0 mil cell size. As a coarse model we use simple transmission lines for modeling each microstrip section and classical formulas [29] to calculate the characteristic impedance and the effective dielectric constant of each transmission line. It is seen that $L_{c2} = L_2 + W_0/2, L_{c1} = L_1 + W_0/2$ and $L_{c0} = L_0 + W_1/2 + W_2/2$. We use OSA90/hope [33] built-in transmission line elements TRL. The fine model and its surrogate coarse model are illustrated in Fig. 3.16 and Fig. 3.17, respectively.

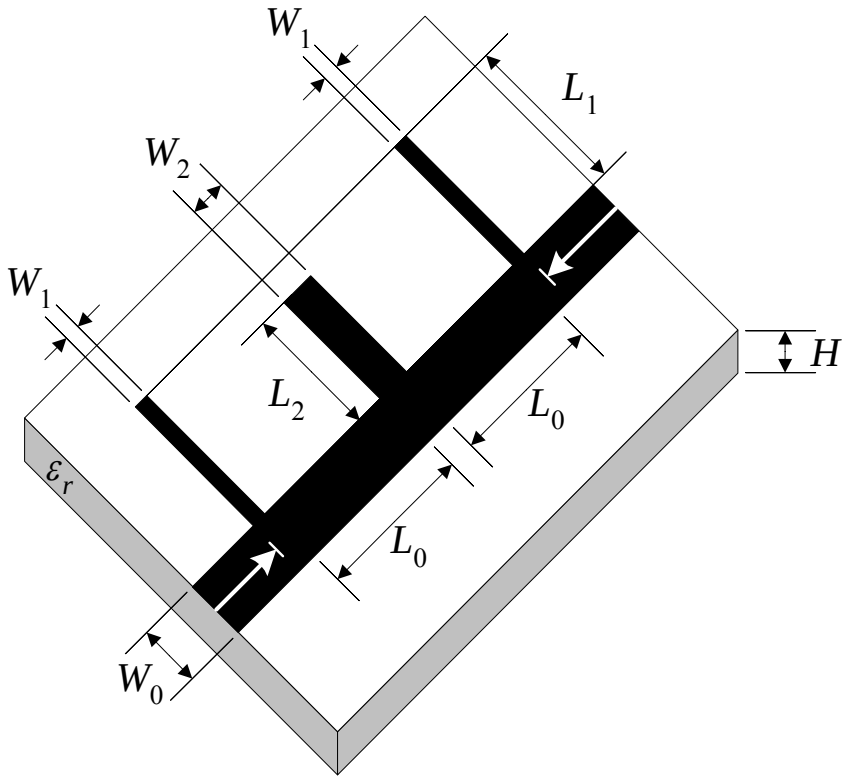

Fig. 3.16 Bandstop microstrip filter with open stubs: “fine” model [5].

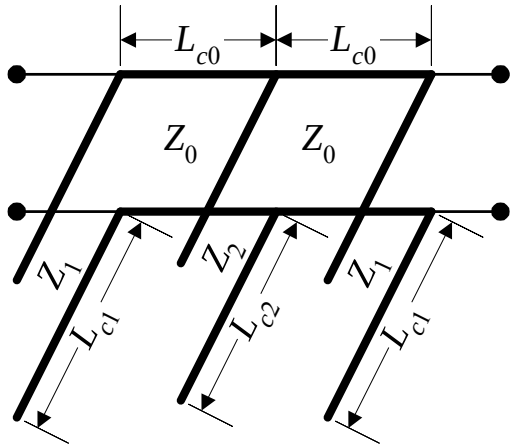

Fig. 3.17 Bandstop microstrip filter with open stubs: “coarse” model [5].

TABLE 3.5

NORMALIZED COARSE MODEL SENSITIVITIES WITH RESPECT TO DESIGN PARAMETERS FOR THE BANDSTOP MICROSTRIP FILTER

Parameter	$\hat{S}_i$
W_1	0.065
W_2	0.077
L_0	0.677
L_1	1.000
L_2	0.873

Using OSA90/hope we can get the optimal coarse solution at 10 GHz as $\boldsymbol{x}_c^* = [4.560 \;\; 9.351 \;\; 107.80 \;\; 111.03 \;\; 108.75]^T$ (in mils). We use 21 points per frequency sweep. The coarse and fine model responses at the optimal coarse solution are shown in Fig. 3.18 (fine sweep is used only for illustration). We utilize the real and imaginary parts of S_{11} and S_{21} in the traditional PE. Normalized sensitivity analysis [22] for the coarse model is given in Table 3.5. During the PE we consider $\boldsymbol{x}_c^{PSM} = [L_1 \;\; L_2]^T$ while $\boldsymbol{x}_f^s = [W_1 \;\; W_2 \;\; L_0]^T$ are held fixed at the optimal coarse solution. Finite differences estimate the fine and coarse Jacobians used to initialize $\boldsymbol{B}^{PSM}$ as in (3.28). A hybrid approach is used to update $\boldsymbol{B}^{PSM}$ at each iteration.

Algorithm 3 converges in 5 iterations. The PE execution time for the whole process is 59 min on an IBM-IntelliStation (AMD Athlon 400MHz) machine. The optimal coarse model response and the final design fine response are depicted in Fig. 3.19. The convergence of the algorithm is depicted in Fig. 3.20, where the reduction of $\left\| \boldsymbol{x}_c - \boldsymbol{x}_c^* \right\|_2$ versus iteration is illustrated. The initial and final design values are shown in Table 3.6. The final mapping is given by

$$\boldsymbol{B}^{PSM} = \begin{bmatrix} 0.570 & 0.168 & 0.209 & 0.911 & 0.214 \\ -0.029 & 0.154 & 0.126 & -0.024 & 0.470 \end{bmatrix}$$

We notice that [L_1 L_2], represented by the last two columns, are dominant parameters.

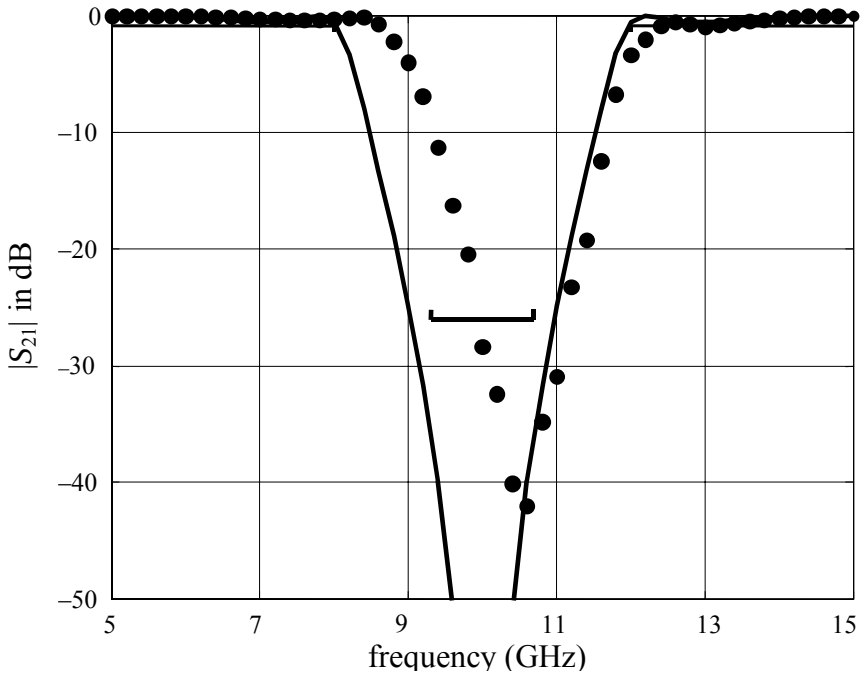

Fig. 3.18 Optimal OSA90/hope coarse target response (—) and ***em*** fine model response at the starting point (•) for the bandstop microstrip filter using a fine frequency sweep (51 points) with L_1 and L_2 as the PSM coarse model parameters.

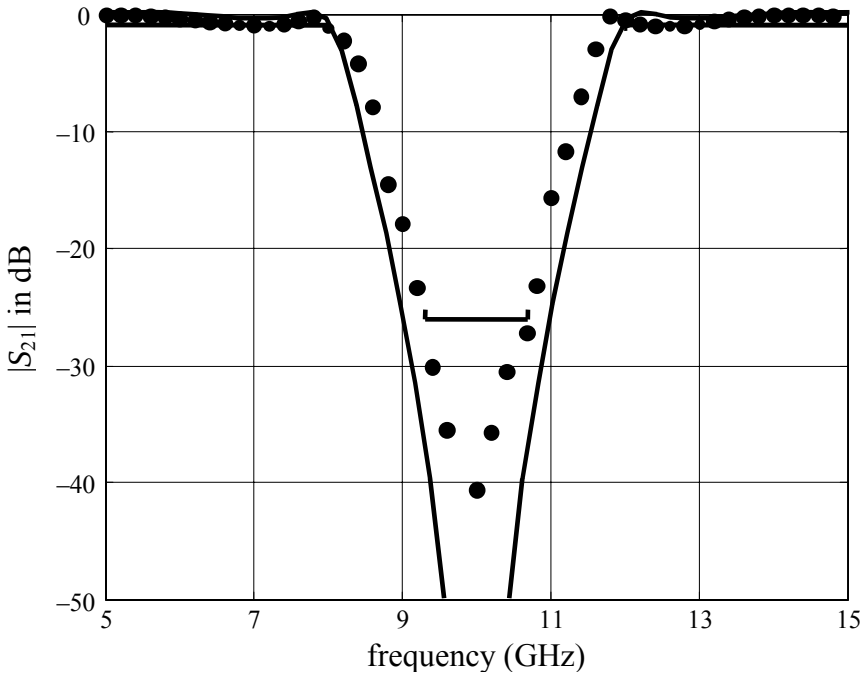

Fig. 3.19 Optimal OSA90/hope coarse target response (—) and ***em*** fine model response at the final design (•) for the bandstop microstrip filter using a fine frequency sweep (51 points) with L_1 and L_2 as the PSM coarse model parameters.

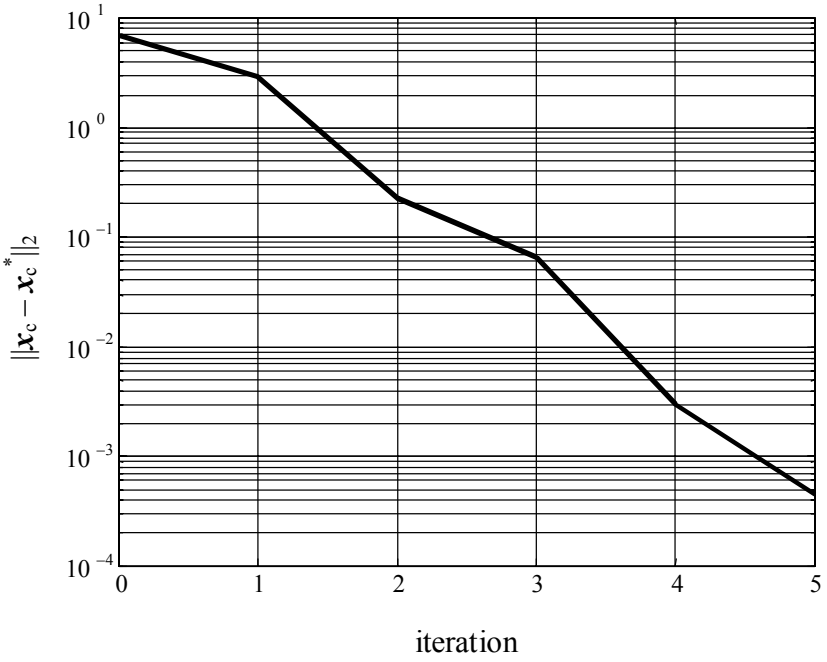

Fig. 3.20 $\left\|\boldsymbol{x}_c - \boldsymbol{x}_c^*\right\|_2$ versus iteration for the bandstop microstrip filter using L_1 and L_2 as the PSM coarse model parameters.

TABLE 3.6

INITIAL AND FINAL DESIGNS FOR
THE BANDSTOP MICROSTRIP FILTER USING L_1 AND L_2

Parameter	$\boldsymbol{x}_f^{(0)}$	$\boldsymbol{x}_f^{(5)}$
W_1	4.560	7.329
W_2	9.351	10.672
L_0	107.80	109.24
L_1	111.03	115.53
L_2	108.75	111.28
all values are in mils		

We run Algorithm 3 using all design parameters in the PE and in calculating the quasi–Newton step in the fine space, i.e., we use a full mapping. The algorithm converges in 5 iterations, however, the PE process takes 75 min on an IBM-IntelliStation (AMD Athlon 400MHz) machine. The initial and final designs are given in Table 3.7. The final mapping is

$$\boldsymbol{B} = \begin{bmatrix} 0.532 & -0.037 & 0.026 & 0.017 & -0.006 \\ -0.051 & 0.543 & 0.022 & -0.032 & 0.026 \\ 0.415 & 0.251 & 1.024 & 0.073 & 0.011 \\ 0.169 & -0.001 & -0.022 & 0.963 & 0.008 \\ -0.213 & -0.003 & -0.045 & -0.052 & 0.958 \end{bmatrix}$$

The reduction of $\left\| \boldsymbol{x}_c - \boldsymbol{x}_c^* \right\|_2$ versus iteration is shown in Fig. 3.21.

The notion of tuning is evident in this example also, where the various lengths and widths which constitute the designable parameters (see Fig. 3.16) have obvious physical interrelations.

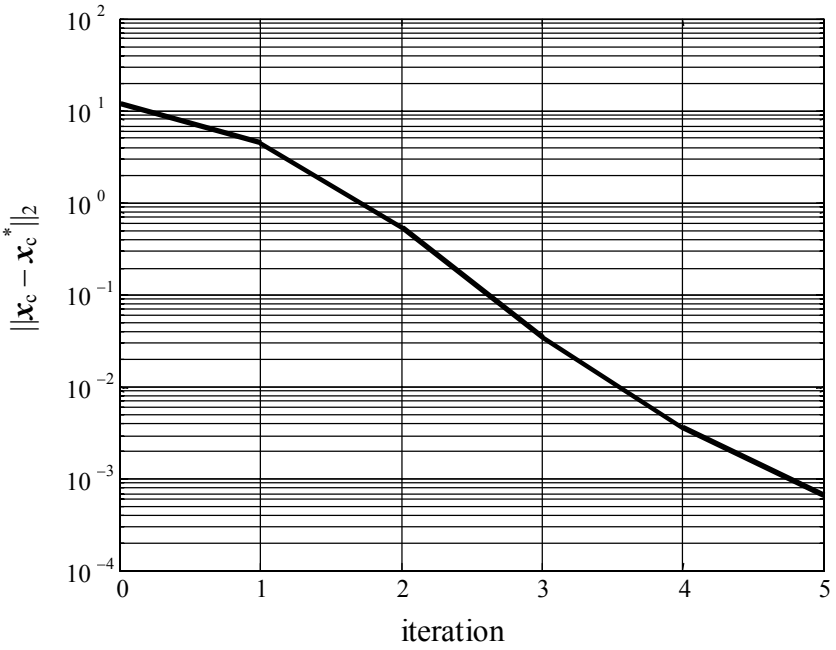

Fig. 3.21 $\left\|\boldsymbol{x}_c - \boldsymbol{x}_c^*\right\|_2$ versus iteration for the bandstop microstrip filter using a full mapping.

TABLE 3.7

INITIAL AND FINAL DESIGNS FOR
THE BANDSTOP MICROSTRIP FILTER USING A FULL MAPPING

Parameter	$\boldsymbol{x}_f^{(0)}$	$\boldsymbol{x}_f^{(5)}$
W_1	4.560	8.7464
W_2	9.351	19.623
L_0	107.80	97.206
L_1	111.03	116.13
L_2	108.75	113.99
all values are in mils		

3.4.4 Comparison with Previous Approaches

All SM-based algorithms, by their very nature, are expected to produce acceptable designs in a small number of fine model evaluations, typically 3 to 10. Hence, a basis for comparison must be simplicity, ease of programming, robustness on many examples and, in particular, avoidance of designer intervention. Our extensive convergence results (Tables 3.1 and 3.2, Figs. 3.14, 3.15, 3.20 and 3.21) of our gradient-based proposal demonstrate that we averted false parameter extractions, do not require sophisticated programming, and do not rely on designer intervention.

3.5 CONCLUDING REMARKS

We present a family of robust techniques for exploiting sensitivities in EM–based circuit optimization through SM. We exploit a Partial Space Mapping (PSM) concept where a reduced set of parameters is sufficient in the Parameter Extraction (PE) process. Available gradients can initialize mapping approximations. Exact or approximate Jacobians of responses can be utilized. For flexibility, we propose different possible "mapping matrices" for the PE processes and SM iterations. Finite differences may be used to initialize the mapping. A hybrid approach incorporating the Broyden formula can be used for mapping updates. Our approaches have been tested on several examples. They demonstrate simplicity of implementation, robustness, and do not rely on designer intervention.

Final mappings are useful in statistical analysis and yield optimization. Furthermore, the notion of exploiting reduced sets of physical parameters reflects the important idea of postproduction tuning.

REFERENCES

[1] J.W. Bandler, R.M. Biernacki, S.H. Chen, P.A. Grobelny and R.H. Hemmers, "Space mapping technique for electromagnetic optimization," *IEEE Trans. Microwave Theory and Tech.*, vol. 42, pp. 2536–2544, Dec. 1994.

[2] J.W. Bandler, R.M. Biernacki, S.H. Chen, R.H. Hemmers and K. Madsen, "Electromagnetic optimization exploiting aggressive space mapping," *IEEE Trans. Microwave Theory and Tech.*, vol. 43, pp. 2874–2882, Dec. 1995.

[3] J.W. Bandler, W. Kellermann and K. Madsen, "A superlinearly convergent minimax algorithm for microwave circuit design," *IEEE Trans. Microwave Theory and Tech.,* vol. MTT-33, pp. 1519–1530, Dec. 1985.

[4] J.W. Bandler, A.S. Mohamed, M.H. Bakr, K. Madsen and J. Søndergaard, "EM-based optimization exploiting partial space mapping and exact sensitivities," *IEEE Trans. Microwave Theory and Tech.*, vol. 50, pp. 2741–2750, Dec. 2002.

[5] M.H. Bakr, J.W. Bandler, M.A. Ismail, J.E. Rayas-Sánchez and Q.J. Zhang, "Neural space-mapping optimization for EM-based design," *IEEE Trans. Microwave Theory and Tech.*, vol. 48, pp. 2307–2315, Dec. 2000.

[6] J. W. Bandler, Q. J. Zhang and R. M. Biernacki, "A unified theory for frequency-domain simulation and sensitivity analysis of linear and nonlinear circuits," *IEEE Trans. Microwave Theory and Tech.*, vol. 36, pp. 1661–1669, Dec. 1988.

[7] J. W. Bandler, Q. J. Zhang, J. Song and R. M. Biernacki, "FAST gradient based yield optimization of nonlinear circuits," *IEEE Trans. Microwave Theory and Tech.*, vol. 38, pp. 1701–1710, Nov. 1990.

[8] F. Alessandri, M. Mongiardo and R. Sorrentino, "New efficient full wave optimization of microwave circuits by the adjoint network method," *IEEE Microwave and Guided Wave Letts.*, vol. 3, pp. 414–416, Nov. 1993.

[9] N.K. Georgieva, S. Glavic, M.H. Bakr and J.W. Bandler, "Feasible adjoint sensitivity technique for EM design optimization," *IEEE Trans. Microwave Theory and Tech.*, vol. 50, pp. 2751–2758, Dec. 2002.

[10] N.K. Nikolova, J.W. Bandler and M. H. Bakr, "Adjoint techniques for sensitivity analysis in high-frequency structure CAD," *IEEE Trans. Microwave Theory Tech.*, vol. 52, pp. 403–419, Jan. 2004.

[11] J.W. Bandler, Q. Cheng, S.A. Dakroury, A.S. Mohamed, M.H. Bakr, K. Madsen and J. Søndergaard, "Space mapping: the state of the art," *IEEE Trans. Microwave Theory Tech.*, vol. 52 pp. 337–361, Jan. 2004.

[12] J.W. Bandler, R.M. Biernacki and S.H. Chen, "Fully automated space mapping optimization of 3D structures," in *IEEE MTT-S Int. Microwave Symp. Dig.*, San Francisco, CA, 1996, pp. 753–756.

[13] J.W. Bandler, R.M. Biernacki, S.H. Chen and D. Omeragic, "Space mapping optimization of waveguide filters using finite element and mode-matching electromagnetic simulators," *Int. J. RF and Microwave CAE*, vol. 9, pp. 54–70, 1999.

[14] M.H. Bakr, J.W. Bandler, R.M. Biernacki, S.H. Chen and K. Madsen, "A trust region aggressive space mapping algorithm for EM optimization," *IEEE Trans. Microwave Theory Tech.*, vol. 46, pp. 2412–2425, Dec. 1998.

[15] M.H. Bakr, J.W. Bandler and N.K. Georgieva, "An aggressive approach to parameter extraction," *IEEE Trans. Microwave Theory and Tech.*, vol. 47, pp. 2428–2439, Dec. 1999.

[16] J.W. Bandler, R.M. Biernacki, S.H. Chen and Y.F. Huang, "Design optimization of interdigital filters using aggressive space mapping and decomposition," *IEEE Trans. Microwave Theory Tech.*, vol. 45, pp. 761–769, May 1997.

[17] J.W. Bandler, M.A. Ismail, J.E. Rayas-Sánchez and Q.J. Zhang, "Neuromodeling of microwave circuits exploiting space mapping technology," *IEEE Trans. Microwave Theory Tech.*, vol. 47, pp. 2417–2427, Dec. 1999.

[18] M.H. Bakr, J.W. Bandler, K. Madsen, J.E. Rayas-Sánchez and J. Søndergaard, "Space mapping optimization of microwave circuits exploiting surrogate models," *IEEE Trans. Microwave Theory and Tech.*, vol. 48, pp. 2297–2306, Dec. 2000.

[19] J.W. Bandler, Q.S. Cheng, N.K. Nikolova and M.A. Ismail, "Implicit space mapping optimization exploiting preassigned parameters," *IEEE Trans. Microwave Theory Tech.*, vol. 52, pp. 378–385, Jan. 2004.

[20] J.W. Bandler, N. Georgieva, M.A. Ismail, J.E. Rayas-Sánchez and Q. J. Zhang, "A generalized space mapping tableau approach to device modeling," *IEEE Trans. Microwave Theory Tech*., vol. 49, pp. 67–79, Jan. 2001.

[21] M.H. Bakr, J.W. Bandler, N.K. Georgieva and K. Madsen, "A hybrid aggressive space-mapping algorithm for EM optimization," *IEEE Trans. Microwave Theory and Tech.*, vol. 47, pp. 2440–2449, Dec. 1999.

[22] J.W. Bandler, M.A. Ismail and J.E. Rayas-Sánchez, "Expanded space mapping EM-based design framework exploiting preassigned parameters," *IEEE Trans. Circuits and Systems—I*, vol. 49, pp. 1833–1838, Dec. 2002.

[23] C.G. Broyden, "A class of methods for solving nonlinear simultaneous equations," *Math. Comp.,* vol. 19, pp. 577–593, 1965.

[24] S. Bila, D. Baillargeat, S. Verdeyme and P. Guillon, "Automated design of microwave devices using full EM optimization method," in *IEEE MTT-S Int. Microwave Symp. Dig.*, Baltimore, MD, 1998, pp. 1771–1774.

[25] A.M. Pavio, "The electromagnetic optimization of microwave circuits using companion models," *Workshop on Novel Methodologies for Device Modeling and Circuit CAD*, *IEEE MTT-S Int. Microwave Symp. Dig.,* Anaheim, CA, 1999.

[26] J.W. Bandler, S.H. Chen, S. Daijavad and K. Madsen, "Efficient optimization with integrated gradient approximations," *IEEE Trans. Microwave Theory Tech.,* vol. 36, pp. 444–455, Feb. 1988.

[27] M.H. Bakr, J.W. Bandler, K. Madsen and J. Søndergaard, "Review of the space mapping approach to engineering optimization and modeling," *Optimization and Engineering*, vol. 1, pp. 241–276, 2000.

[28] R. Fletcher, *Practical Methods of Optimization*, 2nd ed. New York, NY: Wiley, 1987.

[29] M. Pozar, *Microwave Engineering*, 2nd ed. New York, NY: Wiley, 1998.

[30] Matlab, The MathWorks, Inc., 3 Apple Hill Drive, Natick MA 01760–2098, USA.

[31] J.W. Bandler, "Computer-aided circuit optimization," in *Modern Filter Theory and Design,* G.C. Temes and S.K. Mitra, Eds. New York, NY: Wiley, 1973, pp. 211–271.

[32] ***em,*** Sonnet Software, Inc., 100 Elwood Davis Road, North Syracuse, NY 13212, USA.

[33] OSA90/hope and Empipe Version 4.0, formerly Optimization Systems Associates Inc., P.O. Box 8083, Dundas, Ontario, Canada L9H 5E7, 1997, now Agilent Technologies, 1400 Fountaingrove Parkway, Santa Rosa, CA 95403–1799, USA.

CHAPTER 4

TLM-BASED MODELING AND DESIGN EXPLOITING SPACE MAPPING

4.1 INTRODUCTION

In previous implementations of SM technology [1], utilizing either an explicit input mapping [2]–[3], implicit [4] or output mappings [5]–[6], an "idealized" coarse model is assumed to be available. This coarse model, usually empirically based, provides a target optimal response with respect to the predefined design specifications while SM algorithms try to achieve a satisfactory "space-mapped" design $\bar{\boldsymbol{x}}_f$.

In this chapter, we explore the SM methodology in the TLM [7] simulation environment. We design a CPU intensive fine-grid TLM structure utilizing a coarse-grid TLM model with relaxed boundary conditions [8]. Such a coarse model may not faithfully represent the fine-grid TLM model. Furthermore, it may not even satisfy the original design specifications. Hence,

SM techniques such as the aggressive SM [3] will fail to reach a satisfactory solution.

To overcome the aforementioned difficulty, we combine the implicit SM (ISM) [4] and output SM (OSM) [5]–[6] approaches. Parameter extraction (PE), equivalently called surrogate calibration, is responsible for constructing a surrogate of the fine model. As a preliminary PE step, the coarse model's dielectric constant, a convenient preassigned parameter, is first calibrated. If the response deviation between the two TLM models is still large, an output SM scheme absorbs this deviation to make the updated surrogate represent the fine model. The subsequent surrogate optimization step is governed by a trust region (TR) strategy.

The TLM simulator used in the design process is a Matlab [9] implementation. A set of design parameter values represents a point in the TLM simulation space. Because of the discrete nature of the TLM simulator, we employ an interpolation scheme to evaluate the responses, and possibly derivatives, at off-grid points [10]–[11] (see Appendix C). A database system is also created to avoid repeatedly invoking the simulator, to calculate the responses and derivatives, for a previously visited point. The database system is responsible for storage, retrieval and management of all previously performed simulations [11].

Our proposed approach is illustrated through an inductive post, a single-resonator filter and a six-section H-plane waveguide filter [8]. We can achieve

practical designs in a handful of iterations in spite of poor initial surrogate model responses. The results are verified using the commercial time domain TLM simulator MEFiSTo [12].

In Section 4.2 we review the basic concepts of TLM, implicit SM, output SM and TR methodology. The theory of our proposed approach is presented in Section 4.3, explaining the surrogate calibration and surrogate optimization steps. We propose an algorithm in Section 4.4. Examples are illustrated in Section 4.5, including the design of a six-section H-plane waveguide filter with MEFiSTo verification. Conclusions and suggested future developments are drawn in Section 4.6.

4.2 BASIC CONCEPTS

4.2.1 Transmission-Line Matrix (TLM) Method

The TLM method is a time and space discrete method for modeling EM phenomena [13]. A mesh of interconnected transmission lines models the propagation space [7]. The TLM method carries out a sequence of scattering and connection steps [13]. For the *i*th non-metalized node, the scattering relation is given by

$$\boldsymbol{V}_{k+1}^{R,i} = \boldsymbol{S}^{i}(\varepsilon_r^i) \cdot \boldsymbol{V}_k^i \tag{4.1}$$

where $\boldsymbol{V}_k^i$ is the vector of incident impulses on the *i*th node at the *k*th time step, $\boldsymbol{V}_{k+1}^{R,i}$ is the vector of reflected impulses of the *i*th node at the (*k*+1)th time step and

$\boldsymbol{S}^i(\varepsilon_r^i)$ is the scattering matrix at the *i*th node which is a function of the local dielectric constant ε_r^i.

The reflected impulses become incident on neighboring nodes. For a non-dispersive TLM boundary, a single time step is given by

$$\boldsymbol{V}_{k+1} = \boldsymbol{C} \cdot \boldsymbol{S} \cdot \boldsymbol{V}_k + \boldsymbol{V}_k^s \tag{4.2}$$

where $\boldsymbol{V}_k$ is the vector of incident impulses for all nodes at the *k*th time step. The matrix $\boldsymbol{S}$ is a block diagonal matrix whose *i*th diagonal block is $\boldsymbol{S}^i(\varepsilon_r^i)$, $\boldsymbol{C}$ is the connection matrix and the vector $\boldsymbol{V}_k^s$ is the source excitation vector at the *k*th time step.

4.2.2 Design Problem

Our design problem is given by (2.1), where in a TLM-based environment $\boldsymbol{R}_f : X_f \to \mathbb{R}^m$ is a function of $\boldsymbol{V}_k$ for all time steps *k*.

4.2.3 Implicit Space Mapping (ISM)

In the ISM approach, selected preassigned parameters denoted by $\boldsymbol{x} \in X \subseteq \mathbb{R}^p$ are extracted in an attempt to match the coarse model to the fine model [4], [14]. With these parameters fixed in the fine model, the calibrated (implicitly mapped) coarse model denoted by $\boldsymbol{R}_c : X \times X_f \to \mathbb{R}^m$, at the *j*th iteration, is optimized with respect to the design parameters $\boldsymbol{x}_f$ as

$$\boldsymbol{x}_f^{(j)} \triangleq \arg \min_{\boldsymbol{x}_f} U\left(\boldsymbol{R}_c\left(\boldsymbol{x}_f, \boldsymbol{x}^{(j)}\right)\right) \tag{4.3}$$

Refer to Section 2.7, for further discussion.

4.2.4 Output Space Mapping (OSM)

Although the fine and coarse models usually share the same physical background, they are still two different models and a deviation between them in the response space (i.e., the range) always exists. This deviation cannot be compensated by only manipulating the parameters (i.e., the domain) through the regular SM. Output SM $\boldsymbol{O}: \mathbb{R}^m \to \mathbb{R}^m$ is originally proposed to fine-tune the residual response deviation [5]–[6] between the fine model and its surrogate, in the final stages. In this case, the surrogate incorporates a faithful coarse model and could be given by the composite function

$$\boldsymbol{R}_s = \boldsymbol{O} \circ \boldsymbol{R}_c \tag{4.4}$$

4.2.5 Trust Region (TR) Methods [15]

TR strategies are employed to assure convergence of an optimization algorithm and to stabilize the iterative process [16]. The TR approach was first introduced in the context of SM with the aggressive SM technique in [17]. See Section 2.5 for more details.

4.3 THEORY

In this study, we propose an approach to create a surrogate of the fine model that exploits an input implicit mapping (model domain) and also encompasses the response deviation between the fine model and its surrogate (model range) through an output mapping. The proposed output SM scheme absorbs possible response misalignments through a response linear transformation (shift and scale). Fig. 4.1 describes a conceptual scheme for combining an input parameter mapping (implicit in our case) along with an output response mapping.

At the *j*th iteration, a surrogate of the fine model is given by [8]

$$\boldsymbol{R}_s(\boldsymbol{x}_f, \boldsymbol{x}^{(j+1)}, \boldsymbol{\alpha}^{(j+1)}, \boldsymbol{\beta}^{(j+1)}) \triangleq \boldsymbol{\alpha}^{(j+1)} \boldsymbol{R}_c\left(\boldsymbol{x}_f, \boldsymbol{x}^{(j+1)}\right) + \boldsymbol{\beta}^{(j+1)} \tag{4.5}$$

Here, $\boldsymbol{x}^{(j+1)}$ is the preassigned parameter vector whose value is determined by the implicit mapping at $\boldsymbol{x}_f^{(j)}$. The scaling diagonal matrix $\boldsymbol{\alpha}^{(j+1)} \in \mathbb{R}^{m \times m}$ and the shifting vector $\boldsymbol{\beta}^{(j+1)} \in \mathbb{R}^m$ are the output mapping parameters. The preassigned parameters and the output mapping parameters are evaluated through a surrogate calibration, i.e., the parameter extraction process [8].

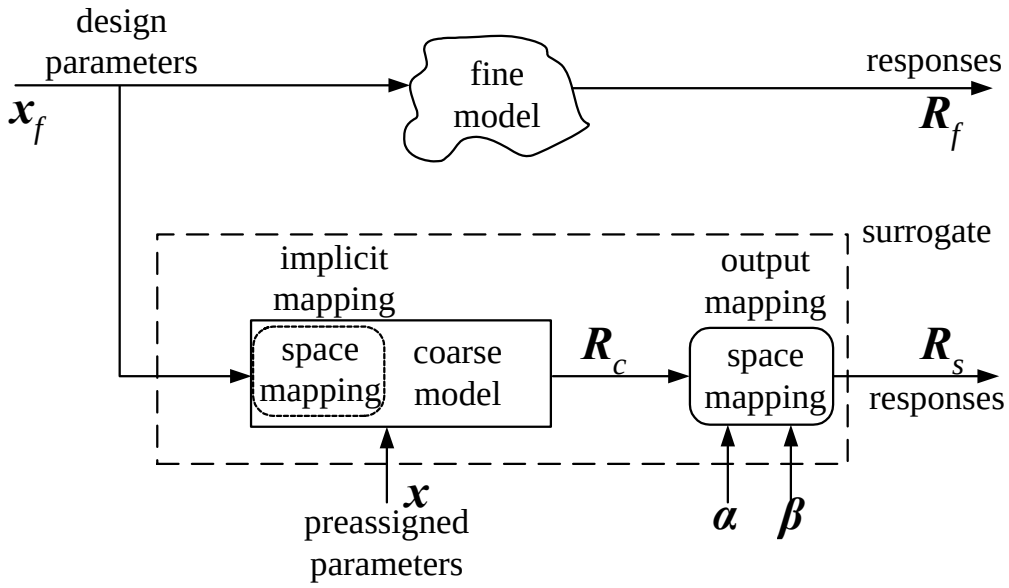

Fig. 4.1 The implicit and output space mapping concepts. We calibrate the surrogate against the fine model utilizing the preassigned parameters $\boldsymbol{x}$, e.g., dielectric constant, and the output response mapping parameters: the scaling matrix $\boldsymbol{\alpha}$ and the shifting vector $\boldsymbol{\beta}$.

4.3.1 Parameter Extraction (Surrogate Calibration)

The PE optimization process is performed here to align the surrogate (4.5) with the fine model by calibrating the mapping(s) parameters.

The deviation between the fine model and the surrogate responses at the current fine model point $\boldsymbol{x}_f^{(j)}$ is given by

$$\boldsymbol{e}\left(\boldsymbol{x}_f^{(j)}, \boldsymbol{x}, \boldsymbol{\alpha}, \boldsymbol{\beta}\right) = \boldsymbol{R}_s\left(\boldsymbol{x}_f^{(j)}, \boldsymbol{x}, \boldsymbol{\alpha}, \boldsymbol{\beta}\right) - \boldsymbol{R}_f\left(\boldsymbol{x}_f^{(j)}\right) \tag{4.6}$$

At the jth iteration, $\boldsymbol{x}^{(j+1)}$ is first extracted keeping the output mapping parameters $\left\{\boldsymbol{\alpha}^{(j)}, \boldsymbol{\beta}^{(j)}\right\}$ fixed as follows

$$\begin{aligned}
&\left[\boldsymbol{x}^{(j+1)}\right] \triangleq \arg\min_{\boldsymbol{x}} \left\|\boldsymbol{E}_r\right\|, \\
&\boldsymbol{E}_r = \begin{bmatrix} \boldsymbol{e}_0^T & \boldsymbol{e}_1^T & \ldots & \boldsymbol{e}_{N_j-1}^T \end{bmatrix}^T, \\
&\boldsymbol{e}_l = \boldsymbol{R}_s\left(\boldsymbol{x}_f^{(l)}, \boldsymbol{x}, \boldsymbol{\alpha}^{(j)}, \boldsymbol{\beta}^{(j)}\right) - \boldsymbol{R}_f\left(\boldsymbol{x}_f^{(l)}\right) \quad \forall \boldsymbol{x}_f^{(l)} \in V^{(j)}
\end{aligned} \tag{4.7}$$

Here, a multipoint PE (MPE) scheme [18], [19] is employed. We calibrate the surrogate model against the fine model at a set of points $\boldsymbol{x}_f^{(l)} \in V^{(j)}$ with $\left|V^{(j)}\right| = N_j$, where N_j is the number of fine model points utilized at the *j*th PE iteration. At each PE iteration, we initially set $V^{(j)} = \left\{\boldsymbol{x}_f^{(j)}\right\}$. Then, some of the fine model points of the previous successful iterates are included into the set $V^{(j)}$ and hence more information about the fine model could be utilized.

Then, we calibrate the surrogate by manipulating $\left\{\boldsymbol{\alpha}^{(j)}, \boldsymbol{\beta}^{(j)}\right\}$ at $\boldsymbol{x}_f^{(j)}$ and $\boldsymbol{x}^{(j+1)}$ to absorb the response deviation [8]

$$\begin{aligned}
&\left[\boldsymbol{\alpha}^{(j+1)}, \boldsymbol{\beta}^{(j+1)}\right] \triangleq \arg\min_{\boldsymbol{\alpha},\boldsymbol{\beta}} \left\| \begin{bmatrix} \boldsymbol{e}^T & w_1\left[(\boldsymbol{\alpha} - \boldsymbol{I})\boldsymbol{u}\right]^T & w_2\boldsymbol{\beta}^T \end{bmatrix}^T \right\|, \\
&\boldsymbol{e} = \boldsymbol{R}_s\left(\boldsymbol{x}_f^{(j)}, \boldsymbol{x}^{(j+1)}, \boldsymbol{\alpha}, \boldsymbol{\beta}\right) - \boldsymbol{R}_f\left(\boldsymbol{x}_f^{(j)}\right); \\
&\boldsymbol{u} = \begin{bmatrix} 1 & 1 & \ldots & 1 \end{bmatrix}^T
\end{aligned} \tag{4.8}$$

$\boldsymbol{\alpha}$ and $\boldsymbol{\beta}$ are ideally $\boldsymbol{I}$ and $\boldsymbol{0}$, respectively. The PE (4.8) is penalized such that $\boldsymbol{\alpha}$ and $\boldsymbol{\beta}$ remain close to their ideal values. w_1 and w_2 are user-defined weighting factors. A suitable norm, denoted by $\|\ \|$, is utilized in (4.7) and (4.8), e.g., the l_2 norm.

4.3.2 Surrogate Optimization (Prediction)

We optimize a suitable objective function of the surrogate (4.5) in effort to obtain a solution of (2.1). We utilize the TR methodology to find the step in the fine space at the *j*th iteration [14], [16]

$$\begin{aligned} \boldsymbol{h}^{(j)} \triangleq \arg\ \min_{\boldsymbol{h}} U(\boldsymbol{R}_s(\boldsymbol{x}_f^{(j)}+\boldsymbol{h}, \boldsymbol{x}^{(j+1)}, \boldsymbol{\alpha}^{(j+1)}, \boldsymbol{\beta}^{(j+1)})), \\ \|\boldsymbol{h}\|_\infty \le \delta^{(j)} \end{aligned} \tag{4.9}$$

where $\delta^{(j)}$ is the TR size at the *j*th iteration. The tentative step $\boldsymbol{h}^{(j)}$ is accepted as a successful step in the fine model parameter space if there is a reduction of the fine model objective function, otherwise the step is rejected.

$$\boldsymbol{x}_f^{(j+1)} = \begin{cases} \boldsymbol{x}_f^{(j)} + \boldsymbol{h}^{(j)}, & \text{if } U(\boldsymbol{R}_f(\boldsymbol{x}_f^{(j)}+\boldsymbol{h}^{(j)})) < U(\boldsymbol{R}_f(\boldsymbol{x}_f^{(j)})) \\ \boldsymbol{x}_f^{(j)}, & \text{otherwise} \end{cases} \tag{4.10}$$

The TR radius is updated according to [16].

4.3.3 Stopping Criteria

The algorithm stops when one of the following stopping criteria satisfied:

- A predefined maximum number of iterations $j_{\max}$ is reached.
- The step length taken by the algorithm is sufficiently small [20]

$$\left\|\boldsymbol{h}^{(j)}\right\| \le \eta\left(1+\left\|\boldsymbol{x}_f^{(j)}\right\|\right) \tag{4.11}$$

where η is a user-defined small number.

- The TR radius $\delta^{(j)}$ reaches the minimum allowed value $\delta_{\min}$

$$\delta^{(j)} \le \delta_{\min} \tag{4.12}$$

4.4 ALGORITHM [8]

Given $\delta^{(0)}, \delta_{\min}, j_{\max}, \eta, \boldsymbol{x}^{(0)}$.

Comment The initial TR radius is $\delta^{(0)}$ and the nominal preassigned parameter value is $\boldsymbol{x}^{(0)}$.

Step 1 Initialize $j = 0$ and $\boldsymbol{\alpha}^{(0)} = \boldsymbol{I}, \boldsymbol{\beta}^{(0)} = \mathbf{0}$.

Step 2 Solve (4.3) to find the initial surrogate optimizer.

Comment The initial surrogate is the coarse model.

Step 3 Evaluate the fine model response $\boldsymbol{R}_f(\boldsymbol{x}_f^{(0)})$.

Step 4 Find surrogate parameters $\left\{\boldsymbol{x}^{(j+1)}, \boldsymbol{\alpha}^{(j+1)}, \boldsymbol{\beta}^{(j+1)}\right\}$ through PE (4.7) and (4.8).

Step 5 Obtain $\boldsymbol{h}^{(j)}$ by solving (4.9).

Step 6 Evaluate $\boldsymbol{R}_f(\boldsymbol{x}_f^{(j)} + \boldsymbol{h}^{(j)})$.

Step 7 Set $\boldsymbol{x}_f^{(j+1)}$ according to (4.10).

Step 8 Update $\delta^{(j+1)}$ according to the criterion in [16].

Step 9 If the stopping criterion is satisfied (Section 4.3.3.), terminate.

Step 10 If the TR step is successful, increment *j* and go to Step 4, else go to Step 5.

4.5 EXAMPLES

A Matlab implementation of a 2D-TLM simulator, developed by Bakr [21], is utilized. We employ the dielectric constant ε_r as a scalar preassigned parameter (i.e., $\boldsymbol{x} = \varepsilon_r$) for the whole region in all the coming examples.

4.5.1 An Inductive Obstacle in a Parallel-Plate Waveguide

Fig. 4.2 shows an inductive post centered in a parallel-plate waveguide with fixed dimensions. Thickness *D* and width *W* of the inductive obstacle are design parameters. We are exciting the dominant TEM mode of propagation. Due to symmetry, only half the structure is simulated.

We use the fine model with a square cell $\Delta x = \Delta y = 1.0$ mm, while the coarse model utilizes a square cell $\Delta x = \Delta y = 5.0$ mm. We utilized 21 frequency points in the frequency range 0.1GHz $\leq \omega \leq$ 2.5 GHz. The objective function is defined to match the real and imaginary parts of S_{11} and S_{21} of a given target response.

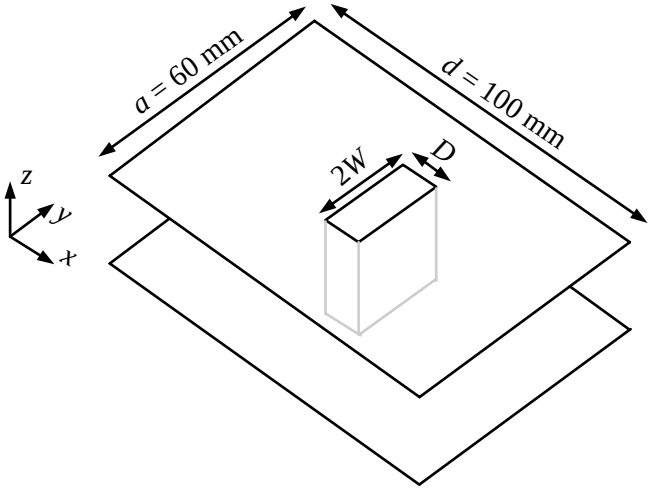

(a)

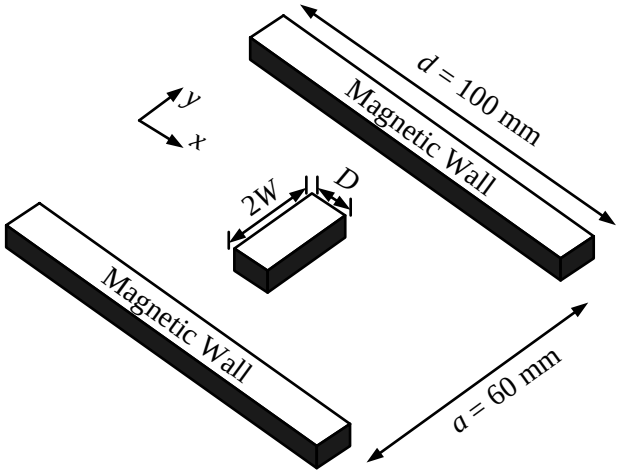

(b)

Fig. 4.2 An inductive post in a parallel-plate waveguide: (a) 3D plot, and (b) cross section with magnetic side walls [13].

An interpolation scheme is used [10] in optimizing the surrogate (calibration and prediction steps). The least-squares Levenberg-Marquardt algorithm available in Matlab [9] is utilized to solve both the PE problem and the TR subproblem in each iteration. The PE is designed to match the fine model with the surrogate at the current point in both (4.7) and (4.8), i.e. $V^{(j)} = \left\{ \boldsymbol{x}_f^{(j)} \right\}$, $\forall j$. The weighting factors w_1 and w_2 are set to zero (unconstrained problem).

The algorithm converges in 7 iterations. The progression of the optimization iterates on the fine modeling grid is shown in Fig. 4.3. The target, fine model and surrogate responses at the initial and the final iterations for $|S_{21}|$ and $|S_{11}|$ are shown in Fig. 4.4 and Fig. 4.5. Fig. 4.6 illustrates the reduction of the fine model and the corresponding surrogate objective functions along iterations. The optimization results are summarized in Table 4.1.

Our proposed approach, without the database system, takes 34 min versus 68 min for direct optimization. Utilizing the database system reduces the execution time to 4 min.

A statistical analysis of the surrogate at the final design is carried out with 100 samples. The relative tolerance used is 2%. The results show good agreement between the fine model (75 min for 100 outcomes) and its surrogate (7 min for 100 outcomes). The real and imaginary parts of S_{21} for both the fine model and its surrogate at the final design are shown in Fig. 4.7 and Fig. 4.8.

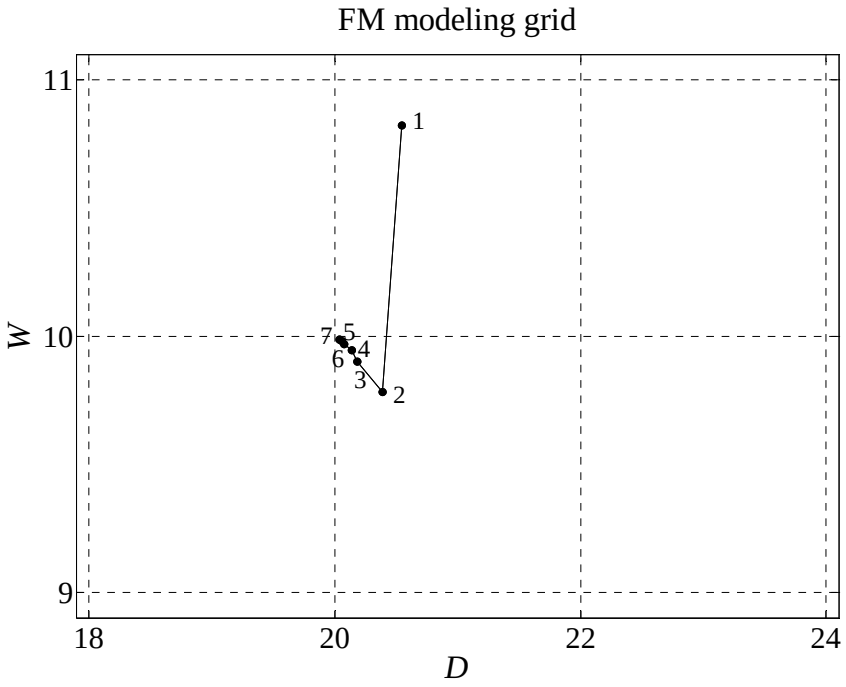

Fig. 4.3 The progression of the optimization iterates for the inductive post on the fine modeling grid (*D* and *W* are in mm).

TABLE 4.1

OPTIMIZATION RESULTS FOR THE INDUCTIVE POST

Iteration	$\boldsymbol{x}_f$ (mm)	ε_r	U_s	U_f
0	$\begin{bmatrix} 20.55 \\ 10.82 \end{bmatrix}$	1.0000	3.15e–4	2.5e–2
1	$\begin{bmatrix} 20.39 \\ 9.78 \end{bmatrix}$	0.9663	2.45e–5	3.06e–4
2	$\begin{bmatrix} 20.18 \\ 9.90 \end{bmatrix}$	0.9683	6.57e–5	5.49e–5
3	$\begin{bmatrix} 20.14 \\ 9.95 \end{bmatrix}$	0.9692	1.04e–5	9.10e–6
4	$\begin{bmatrix} 20.08 \\ 9.97 \end{bmatrix}$	0.9695	3.90e–6	2.74e–6
5	$\begin{bmatrix} 20.06 \\ 9.982 \end{bmatrix}$	0.9697	1.60e–6	1.12e–6
6	$\begin{bmatrix} 20.04 \\ 9.987 \end{bmatrix}$	0.9698	6.0e–7	5.30e–7

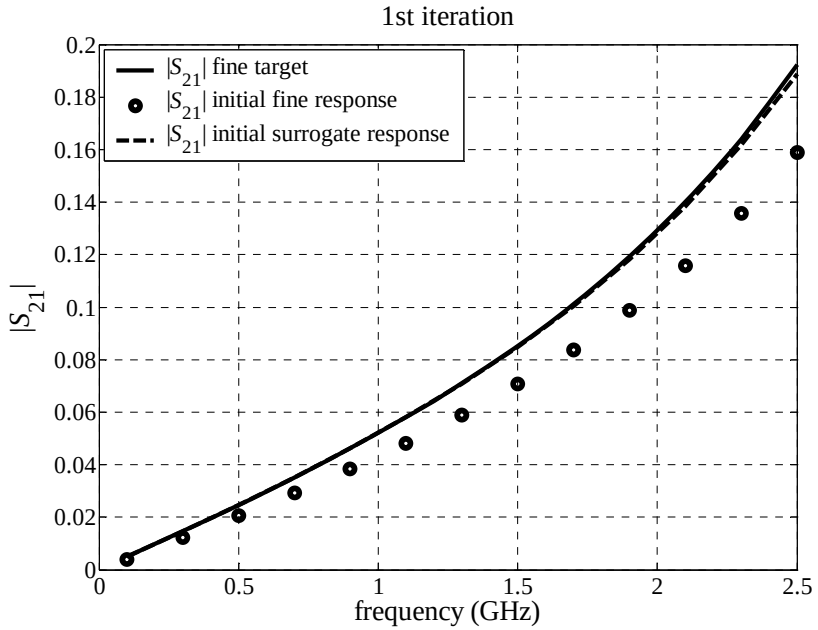

(a)

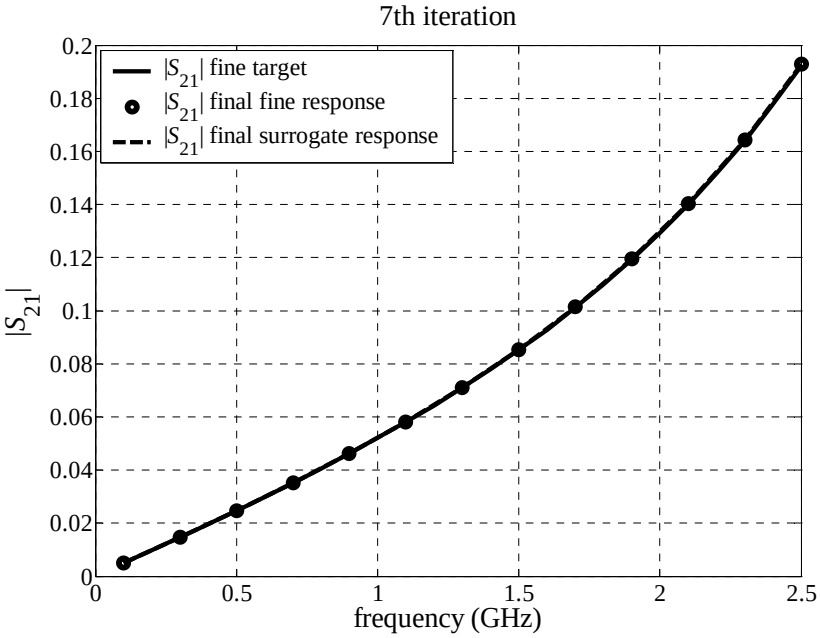

(b)

Fig. 4.4 Optimal target response (—), the fine model response (•) and the surrogate response (--) for the inductive post ($|S_{21}|$): (a) at the initial design, and (b) at the final design.

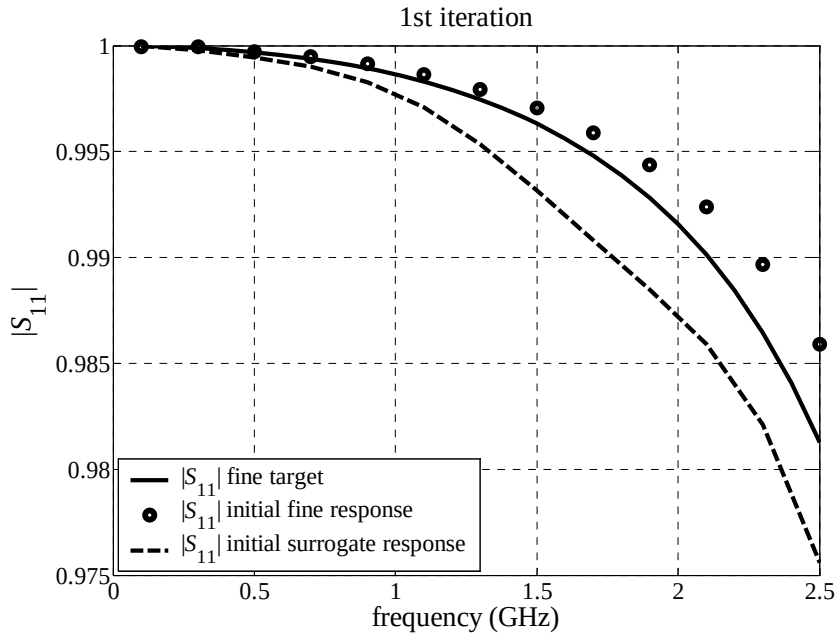

(a)

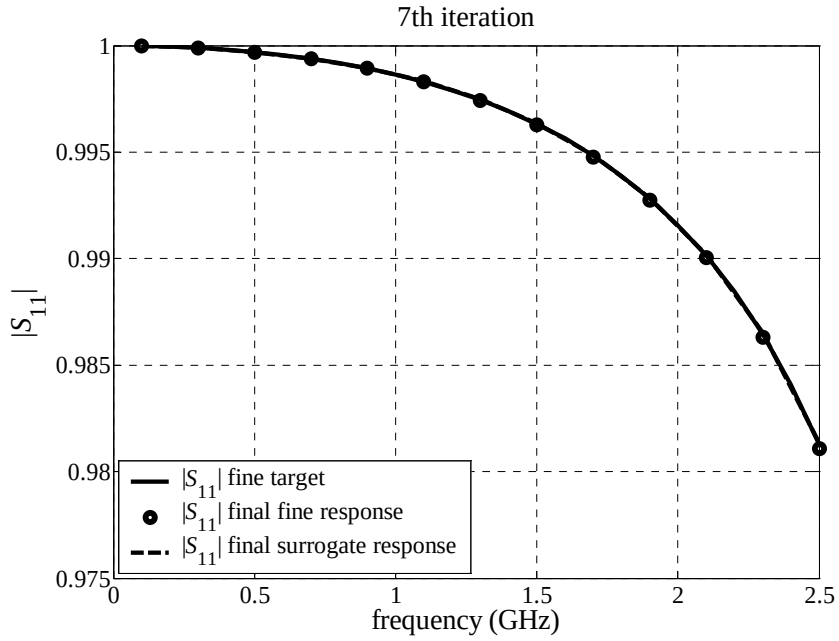

(b)

Fig. 4.5 Optimal target response (—), the fine model response (•) and the surrogate response (--) for the inductive post ($|S_{11}|$): (a) at the initial design, and (b) at the final design.

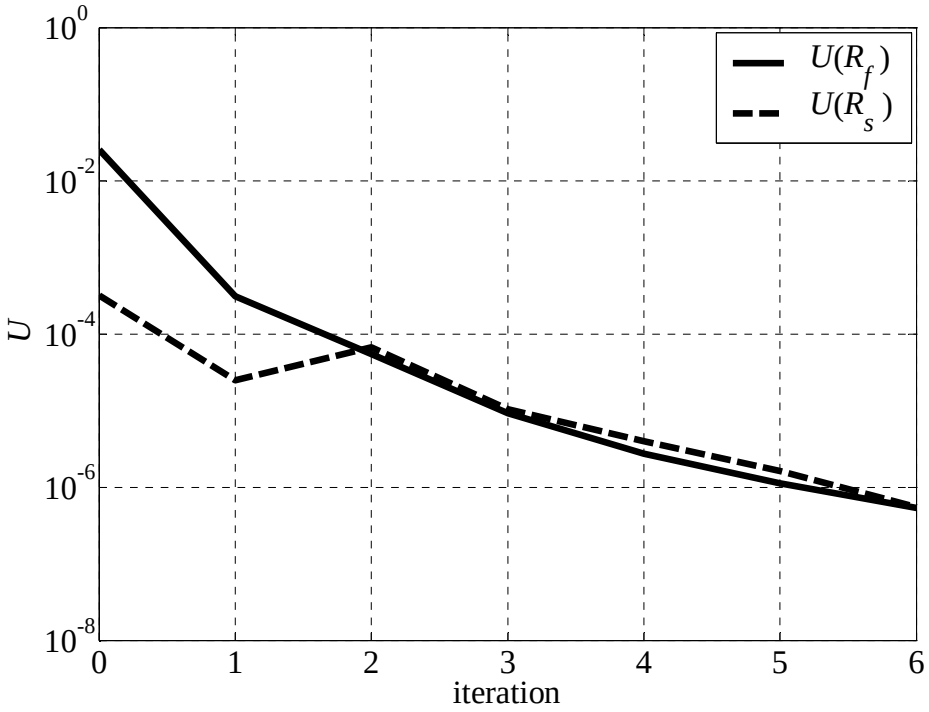

Fig. 4.6 The reduction of the objective function (U) for the fine model (—) and the surrogate (--) for the inductive post.

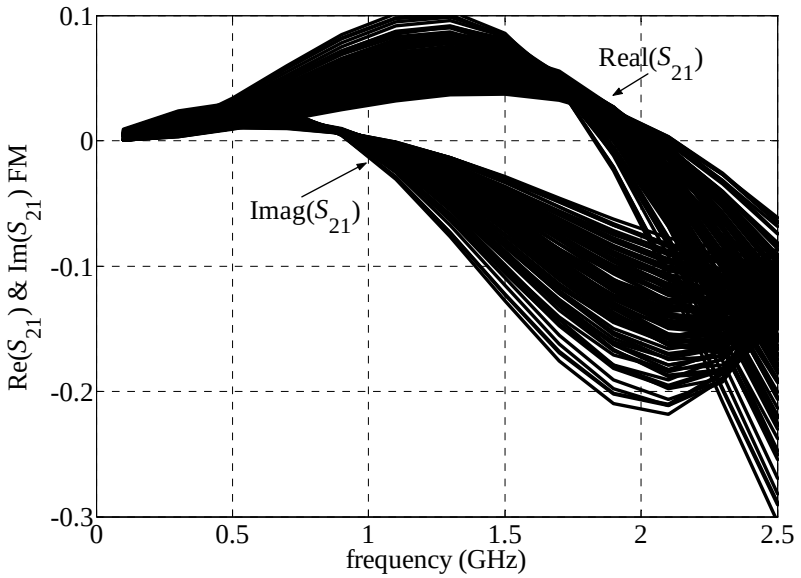

(a)

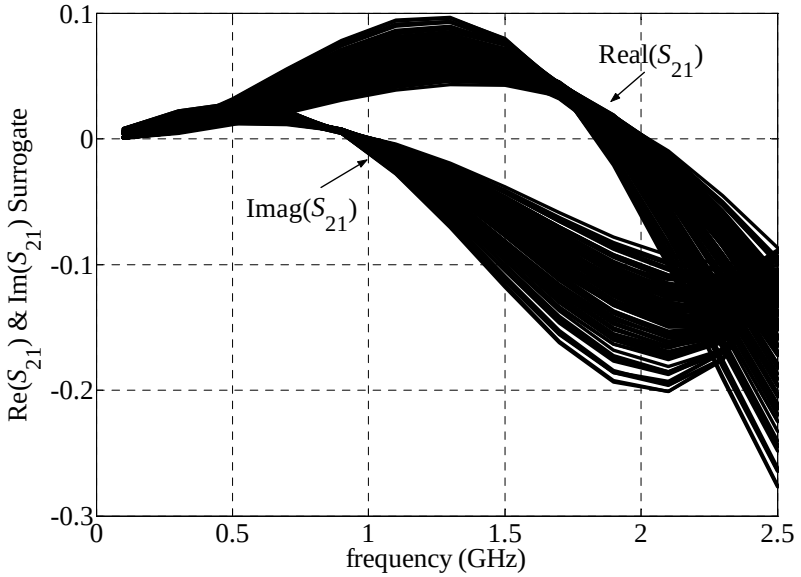

(b)

Fig. 4.7 Statistical analysis for the real and imaginary of S_{21} of the inductive post with 2% relative tolerances: (a) using the fine model, and (b) using the surrogate at the final iteration of the optimization. 100 outcomes are used.

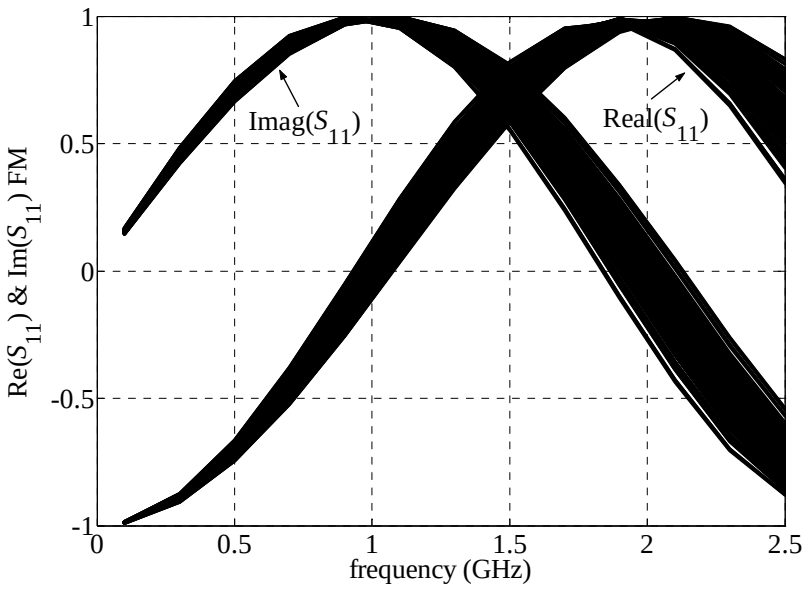

(a)

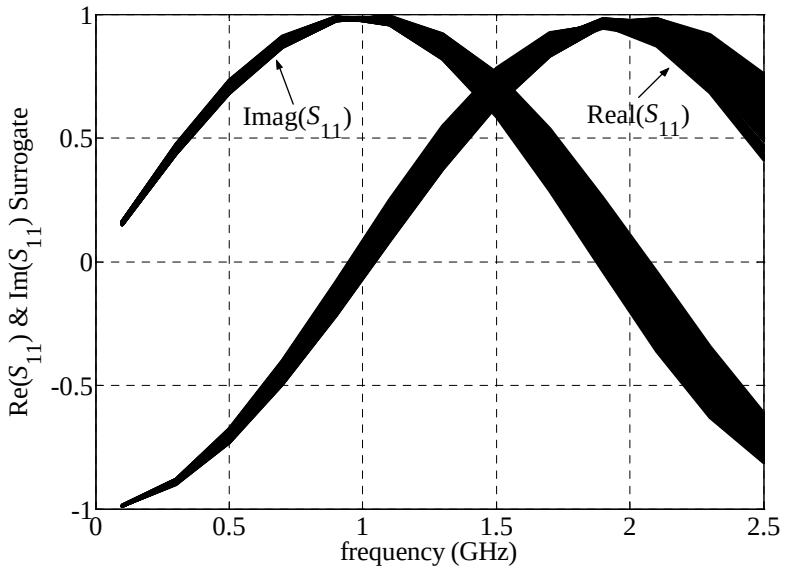

(b)

Fig. 4.8 Statistical analysis for the real and imaginary of S_{11} of the inductive post with 2% relative tolerances: (a) using the fine model, and (b) using the surrogate at the final iteration of the optimization. 100 outcomes are used.

4.5.2 Single-Resonator Filter

A single-resonator filter is shown in Fig. 4.9. The design parameters are the width *W* and the resonator length *d*. The rectangular waveguide width and length are fixed as shown. The propagating mode is TE_{10} with cutoff frequency 2.5 GHz.

We use the fine model with a square cell $\Delta x = \Delta y = 1.0$ mm. The coarse model utilizes a square cell $\Delta x = \Delta y = 5.0$ mm. We utilize 21 frequency points uniformly distributed in the range $\omega \in [3.0, 5.0]$ GHz.

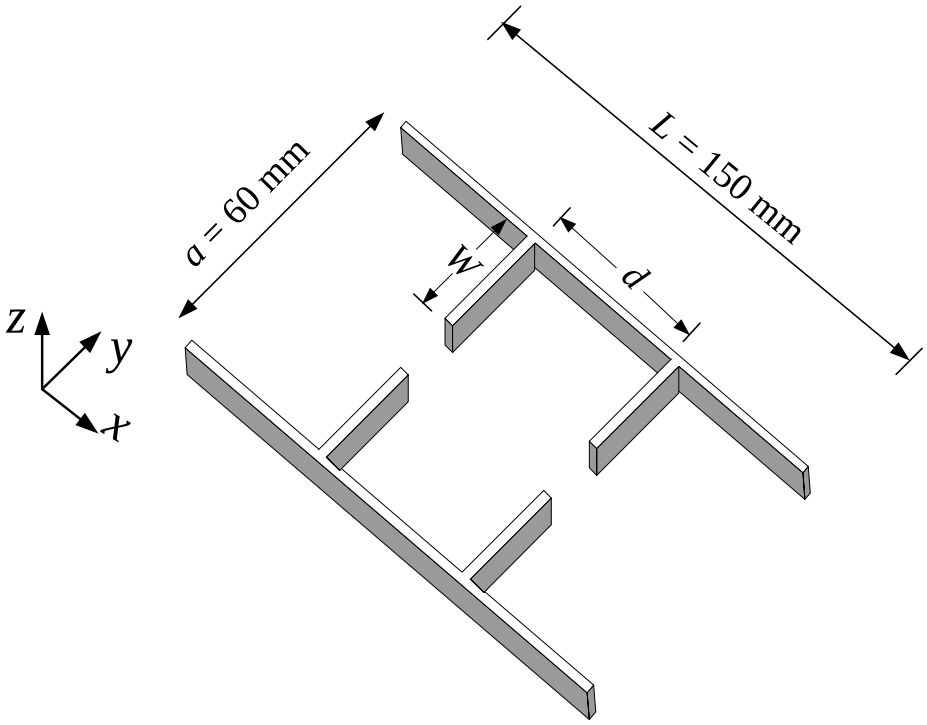

Fig. 4.9 Topology of the single-resonator filter [13].

The fine model employs a Johns matrix boundary [22], [23], [24] as an absorbing boundary condition while the coarse model utilizes a single impulse reflection coefficient calculated at the center frequency (4.0 GHz). Hence, we do not need to calculate the Johns matrix for the coarse model each time we change ε_r. This introduces another source of inaccuracy in the coarse model.

A minimax objective function is used in the design process with upper and lower design specifications

$$\begin{aligned} |S_{21}| &\le 0.65 \text{ for } 3.0 \text{ GHz } \le \omega \le \text{ } 3.4 \text{ GHz} \\ |S_{21}| &\ge 0.95 \text{ for } 3.9 \text{ GHz } \le \omega \le \text{ } 4.1 \text{ GHz} \\ |S_{21}| &\le 0.75 \text{ for } 4.7 \text{ GHz } \le \omega \le \text{ } 5.0 \text{ GHz} \end{aligned}$$

The Matlab [9] least-squares Levenberg-Marquardt algorithm solves the PE problem. The TR subproblem (4.9) is solved by the minimax routine by Hald and Madsen [25], [26] described in [27]. An interpolation scheme with database system is used [10]. The surrogate is calibrated to match the fine model at the last two points in (4.7) and the current point in (4.8). The weighting factors are set to $w_1 = 1$ and $w_2 = 0$.

The algorithm converges in 5 iterations to an optimal fine model response although the coarse model initially exhibits a very poor response (see Fig. 4.10(a)). Fig. 4.10(b) depicts the fine-grid TLM response along with its surrogate response at the final design. The reduction of the objective function of the fine model and the surrogate versus iteration and the progression of the optimization iterates are shown in Fig. 4.11 and Fig. 4.12, respectively. The optimal design

reached by the algorithm is given by d = 32.99 mm and W = 14.59 mm (see Table 4.2 for the optimization summary).

Our proposed approach, without the database system, takes 88 min versus 172 min for direct optimization. Utilizing the database system reduces the execution time to 15 min.

We utilize the time domain TLM simulator MEFiSTo [12] to verify our results. We employ the rubber cell feature [12] in MEFiSTo to examine our interpolation scheme. Using the TLM conformal (rubber) cell [28], the dimensions of the underlying structure, which are not located at multiple integers of the mesh size, will not be shifted to the closest cell boundary. Rather, a change in the size and shape of the TLM boundary cell, due to an irregular boundary position, is translated into a change in its input impedance at the cell interface with a regular computational mesh [28]. Fig. 4.13 shows a good agreement between the interpolated results of the final design obtained from our algorithm and the MEFiSTo simulation utilizing rubber cell.

TABLE 4.2

OPTIMIZATION RESULTS FOR THE SINGLE-RESONATOR FILTER

Iteration	$\boldsymbol{x}_f$ (mm)	ε_r	U_s	U_f
0	$\begin{bmatrix} 29.25 \\ 11.05 \end{bmatrix}$	1.0000	0.1341	0.1870
1	$\begin{bmatrix} 29.98 \\ 12.15 \end{bmatrix}$	1.0637	0.1152	0.1417
2	$\begin{bmatrix} 32.27 \\ 13.37 \end{bmatrix}$	1.0845	0.0543	0.0523
3	$\begin{bmatrix} 33.80 \\ 14.95 \end{bmatrix}$	1.0721	0.0052	0.0001
4	$\begin{bmatrix} 32.99 \\ 14.59 \end{bmatrix}$	1.0139	-0.0072	-0.0072

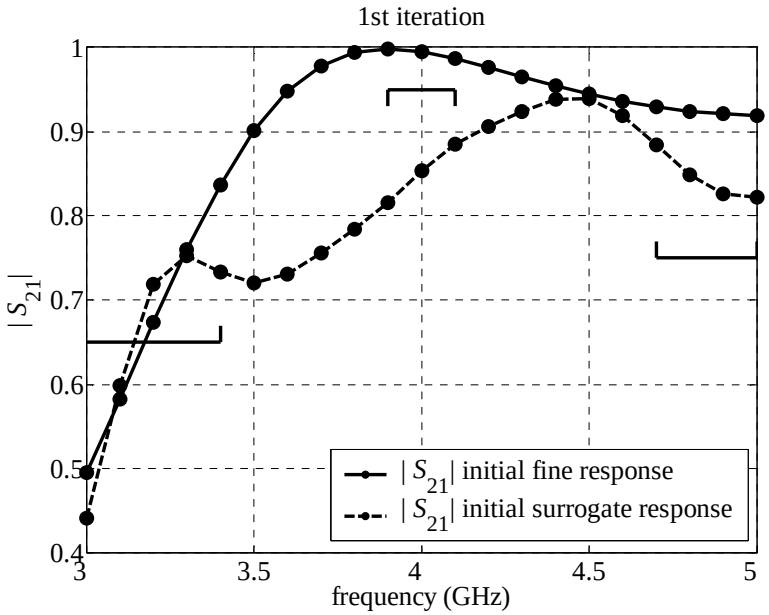

(a)

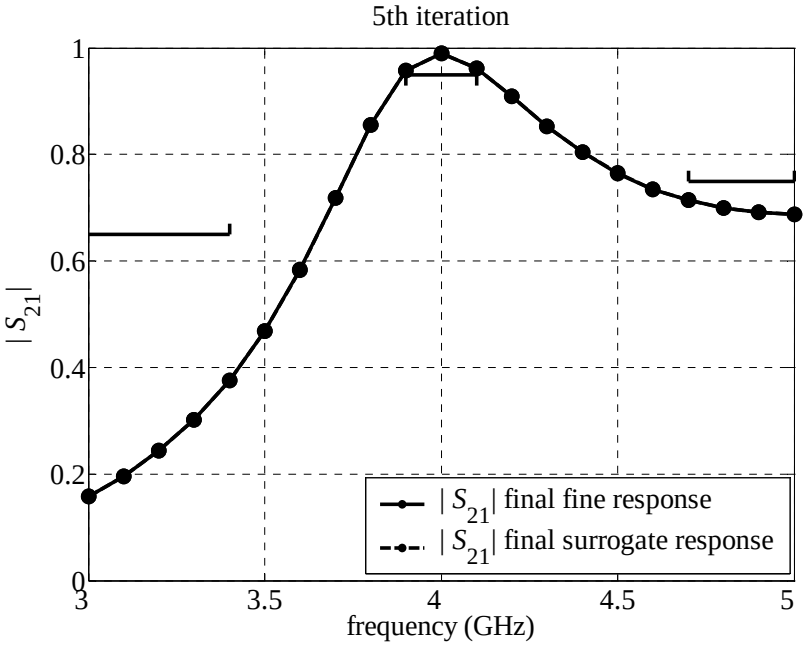

(b)

Fig. 4.10 The surrogate response (--•--) and the corresponding fine model response (–•–) at: (a) the initial design, and (b) the final design (using linear interpolation) for the single-resonator filter.

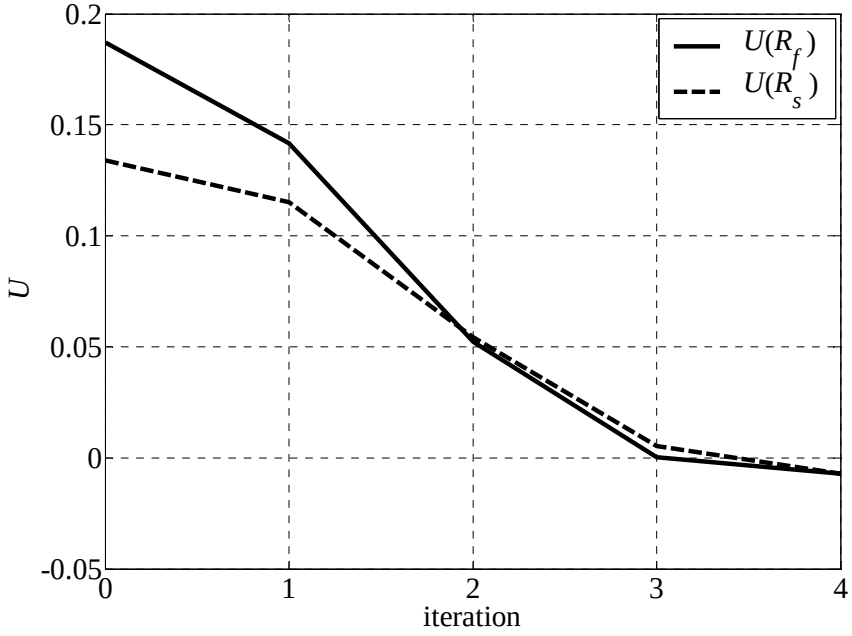

Fig. 4.11 The reduction of the objective function (U) for the fine model (—) and the surrogate (--) for the single-resonator filter.

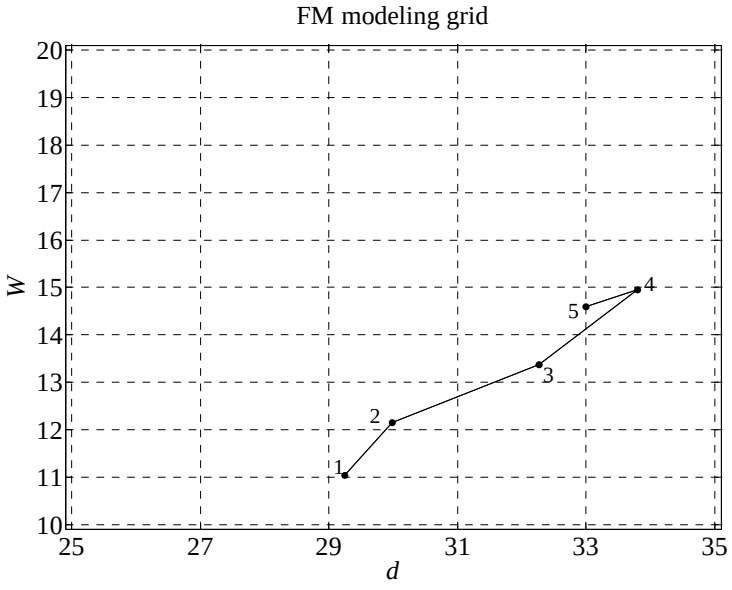

Fig. 4.12 The progression of the optimization iterates for the single-resonator filter on the fine modeling grid (d and W are in mm).

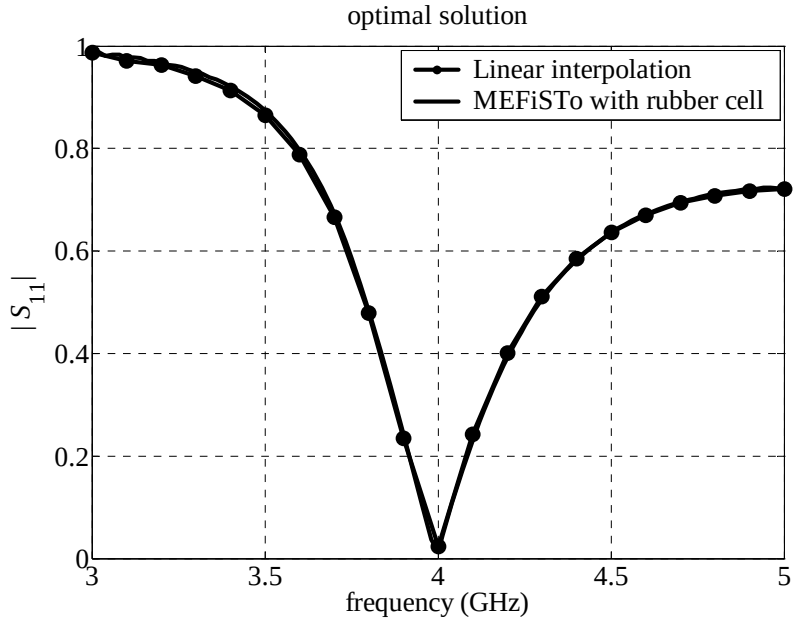

(a)

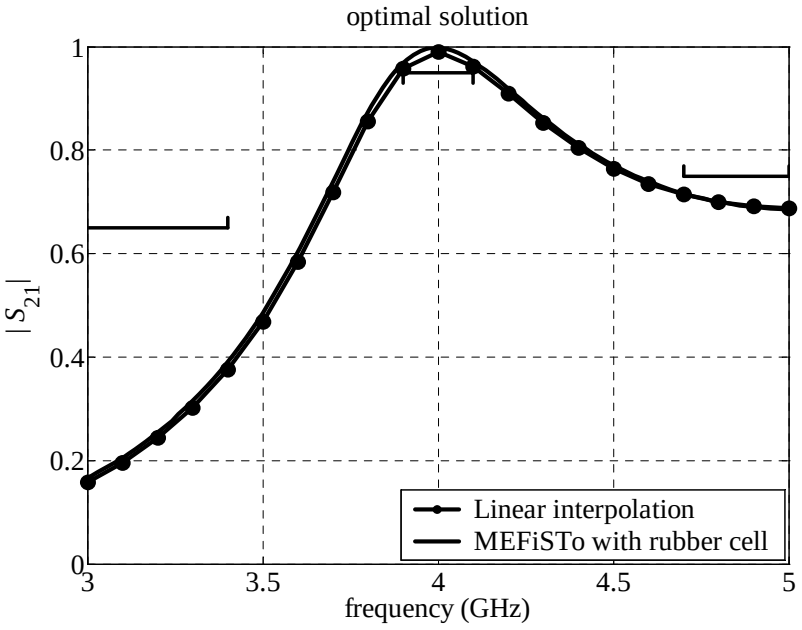

(b)

Fig. 4.13 The final design reached by the algorithm (–•–) versus the simulation results using MEFiSTo 2D with the rubber cell feature (—) for the single-resonator filter: (a) $|S_{11}|$ and (b) $|S_{21}|$.

4.5.3 Six-Section H-plane Waveguide Filter

We consider the six-section H-plane waveguide filter [29], [30] (see 3D view and 2D cross section in Fig. 4.14(a) and (b), respectively). A waveguide with a width 1.372 inches (3.485cm) is used. The propagation mode is TE_{10} with a cutoff frequency of 4.3 GHz. The six-waveguide sections are separated by seven H-plane septa, which have a finite thickness of 0.0245 inches (0.6223 mm). The design parameters are the three waveguide-section lengths L_1, L_2 and L_3 and the septa widths W_1, W_2, W_3 and W_4. A minimax objective function is employed with upper and lower design specifications given by

$$\begin{aligned} &|S_{11}| \le 0.16 \text{ for } 5.4 \text{ GHz } \le \omega \le \text{ } 9.0 \text{ GHz} \\ &|S_{11}| \ge 0.85 \text{ for } \omega \le \text{ } 5.2 \text{ GHz} \\ &|S_{11}| \ge 0.5 \quad \text{for } \omega \ge 9.5 \text{ GHz} \end{aligned}$$

We use the fine model with a square cell $\Delta x = \Delta y = 0.6223$ mm. The number of TLM cells in the x and y directions are $N_x = 301$ and $N_y = 28$, respectively. A Johns matrix boundary [22]–[24] is used as a dispersive absorbing boundary condition with $N_t = 8000$ time steps. We utilize 23 points in the frequency range $\omega \in [5.0, 10.0]$ GHz. We consider the filter design using two different coarse models: empirical coarse model and coarse-grid TLM model. In both cases, we use the least-squares Levenberg-Marquardt algorithm in Matlab [9] for the PE. A linear interpolation scheme with a data base system is utilized for the surrogate optimization using the minimax routine [25]–[27]. The PE is designed to match the fine model with its surrogate utilizing the most recent three

points in (4.7) and the current point in (4.8). We set the weighting factors to w_1 =1 and w_2 = 0.

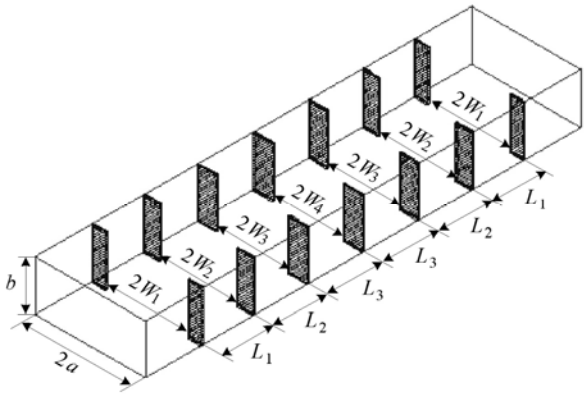

(a)

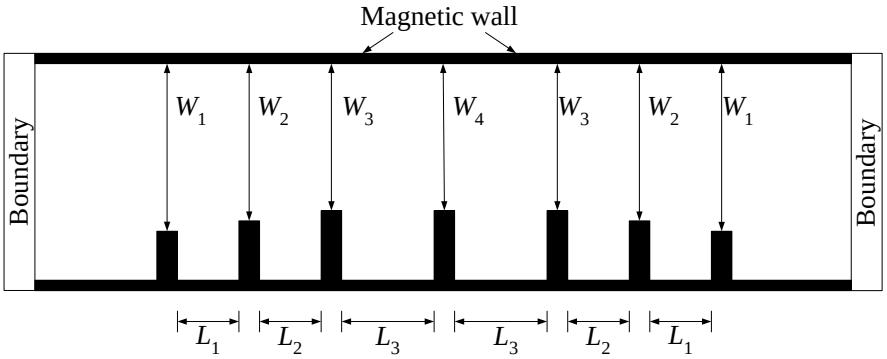

(b)

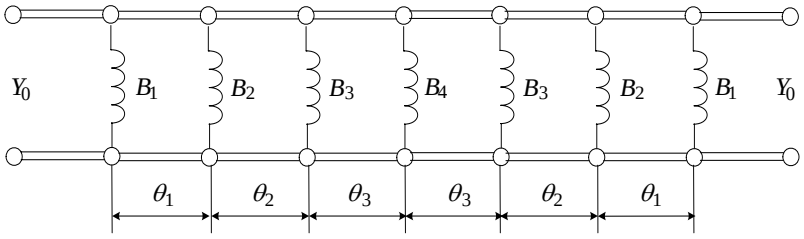

(c)

Fig. 4.14 The six-section H-plane waveguide filter: (a) the 3D view [30], (b) one half of the 2D cross section, and (c) the equivalent empirical circuit model [30].

4.5.3.1 Case 1: Empirical Coarse Model

A coarse model with lumped inductances and dispersive transmission line sections is utilized. We simplify formulas due to Marcuvitz [31] for the inductive susceptances corresponding to the H-plane septa. They are connected to the transmission line sections through circuit theory [32]. The model is implemented and simulated in the Matlab [9] environment. Fig. 4.14(c) shows the empirical circuit model.

The algorithm converges to an optimal solution in 10 iterations. The initial and final designs are shown in Table 4.3. The final value of ε_r = 1.02. The initial and final responses for the fine model and its surrogate are illustrated in Fig. 4.15. Fig. 4.16 depicts the reduction of objective function of the fine model and its surrogate. The final design response using our algorithm is compared with MEFiSTo in Fig. 4.17.

TABLE 4.3

INITIAL AND FINAL DESIGNS FOR
THE SIX-SECTION H-PLANE WAVEGUIDE FILTER
DESIGNED USING THE EMPIRICAL COARSE MODEL

Parameter	Initial design (mm)	Final design (mm)
L_1	16.5440	16.1551
L_2	16.7340	16.1608
L_3	17.1541	16.6330
W_1	12.8118	12.7835
W_2	11.7704	11.7885
W_3	11.2171	11.2415
W_4	11.0982	11.1621

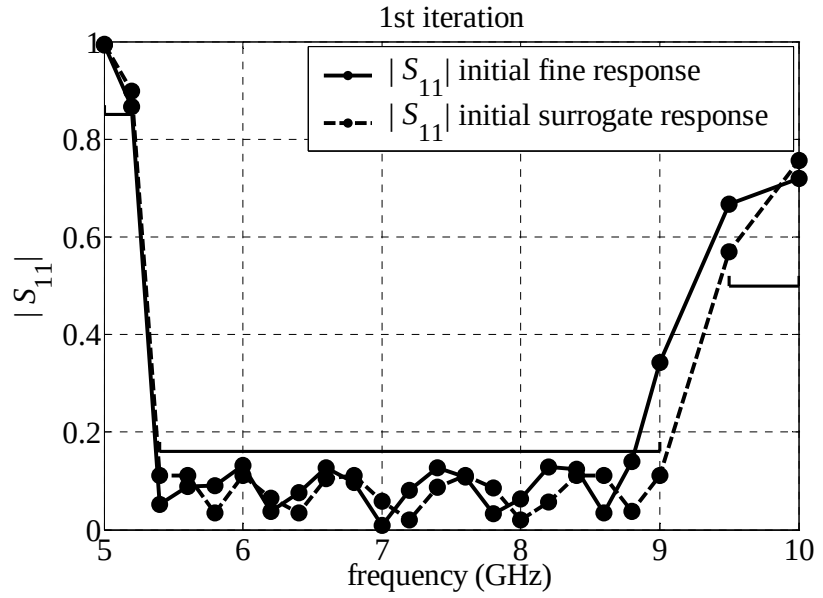

(a)

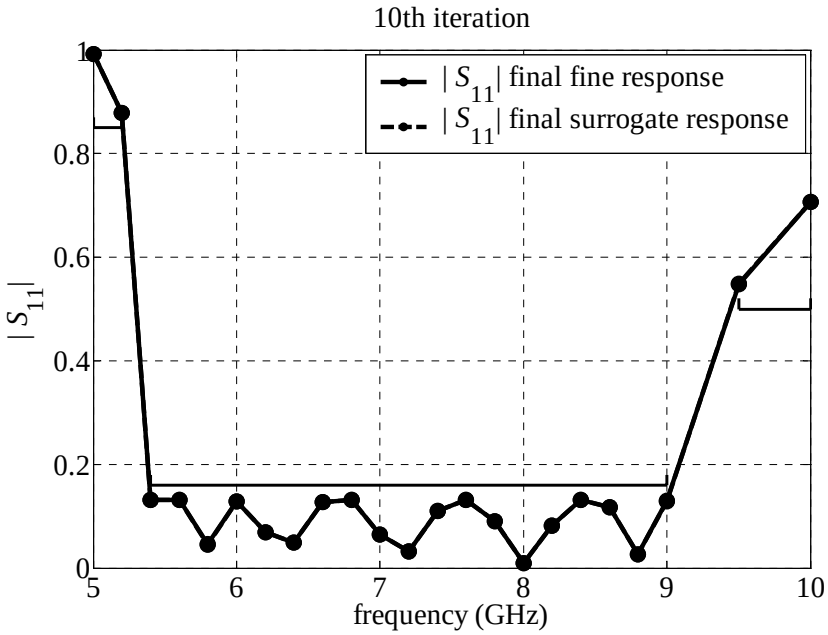

(b)

Fig. 4.15 The surrogate response (--•--) and the corresponding fine model response (–•–) at: (a) the initial design, and (b) the final design (using linear interpolation) for the six-section H-plane waveguide filter designed using the empirical coarse model.

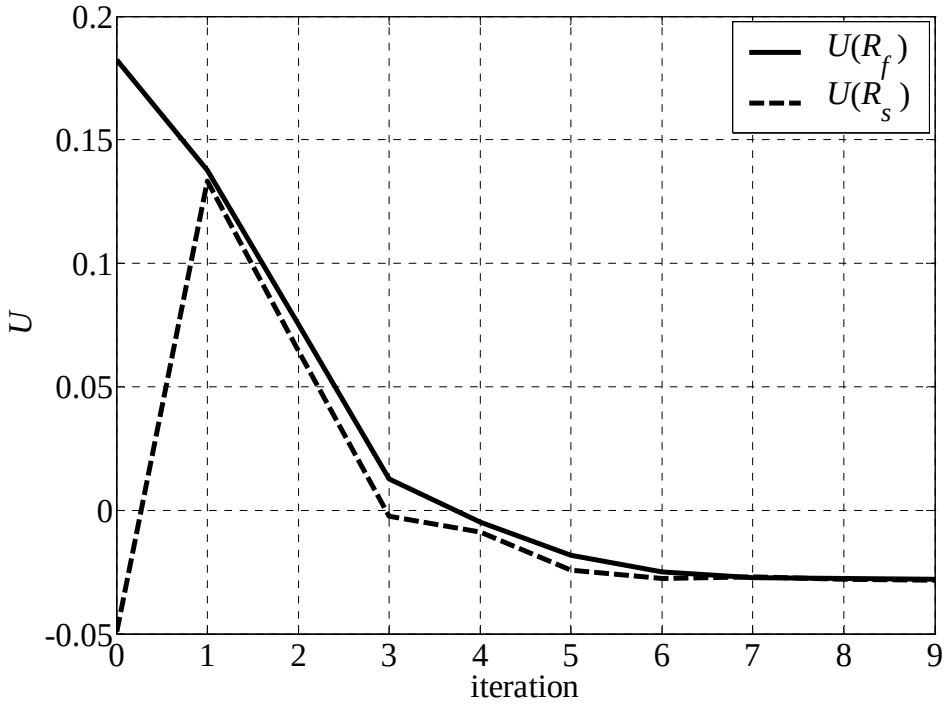

Fig. 4.16 The reduction of the objective function (U) of the fine model (—) and the surrogate (--) for the six-section H-plane waveguide filter designed using the empirical coarse model.

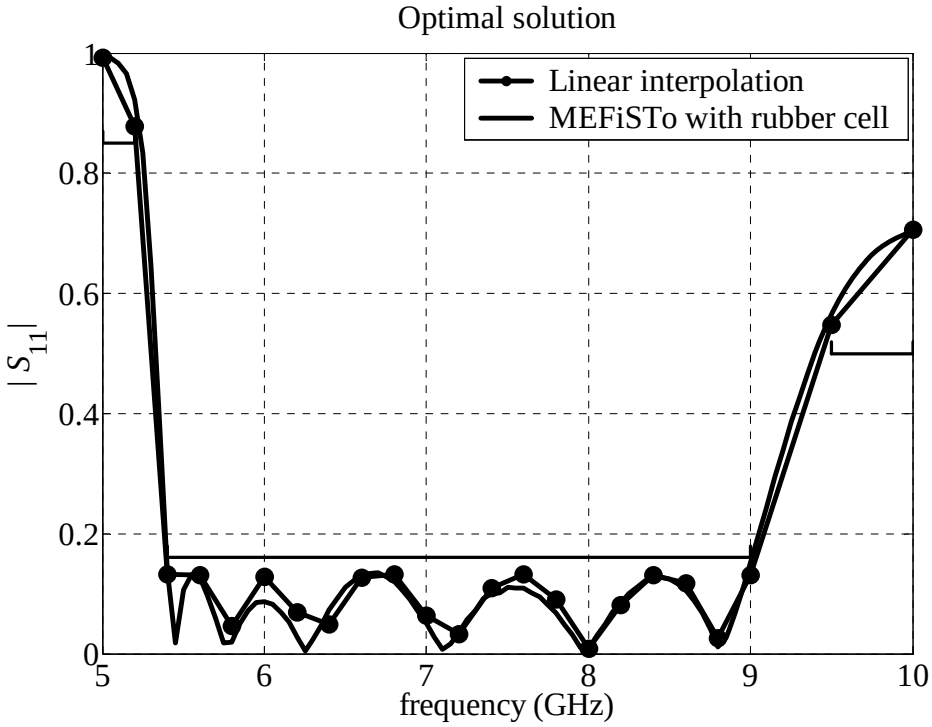

Fig. 4.17 The final design reached by the algorithm (–•–) compared with MEFiSTo 2D simulation with the rubber cell feature (—) for the six-section H-plane waveguide filter designed using the empirical coarse model.

4.5.3.2 Case 2: Coarse-grid TLM Model

We utilize a coarse-grid TLM model with a square cell $\Delta x = \Delta y = 1.2446$ mm. The number of TLM cells in the x and y directions are $N_x = 150$ and $N_y = 14$, respectively. The number of time steps is $N_t = 1000$ time steps. A single impulse reflection coefficient calculated at the center frequency (7.5 GHz) is utilized. We have three sources of inaccuracy of the coarse-grid TLM model, namely, the coarser grid, the inaccurate absorbing boundary conditions and the reduced number of time steps. This reduces the computation time of the coarse model versus the fine model.

Despite the poor starting surrogate response (see Fig. 4.18(a)), the algorithm reaches an optimal solution in 8 iterations. The initial and final designs are shown in Table 4.4. The final value of $\varepsilon_r = 0.991$. The initial and final responses for the fine model and its surrogate are illustrated in Fig. 4.18. The reduction of the objective function of the fine model and its surrogate is shown in Fig. 4.19. The final design response obtained using our algorithm is compared with MEFiSTo simulation in Fig. 4.20. It shows good agreement.

TABLE 4.4

INITIAL AND FINAL DESIGNS FOR
THE SIX-SECTION H-PLANE WAVEGUIDE FILTER
DESIGNED USING THE COARSE-GRID TLM MODEL

Parameter	Initial design (mm)	Final design (mm)
L_1	16.5440	16.1527
L_2	16.7340	16.1788
L_3	17.1541	16.6403
W_1	12.8118	12.7906
W_2	11.7704	11.7694
W_3	11.2171	11.2509
W_4	11.0982	11.1558

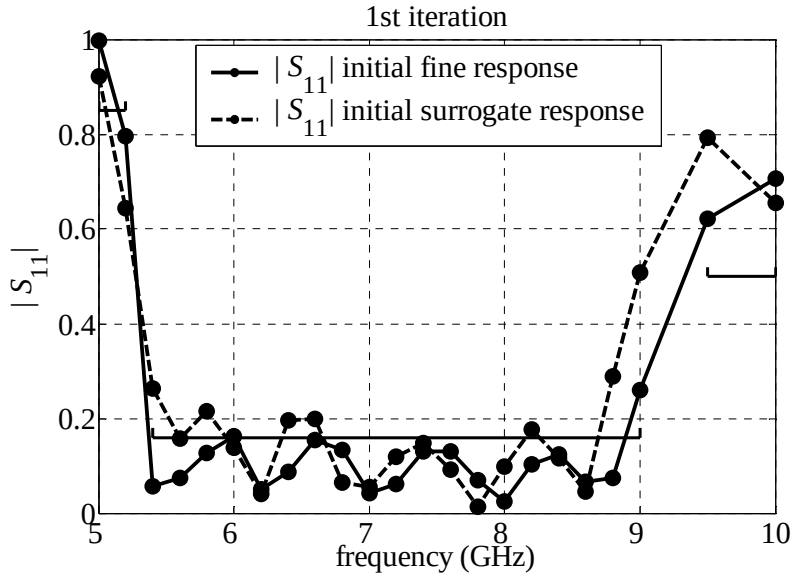

(a)

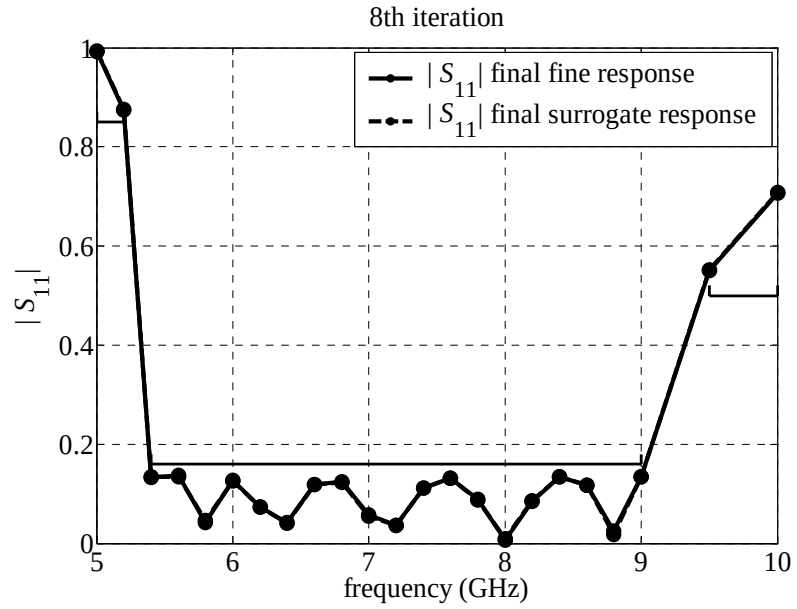

(b)

Fig. 4.18 The surrogate response (--•--) and the corresponding fine model response (–•–) at: (a) the initial design, and (b) the final design (using linear interpolation) for the six-section H-plane waveguide filter designed using the coarse-grid TLM model.

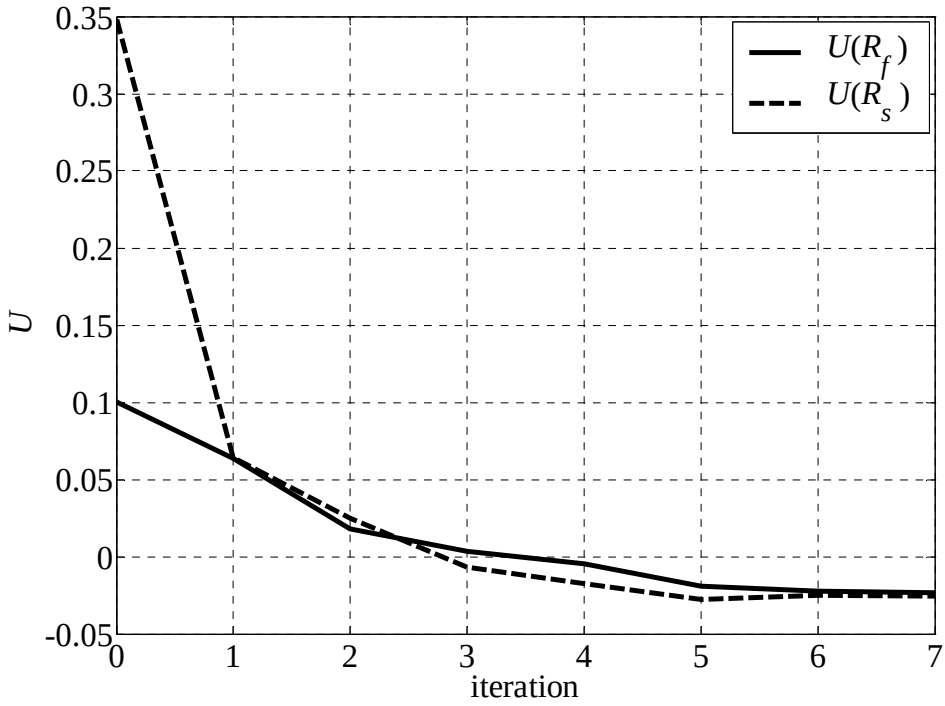

Fig. 4.19 The reduction of the objective function (U) of the fine model (—) and the surrogate (--) for the six-section H-plane waveguide filter designed using the coarse-grid TLM model.

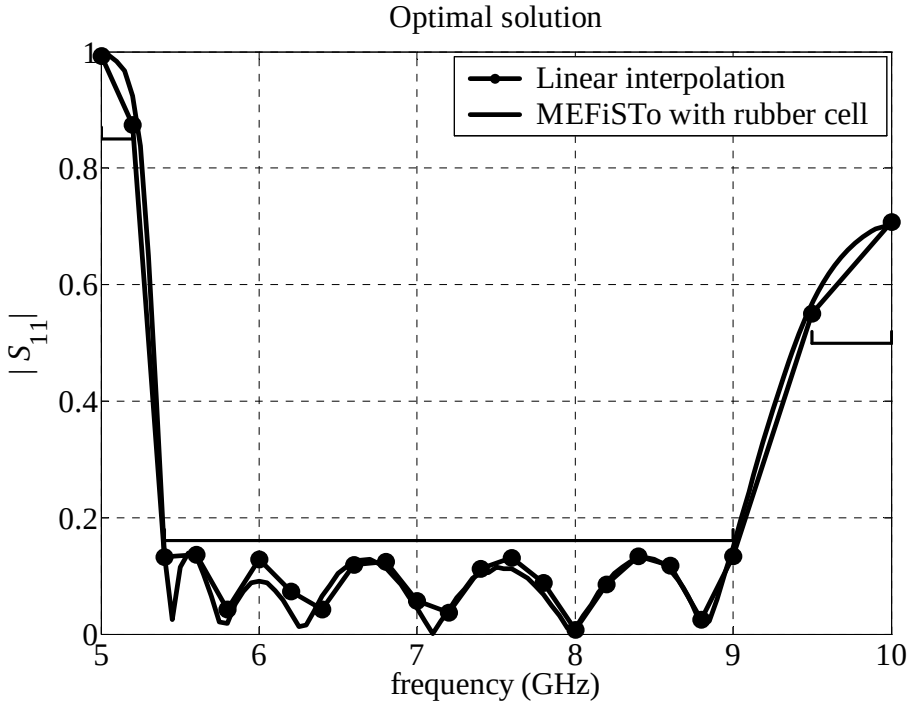

Fig. 4.20 The final design reached by the algorithm (–•–) compared with MEFiSTo 2D simulation with the rubber cell feature (—) for the six-section H-plane waveguide filter designed using the coarse-grid TLM model.

Using the proposed approach, the optimization time is reduced by 66% with respect to direct optimization, as shown in Table V. The dynamically-updated database system, implemented in the algorithm, reduces the optimization time even more, as reported in Table V. The run time for the PE process, surrogate optimization and fine model simulation of our proposed approach are 15, 4 and 58 min, respectively.

TABLE 4.5

OUR APPROACH WITH/WITHOUT DATABASE SYSTEM
VERSUS DIRECT OPTIMIZATION FOR
THE SIX-SECTION H-PLANE WAVEGUIDE FILTER
DESIGNED USING COARSE-GRID TLM MODEL

The proposed approach with database system (hrs)	The proposed approach without database system (hrs)	Direct optimization (hrs)
1.3	10	30

4.6 CONCLUDING REMARKS

In this chapter, we investigate the space mapping approach to modeling and design when the coarse model does not faithfully represent the fine model. In this work, a coarse-grid TLM model with relaxed boundary conditions is utilized as a coarse model. Such a model may provide a response that deviates significantly from the original design specifications and, hence, previous SM

implementations may fail to reach a satisfactory solution. We propose a technique exploiting Implicit SM and Output SM. The dielectric constant, a convenient preassigned parameter, is first calibrated for a rough (preprocessing) alignment between the coarse and fine TLM models. Output SM absorbs the remaining response deviation between the TLM fine-grid model and the implicitly mapped TLM coarse-grid model (the surrogate). To accommodate the discrete nature of our EM simulator, we designed the algorithm to have interpolation and dynamically-updated database capabilities, key to efficient design automation. Our approach is illustrated through the TLM-based design of an inductive post, a single-resonator filter and a six-section H-plane waveguide filter. Our algorithm converges to a good design for the fine-grid TLM model in spite of poor initial behavior of the coarse-grid TLM surrogate.

REFERENCES

[1] J.W. Bandler, Q. Cheng, S.A. Dakroury, A.S. Mohamed, M.H. Bakr, K. Madsen and J. Søndergaard, "Space mapping: the state of the art," *IEEE Trans. Microwave Theory and Tech.*, vol. 52, pp. 337–361, Jan. 2004.

[2] J.W. Bandler, R.M. Biernacki, S.H. Chen, P.A. Grobelny and R.H. Hemmers, "Space mapping technique for electromagnetic optimization," *IEEE Trans. Microwave Theory and Tech.*, vol. 42, pp. 2536–2544, Dec. 1994.

[3] J.W. Bandler, R.M. Biernacki, S.H. Chen, R.H. Hemmers and K. Madsen, "Electromagnetic optimization exploiting aggressive space mapping," *IEEE Trans. Microwave Theory and Tech.*, vol. 43, pp. 2874–2882, Dec. 1995.

[4] J.W. Bandler, Q.S. Cheng, N.K. Nikolova and M.A. Ismail, "Implicit space mapping optimization exploiting preassigned parameters," *IEEE Trans. Microwave Theory and Tech.*, vol. 52, pp. 378–385, Jan. 2004.

[5] J.W. Bandler, Q.S. Cheng, D. Gebre-Mariam, K. Madsen, F. Pedersen and J. Søndergaard, "EM-based surrogate modeling and design exploiting implicit, frequency and output space mappings," in *IEEE MTT-S Int. Microwave Symp. Dig.*, Philadelphia, PA, 2003, pp. 1003–1006.

[6] J.W. Bandler, D.M. Hailu, K. Madsen, and F. Pedersen, "A space-mapping interpolating surrogate algorithm for highly optimized EM-based design of microwave devices," *IEEE Trans. Microwave Theory and Tech.*, vol. 52, pp. 2593–2600, Nov. 2004.

[7] W.J.R. Hoefer, "The transmission-line matrix method—Theory and applications," *IEEE Trans. Microwave Theory and Tech.*, vol. MTT-33, pp. 882–893, Oct. 1985.

[8] J.W. Bandler, A.S. Mohamed and M.H. Bakr, "TLM modeling and design exploiting space mapping," *IEEE Trans. Microwave Theory Tech.*, vol. 53, 2005.

[9] Matlab, The MathWorks, Inc., 3 Apple Hill Drive, Natick, MA 01760–2098, USA.

[10] J.W. Bandler, R.M. Biernacki, S.H. Chen, L.W. Hendrick and D. Omeragic, "Electromagnetic optimization of 3D structures," *IEEE Trans. Microwave Theory and Tech.*, vol. 45, pp. 770–779, May 1997.

[11] P.A. Grobelny, *Integrated Numerical Modeling Techniques for Nominal and Statistical Circuit Design*, Ph.D. Thesis, Department of Electrical and Computer Engineering, McMaster University, Hamilton, ON, Canada, 1995.

[12] MEFiSTo-3D, Faustus Scientific Corporation, 1256 Beach Drive, Victoria, BC, V8S 2N3, Canada.

[13] M.H. Bakr, P.P.M. So and W.J.R. Hoefer, "The generation of optimal microwave topologies using time-domain field synthesis," *IEEE Trans. Microwave Theory and Tech*., vol. 50, pp. 2537–2544, Nov. 2002.

[14] J.W. Bandler, M.A. Ismail and J.E. Rayas-Sánchez, "Expanded space mapping EM-based design framework exploiting preassigned parameters," *IEEE Trans. Circuits and Systems—I*, vol. 49, pp. 1833–1838, Dec. 2002.

[15] A.R. Conn, N.I.M. Gould and P.L. Toint, *Trust-Region Methods*. Philadelphia, PA: SIAM and MPS, 2000.

[16] N.M. Alexandrov, J.E. Dennis Jr, R.M. Lewis and V. Torczon, "A trust-region framework for managing the use of approximation models in optimization," *Struct. Optim.*, vol. 15, pp. 16–23, 1998.

[17] M.H. Bakr, J.W. Bandler, R.M. Biernacki, S.H. Chen and K. Madsen, "A trust region aggressive space mapping algorithm for EM optimization," *IEEE Trans. Microwave Theory and Tech.*, vol. 46, pp. 2412–2425, Dec. 1998.

[18] J.W. Bandler, R.M. Biernacki and S.H. Chen, "Fully automated space mapping optimization of 3D structures," in *IEEE MTT-S Int. Microwave Symp. Dig.*, San Francisco, CA, 1996, pp. 753–756.

[19] J.W. Bandler, R.M. Biernacki, S.H. Chen and D. Omeragic, "Space mapping optimization of waveguide filters using finite element and mode-matching electromagnetic simulators," *Int. J. RF and Microwave CAE*, vol. 9, pp. 54–70, 1999.

[20] J. Søndergaard, *Optimization Using Surrogate Models—by the Space Mapping Technique*, Ph.D. Thesis, Informatics and Mathematical Modelling (IMM), Technical University of Denmark (DTU), Lyngby, Denmark, 2003.

[21] M.H. Bakr, *2D-TLM Matlab Implementation*, Department of Electrical and Computer Engineering, McMaster University, Hamilton, ON, Canada, 2004.

[22] P.B. Johns and K. Akhtarzad, "The use of time domain diakoptics in time discrete models of fields," *Int. J. Num. Methods Eng.*, vol. 17, pp. 1–14, 1981.

[23] P.B. Johns and K. Akhtarzad, "Time domain approximations in the solution of fields by time domain diakoptics," *Int. J. Num. Methods Eng.*, vol. 18, pp. 1361–1373, 1982.

[24] Eswarappa, G.I. Costache and W.J.R. Hoefer, "Transmission line matrix modeling of dispersive wide-band absorbing boundaries with time-domain diakoptics for S-parameter extraction", *IEEE Trans. Microwave Theory and Tech.*, vol. 38, pp 379–386, Apr. 1990.

[25] K. Madsen, "An algorithm for minimax solution of overdetermined systems of non-linear equations," *J. Inst. Mathematics and its Applications*, vol. 16, pp. 321–328, 1975.

[26] J. Hald and K. Madsen, "Combined LP and quasi-Newton methods for minimax optimization," *Mathematical Programming*, vol. 20, pp. 49–62, 1981.

[27] K. Madsen, H.B. Nielsen and J. Søndergaard, "Robust subroutines for non-linear optimization," DTU, Lyngby, Denmark, *Technical Report IMM-REP-2002-02,* 2002.

[28] P.P.M. So and W.J.R. Hoefer, "Locally conformal cell for two-dimensional TLM," in *IEEE MTT-S Int. Microwave Symp. Dig.*, Philadelphia, PA, 2003, pp. 977–980.

[29] G.L. Matthaei, L. Young and E.M.T. Jones, *Microwave Filters, Impedance-Matching Networks, and Coupling Structures*, 1st ed. New York, NY: McGraw-Hill, 1964.

[30] M.H. Bakr, J.W. Bandler, N. Georgieva and K. Madsen, "A hybrid aggressive space mapping algorithm for EM optimization," *IEEE Trans. Microwave Theory and Tech.*, vol. 47, pp. 2440–2449, Dec. 1999.

[31] N. Marcuvitz, *Waveguide Handbook*, 1st ed. New York, NY: McGraw-Hill, 1951, p.221.

[32] M. Pozar, *Microwave Engineering*, 2nd ed. New York, NY: Wiley, 1998.

CHAPTER 5

CONCLUSIONS

This thesis describes the recent trends in the microwave circuit CAD tools exploiting the SM technology. The simple CAD methodology follows the traditional experience and intuition of engineers, yet appears to be amenable to rigorous mathematical treatment.

In Chapter 2, the SM technique and the SM-oriented surrogate (modeling) concept and their applications in engineering design optimization are reviewed. The aim and advantages of SM are described. Proposed approaches to SM-based optimization include the original SM algorithm, the Broyden-based aggressive space mapping, trust region aggressive space mapping, hybrid aggressive space mapping, neural space mapping and implicit space mapping. We also present a mathematical motivation for SM. We place SM into the context of classical optimization, which is based on local Taylor approximations. The SM model is seen as a good approximation over a large region, i.e., it is efficient in the initial phase when large iteration steps are needed, whereas the first-order Taylor model is better close to the solution. We briefly discuss convergence issues for the SM algorithms which are now emerging. Interesting SM and surrogate applications

are reviewed. They indicate that exploitation of properly managed "space mapped" surrogates promises significant efficiency in all branches of engineering design.

In Chapter 3, we present a family of robust techniques for exploiting sensitivities in EM–based circuit optimization through SM. We exploit a partial SM concept where a reduced set of parameters is sufficient in the PE process. Available gradients can initialize mapping approximations. Exact or approximate Jacobians of responses can be utilized. For flexibility, we propose different possible "mapping matrices" for the PE processes and SM iterations. Finite differences may be used to initialize the mapping. A hybrid approach incorporating the Broyden formula can be used for mapping updates. Our approaches have been tested on several examples. They demonstrate simplicity of implementation, robustness, and do not rely on designer intervention. Final mappings are useful in statistical analysis and yield optimization. Furthermore, the notion of exploiting reduced sets of physical parameters reflects the important idea of postproduction tuning.

In Chapter 4, we investigate, for the first time, the space mapping approach to modeling and design when the coarse model does not faithfully represent the fine model. In this work, a coarse-grid TLM model with relaxed boundary conditions is utilized as a coarse model. Such a model may provide a response that deviates significantly from the original design specifications and, hence, previous SM implementations may fail to reach a satisfactory solution.

We propose a technique exploiting implicit SM and output SM. The dielectric constant, a convenient preassigned parameter, is first calibrated for a rough (preprocessing) alignment between the coarse and fine TLM models. Output SM absorbs the remaining response deviation between the TLM fine-grid model and the implicitly mapped TLM coarse-grid model (the surrogate). To accommodate the discrete nature of our EM simulator, we designed the algorithm to have interpolation and dynamically-updated database capabilities, key to efficient design automation. Our approach is illustrated through the TLM-based design of an inductive post, a single-resonator filter and a six-section H-plane waveguide filter. Our algorithm converges to a good design for the fine-grid TLM model in spite of poor initial behavior of the coarse-grid TLM surrogate.

From the experience gained during the course of this work, the author suggests the following research topics to be addressed in future developments.

(1) Exploiting the gradient-based SM approach in statistical analysis and yield optimization.

(2) Applying SM optimization algorithms exploiting sensitivity formulations in problems of special interest such as the design of antenna structures.

(3) Utilizing the gradient-based SM technique to produce enhanced models for microwave structures and build library models for the microwave components.

(4) Employing different dielectric constants, as preassigned parameters, for different regions of the underlying microwave structure to provide better results in the modeling process.

(5) Incorporating the gradient PE process within the TLM environment to improve the construction of the surrogate, e.g., exploiting adjoint variable methods.

(6) Building an SM engine that incorporates different SM algorithms for modeling and design. This emerges from our capability to drive different full EM solvers such as Sonnet's ***em***, Ansoft HFSS, MEFiSTo Pro, etc., from programming environments such as Matlab or Visual C++.

APPENDIX A

BROYDEN VERSUS BFGS UPDATE

The SM techniques incorporate a procedure to update (extract) the mapping $\boldsymbol{P}$ [1]–[2]. The mapping Jacobian is approximated by the matrix $\boldsymbol{B}$, i.e., $\boldsymbol{B} \approx \boldsymbol{J}_P(\boldsymbol{x}_f)$ (See Chapter 2 for further details). In Chapter 3, we reviewed different schemes proposed in the literature to update the matrix $\boldsymbol{B}$. In the aggressive SM approach [2], a proposed technique based on the Broyden rank-1 formula [3] is employed to update $\boldsymbol{B}$. The Broyden-based scheme exhibits good results [2]. In this appendix, we compare the usage of BFGS rank-2 updating formula versus the Broyden rank-1 formula for the aggressive SM techniques. We propose a modified BFGS rank-2 updating formula for the non-symmetric case, e.g., Jacobian matrix. We start with a theoretical discussion followed by an illustrative example.

A.1 THEORETICAL DISCUSSION

The aggressive SM solves the nonlinear system

$$\boldsymbol{f} \triangleq \boldsymbol{f}(\boldsymbol{x}_f) = \boldsymbol{P}(\boldsymbol{x}_f) - \boldsymbol{x}_c^* = \boldsymbol{0} \tag{A.1}$$

for $\boldsymbol{x}_f \in X_f \subseteq \mathbb{R}^n$ where $\boldsymbol{f}: \mathbb{R}^n \mapsto \mathbb{R}^n$ is a vector valued function. According to Newton Method for nonlinear equations [4], the solution of (A.1) at the *j*th iteration is given by

$$\begin{aligned} \boldsymbol{x}_f^{(j+1)} &= \boldsymbol{x}_f^{(j)} + \boldsymbol{h}^{(j)} \\ \boldsymbol{J}_P^{(j)} \boldsymbol{h}^{(j)} &= -\boldsymbol{f}^{(j)} \end{aligned} \tag{A.2}$$

A.1.1 The Broyden Method

Since the first-order information (required to evaluate $\boldsymbol{J}_P$) may be difficult to obtain, Broyden [3] suggested a formula which updates an estimate of the Jacobian matrix $\boldsymbol{B}^{(j+1)} \approx \boldsymbol{J}_P^{(j+1)}$ iteratively by satisfying the secant condition [4]

$$\boldsymbol{y}^{(j)} = \boldsymbol{B}^{(j+1)} \boldsymbol{h}^{(j)} \tag{A.3}$$

where $\boldsymbol{h}^{(j)}$ and $\boldsymbol{y}^{(j)}$ denotes the difference between the successive iterates and the successive function values, respectively, i.e.,

$$\boldsymbol{h}^{(j)} = \boldsymbol{x}_f^{(j+1)} - \boldsymbol{x}_f^{(j)}, \qquad \boldsymbol{y}^{(j)} = \boldsymbol{f}^{(j+1)} - \boldsymbol{f}^{(j)} \tag{A.4}$$

Broyden proposed a correction matrix $\boldsymbol{C}^{(j)}$ to iteratively approximate the Jacobian matrix as [5], [6]

$$\boldsymbol{B}^{(j+1)} = \boldsymbol{B}^{(j)} + \boldsymbol{C}^{(j)} \tag{A.5}$$

In the case of a rank-1 updating matrix, $\boldsymbol{C}^{(j)}$ can be given by the outer product of two vectors $\boldsymbol{a}^{(j)}, \boldsymbol{b}^{(j)} \in \mathbb{R}^n$ as

$$\boldsymbol{B}^{(j+1)} = \boldsymbol{B}^{(j)} + \alpha \boldsymbol{a}^{(j)} \boldsymbol{b}^{(j)T} \tag{A.6}$$

where α is a real constant. Broyden chose $\boldsymbol{a}^{(j)}$ and $\boldsymbol{b}^{(j)}$ as [3]

$$\begin{aligned} \boldsymbol{a}^{(j)} &= \boldsymbol{y}^{(j)} - \boldsymbol{B}^{(j)}\boldsymbol{h}^{(j)}, \text{ and} \\ \boldsymbol{b}^{(j)} &= \boldsymbol{h}^{(j)} \end{aligned} \tag{A.7}$$

By substituting (A.7) in (A.6) and then multiplying both sides by $\boldsymbol{h}^{(j)}$, we get

$$\boldsymbol{B}^{(j+1)}\boldsymbol{h}^{(j)} = \boldsymbol{B}^{(j)}\boldsymbol{h}^{(j)} + \alpha\left(\boldsymbol{y}^{(j)} - \boldsymbol{B}^{(j)}\boldsymbol{h}^{(j)}\right)\boldsymbol{h}^{(j)T}\boldsymbol{h}^{(j)} \tag{A.8}$$

To satisfy the secant condition $\boldsymbol{y}^{(j)} = \boldsymbol{B}^{(j+1)}\boldsymbol{h}^{(j)}$, the coefficient α can be calculated as

$$\alpha\boldsymbol{h}^{(j)T}\boldsymbol{h}^{(j)} = 1 \Rightarrow \alpha = \frac{1}{\boldsymbol{h}^{(j)T}\boldsymbol{h}^{(j)}} \tag{A.9}$$

This produces the Broyden non-symmetric rank-1 formula for updating the Jacobian [3], [4]

$$\boldsymbol{B}^{(j+1)} = \boldsymbol{B}^{(j)} + \frac{\boldsymbol{y}^{(j)} - \boldsymbol{B}^{(j)}\boldsymbol{h}^{(j)}}{\boldsymbol{h}^{(j)T}\boldsymbol{h}^{(j)}}\boldsymbol{h}^{(j)T} \tag{A.10}$$

From another prospective, the secant condition (A.3) can be viewed as a system of n linear equations in n^2 unknowns, where the unknowns are the elements of the matrix $\boldsymbol{B}^{(j+1)}$. This system is an underdetermined system with non-unique solution [4]. To determine $\boldsymbol{B}^{(j+1)}$ uniquely, the Broyden's method makes the smallest possible change to the Jacobian measured by the Euclidean norm $\left\|\boldsymbol{B}^{(j+1)} - \boldsymbol{B}^{(j)}\right\|$. Dennis and Schnabel [7] presented a Lemma showing that among all matrices $\boldsymbol{B}$ satisfying the secant condition $\boldsymbol{B}\boldsymbol{h}^{(j)} = \boldsymbol{y}^{(j)}$, the matrix

$\boldsymbol{B}^{(j+1)}$ defined by (A.10) minimizes the difference $\left\|\boldsymbol{B}-\boldsymbol{B}^{(j)}\right\|$. In other words, $\boldsymbol{B}^{(j+1)}$ in (A.10) is the solution to the optimization problem [4]

$$\begin{aligned} \boldsymbol{B}^{(j+1)} &= \arg\min_{\boldsymbol{B}} \left\|\boldsymbol{B}-\boldsymbol{B}^{(j)}\right\| \\ s.t. \quad & \boldsymbol{B}\boldsymbol{h}^{(j)} = \boldsymbol{y}^{(j)} \end{aligned} \tag{A.11}$$

A.1.2 The BFGS Method

The BFGS method was introduced in the context of quasi-Newton methods for nonlinear optimization [4]. In unconstrained optimization, the following objective function is used

$$\min_{\boldsymbol{x}} g(\boldsymbol{x}) \tag{A.12}$$

where $\boldsymbol{x} \in \mathbb{R}^n$ and $g : \mathbb{R}^n \mapsto \mathbb{R}$ is a scalar function.

In this case, the BFGS method primarily forms the local quadratic model $m^{(j)}$ of the objective function at the current iterate as

$$m^{(j)}(\boldsymbol{x}^{(j)}+\boldsymbol{h}) = g^{(j)} + \nabla g^{(j)T}\boldsymbol{h} + \tfrac{1}{2}\boldsymbol{h}^T\boldsymbol{H}^{(j)}\boldsymbol{h} \tag{A.13}$$

where $\boldsymbol{h}$ is the step suggested by the algorithm and $\nabla g^{(j)}$ and $\boldsymbol{H}^{(j)}$ are the function gradient and Hessian, in a vector and matrix forms, at the current iterate, respectively.

Instead of computing the Hessian matrix $\boldsymbol{H}^{(j)}$ at every iteration, Davidon [8] proposed to update it using an approximating matrix $\boldsymbol{B}^{(j)}$ to account for the

curvature measured during the most recent steps [4]. Here, $\boldsymbol{B}^{(j)}$ is a symmetric and positive definite matrix that satisfies the secant condition [4]

$$\boldsymbol{y}^{(j)} = \boldsymbol{B}^{(j+1)}\boldsymbol{h}^{(j)} \tag{A.14}$$

where $\boldsymbol{h}^{(j)}$ and $\boldsymbol{y}^{(j)}$ are given by

$$\boldsymbol{h}^{(j)} = \boldsymbol{x}_f^{(j+1)} - \boldsymbol{x}_f^{(j)}, \qquad \boldsymbol{y}^{(j)} = \nabla g^{(j+1)} - \nabla g^{(j)} \tag{A.15}$$

The secant condition admits infinite number of solutions, since there are $n(n+1)/2$ degrees of freedom in a symmetric matrix, and the secant condition has only n equations. The requirement of positive definiteness imposes n additional inequalities. However, there are still remaining degrees of freedom [4].

In [4], it is shown that to determine $\boldsymbol{B}^{(j+1)}$ uniquely, an additional condition is imposed that among all symmetric matrices satisfying the secant condition, $\boldsymbol{B}^{(j+1)}$ is closest to the current matrix $\boldsymbol{B}^{(j)}$. In other words, $\boldsymbol{B}^{(j+1)}$ is the solution to the optimization problem [4]

$$\begin{aligned} &\boldsymbol{B}^{(j+1)} = \arg\min_{\boldsymbol{B}} \left\| \boldsymbol{B} - \boldsymbol{B}^{(j)} \right\| \\ &s.t. \qquad \boldsymbol{B}\boldsymbol{h}^{(j)} = \boldsymbol{y}^{(j)}, \qquad \boldsymbol{B} = \boldsymbol{B}^T \end{aligned} \tag{A.16}$$

where, $\boldsymbol{h}^{(j)}$ and $\boldsymbol{y}^{(j)}$ are given by (A.15) and the norm used is the weighted Frobenius norm [4].

By imposing the conditions (A.16) on the inverse of the Hessian approximation instead of the Hessian itself and then applying the Sherman-Morrison-Woodbury formula [4], the rank-2 BFGS updating formula for the Hessian approximation matrix $\boldsymbol{B}^{(j+1)}$ can be given by [3]–[5]

$$\boldsymbol{B}^{(j+1)} = \boldsymbol{B}^{(j)} + \frac{\boldsymbol{y}^{(j)}\boldsymbol{y}^{(j)T}}{\boldsymbol{y}^{(j)T}\boldsymbol{h}^{(j)}} - \frac{\boldsymbol{B}^{(j)}\boldsymbol{h}^{(j)}\boldsymbol{h}^{(j)T}\boldsymbol{B}^{(j)T}}{\boldsymbol{h}^{(j)T}\boldsymbol{B}^{(j)}\boldsymbol{h}^{(j)}} \tag{A.17}$$

A.1.3 Comment

Based on our discussion, we conclude that the techniques for solving nonlinear equations have similar characteristics with nonlinear optimization techniques. Despite these similarities, there are some important differences. One of those differences is the derivative information requirement. In optimization, knowledge of the second-order information (by approximating the Hessian) of the objective function is essential, whereas first-order information is sufficient in solving a system of nonlinear equations [4].

Comparing, (A.11), to obtain the Jacobian approximation, and (A.16), to approximate the Hessian, we realize that the use of the BFGS updating formula (A.17) to update the Jacobian matrix has no relevance. This is because the conditions imposed in (A.16) that produce the BFGS updating formula (A.17), symmetry and positive definiteness of the Hessian matrix, do not hold in the case of the Jacobian matrix. The Jacobian matrix is not symmetric and not necessarily positive definite but the Hessian matrix is. Therefore, we expect that using the BFGS updating formula (A.17) directly instead of the Broyden formula (A.10) in solving the system of nonlinear equation (A.1) will give poor results.

We propose a new approach to update the Jacobian matrix used in solving the system of nonlinear equations (A.1) employing a rank-2 updating formula. In this approach, we develop a non-symmetric rank-2 updating formula to adopt the

Jacobian matrix characteristics. The proposed formula is based on the BFGS method.

A.1.4 A Non-Symmetric BFGS Updating Formula

In the case of a rank-2 updating matrix, the successive approximation formula (A.5) can be given by [5]

$$\boldsymbol{B}^{(j+1)} = \boldsymbol{B}^{(j)} + \alpha \boldsymbol{a}^{(j)} \boldsymbol{b}^{(j)T} + \beta \boldsymbol{c}^{(j)} \boldsymbol{d}^{(j)T} \tag{A.18}$$

where α and β are real constants. $\boldsymbol{a}^{(j)}, \boldsymbol{b}^{(j)}, \boldsymbol{c}^{(j)}$ and $\boldsymbol{d}^{(j)} \in \mathbb{R}^n$ and they can be chosen for symmetric BFGS update as follows [5]

$$\begin{aligned} \boldsymbol{a}^{(j)} &= \boldsymbol{b}^{(j)} = \boldsymbol{u}^{(j)}, \\ \boldsymbol{c}^{(j)} &= \boldsymbol{d}^{(j)} = \boldsymbol{v}^{(j)} \end{aligned} \tag{A.19}$$

Here, for the proposed non-symmetric update, we choose

$$\begin{aligned} &\boldsymbol{a}^{(j)} = \boldsymbol{u}^{(j)}, \boldsymbol{b}^{(j)} = \boldsymbol{v}^{(j)}, \text{ and} \\ &\boldsymbol{c}^{(j)} = \boldsymbol{v}^{(j)}, \boldsymbol{d}^{(j)} = \boldsymbol{u}^{(j)} \end{aligned} \tag{A.20}$$

Hence, the general updating formula for non-symmetric case becomes

$$\boldsymbol{B}^{(j+1)} = \boldsymbol{B}^{(j)} + \alpha \boldsymbol{u}^{(j)} \boldsymbol{v}^{(j)T} + \beta \boldsymbol{v}^{(j)} \boldsymbol{u}^{(j)T} \tag{A.21}$$

We apply the secant condition (A.3) by multiplying both sides of (A.21) by $\boldsymbol{h}^{(j)}$ where $\boldsymbol{y}^{(j)}$ and $\boldsymbol{h}^{(j)}$ are given by (A.4)

$$\boldsymbol{y}^{(j)} = \boldsymbol{B}^{(j+1)} \boldsymbol{h}^{(j)} = \boldsymbol{B}^{(j)} \boldsymbol{h}^{(j)} + \alpha \boldsymbol{u}^{(j)} \boldsymbol{v}^{(j)T} \boldsymbol{h}^{(j)} + \beta \boldsymbol{v}^{(j)} \boldsymbol{u}^{(j)T} \boldsymbol{h}^{(j)} \tag{A.22}$$

Fletcher [5] points out that an obvious choice is to use

$$\begin{aligned} \boldsymbol{u}^{(j)} &= \boldsymbol{B}^{(j)}\boldsymbol{h}^{(j)}, \text{ and} \\ \boldsymbol{v}^{(j)} &= \boldsymbol{y}^{(j)} \end{aligned} \tag{A.23}$$

and to satisfy the secant condition, the coefficients α and β are given by

$$\begin{aligned} \alpha \boldsymbol{v}^{(j)T}\boldsymbol{h}^{(j)} = -1 \Rightarrow \alpha &= \frac{-1}{\boldsymbol{v}^{(j)T}\boldsymbol{h}^{(j)}} = \frac{-1}{\boldsymbol{y}^{(j)T}\boldsymbol{h}^{(j)}}, \text{ and} \\ \beta \boldsymbol{u}^{(j)T}\boldsymbol{h}^{(j)} = 1 \Rightarrow \beta &= \frac{1}{\boldsymbol{u}^{(j)T}\boldsymbol{h}^{(j)}} = \frac{1}{\boldsymbol{h}^{(j)T}\boldsymbol{B}^{(j)T}\boldsymbol{h}^{(j)}} \end{aligned} \tag{A.24}$$

By substituting the values of α and β (A.24) and $\boldsymbol{u}^{(j)}$ and $\boldsymbol{v}^{(j)}$ (A.23) into (A.21), the proposed non-symmetric rank-2 updating formula becomes

$$\boldsymbol{B}^{(j+1)} = \boldsymbol{B}^{(j)} - \frac{\boldsymbol{B}^{(j)}\boldsymbol{h}^{(j)}\boldsymbol{y}^{(j)T}}{\boldsymbol{y}^{(j)T}\boldsymbol{h}^{(j)}} + \frac{\boldsymbol{y}^{(j)}\boldsymbol{h}^{(j)T}\boldsymbol{B}^{(j)T}}{\boldsymbol{h}^{(j)T}\boldsymbol{B}^{(j)T}\boldsymbol{h}^{(j)}} \tag{A.25}$$

A.2 EXAMPLES

We apply the aggressive SM algorithm to the seven-section transmission line impedance transformer example by solving (A.1). We compare the usage of the Broyden (A.10), the original BFGS (A.17) and the proposed non-symmetric BFGS (A.25) updating formulas.

A.2.1 Seven-section Capacitively Loaded Impedance Transformer

The seven-section transmission line (TL) capacitively loaded impedance transformer example is described in [9]–[10]. We consider a "coarse" model as an ideal seven-section TL, where the "fine" model is a capacitively-loaded TL with capacitors $C_1 = \cdots = C_8 = 0.025$ pF. The fine and coarse models are shown in Fig. A.1 and Fig. A.2, respectively. Design parameters are normalized lengths

$\boldsymbol{x}_f = \left[L_1\ L_2\ L_3\ L_4\ L_5\ L_6\ L_7\right]^T$, with respect to the quarter-wave length L_q at the center frequency 4.35 GHz. Design specifications are

$$\left|S_{11}\right| \le 0.07, \text{ for } 1 \text{ GHz} \le \omega \le 7.7 \text{ GHz} \tag{A.1}$$

with 68 points per frequency sweep (m = 68). The characteristic impedances for the transformer are fixed as in Table A.1. The Jacobians of both the coarse and fine models were obtained analytically using the adjoint network method [11]. We solve the PE problem using the Levenberg-Marquardt algorithm for nonlinear least squares optimization available in the Matlab Optimization Toolbox [12]. The gradient-based minimax optimization routine by Hald and Madsen [13]–[14] is used for direct optimization of the fine and coarse models.

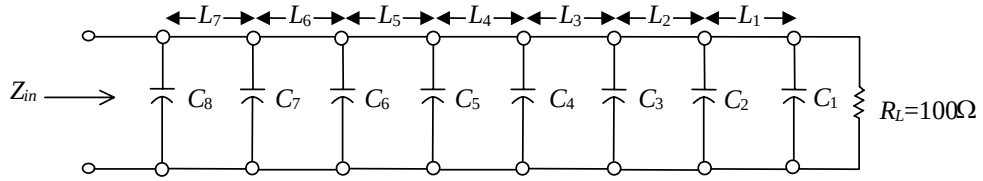

Fig. A.1. Seven-section capacitively-loaded impedance transformer: “fine” model [9].

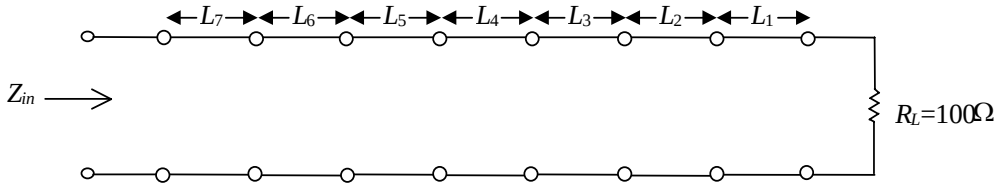

Fig. A.2. Seven-section capacitively-loaded impedance transformer: “coarse” model [9].

TABLE A.1

THE CHARACTERISTIC IMPEDANCES FOR THE SEVEN-SECTION CAPACITIVELY LOADED IMPEDANCE TRANSFORMER

Impedance	Value (Ohm)
Z_1	91.9445
Z_2	85.5239
Z_3	78.1526
Z_4	70.7107
Z_5	63.9774
Z_6	58.4632
Z_7	54.3806

We apply the ASM algorithm [2] utilizing three different formulas to update the mapping Jacobian matrix $\boldsymbol{B}$ utilizing 6 iterations.

Firstly, utilizing the Broyden formula, $\boldsymbol{B}$ is given by (non-symmetric matrix)

$$\boldsymbol{B}_{Broyden}^{(6)} = \begin{bmatrix} 1.5262 & 0.0074 & 0.1969 & 0.3278 & 0.3875 & 0.2015 & -0.4844 \\ -0.3199 & 1.1018 & -0.0474 & -0.0149 & 0.0207 & 0.0093 & -0.0788 \\ 0.0351 & -0.0371 & 1.0095 & 0.0412 & 0.0950 & 0.1310 & -0.0126 \\ -0.0861 & 0.0257 & -0.0169 & 1.0389 & 0.1064 & 0.1678 & 0.0269 \\ -0.1327 & 0.0375 & -0.0562 & -0.0146 & 1.0357 & 0.1690 & 0.1977 \\ -0.1182 & 0.0350 & -0.0751 & -0.1134 & -0.1515 & 0.9637 & 0.3956 \\ 0.0722 & -0.1064 & -0.0168 & -0.2013 & -0.3640 & -0.4405 & 1.1873 \end{bmatrix}$$

Secondly, using the BFGS formula, we get the following $\boldsymbol{B}$ (symmetric and positive definite matrix)

$$\boldsymbol{B}_{BFGS}^{(6)} = \begin{bmatrix} 1.4639 & -0.1274 & 0.1310 & 0.1613 & 0.2002 & 0.1367 & -0.3153 \\ -0.1274 & 1.0480 & -0.0403 & -0.0275 & -0.0207 & 0.0056 & 0.0304 \\ 0.1310 & -0.0403 & 1.0299 & 0.0459 & 0.0661 & 0.0941 & -0.0329 \\ 0.1613 & -0.0275 & 0.0459 & 1.0835 & 0.1231 & 0.1425 & -0.1347 \\ 0.2002 & -0.0207 & 0.0661 & 0.1231 & 1.1817 & 0.2008 & -0.2272 \\ 0.1367 & 0.0056 & 0.0941 & 0.1425 & 0.2008 & 1.1584 & -0.3821 \\ -0.3153 & 0.0304 & -0.0329 & -0.1347 & -0.2272 & -0.3821 & 0.9123 \end{bmatrix}$$

Finally, we utilize our proposed non-symmetric BFGS updating formula

$$\boldsymbol{B}_{modified\ BFGS}^{(6)} = \begin{bmatrix} 1.5614 & 0.2822 & 0.3425 & 0.4108 & 0.2272 & -0.0559 & -0.4612 \\ -0.6924 & 1.0861 & 0.0317 & 0.0308 & 0.0500 & -0.0399 & -0.0059 \\ -0.1343 & -0.0949 & 1.0299 & 0.0706 & 0.1742 & 0.1718 & -0.0065 \\ -0.2252 & -0.0785 & -0.0090 & 1.0365 & 0.1520 & 0.1929 & 0.0745 \\ -0.0204 & -0.1067 & -0.1073 & -0.0680 & 1.0513 & 0.2024 & 0.1897 \\ 0.2685 & -0.0440 & -0.1482 & -0.1559 & -0.1405 & 1.0621 & 0.3304 \\ 0.3183 & 0.0390 & -0.0820 & -0.1657 & -0.2742 & -0.2693 & 1.1663 \end{bmatrix}$$

Convergence results utilizing the three updating formulas are given in Table A.2. As we expect, the original BFGS update provides poor convergence w.r.t. the non-symmetric (Broyden and modified BFGS) updates (see the last column in Table A.2). The initial responses are depicted in Fig. A.3. The final responses, the reduction of $\|\boldsymbol{f}\|_2$ and $U - U_{opt}$ versus iteration using the Broyden and the modified BFGS formulas are shown in Fig. A.4–Fig. A.9. $U = \max\left|S_{11,i}\right|, i = 1, 2, .., m$ and U_{opt} is obtained by fine model optimization. The final response using the original BFGS is similar to Fig. A.4. Convergence of $\|\boldsymbol{f}\|_2$ and $U - U_{opt}$ versus iteration using the original BFGS formula are depicted in Fig. A.10 and Fig. A.11, respectively.

TABLE A.2

ASM ALGORITHM USING
BROYDEN RANK-1 VERSUS MODIFIED BFGS RANK-2 UPDATING
FORMULAS FOR THE SEVEN-SECTION CAPACITIVELY LOADED
IMPEDANCE TRANSFORMER

Updating method	Iterations	$U - U_{opt}$	$\|\boldsymbol{f}\|_2$
Broyden	6	5.34e–4	7.39e–4
BFGS	6	7.64e–4	1.98e–2
modified BFGS	6	5.38e–4	3.68e–4

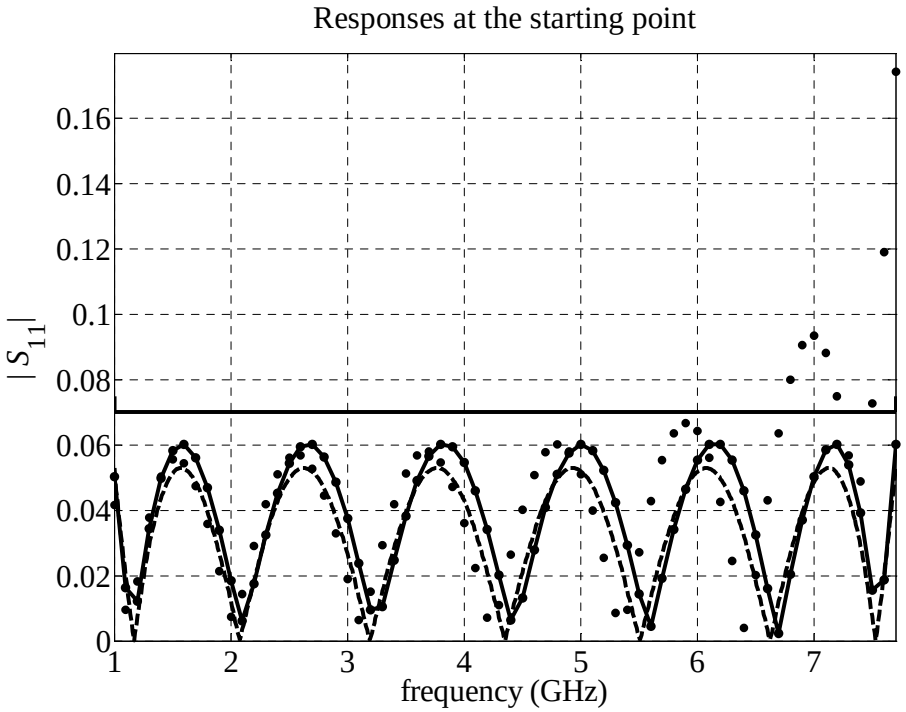

Fig. A.3. Optimal coarse model response (--), optimal fine model response (–•–) and the fine model response (•) at the starting point for the seven-section transmission line capacitively loaded impedance transformer.

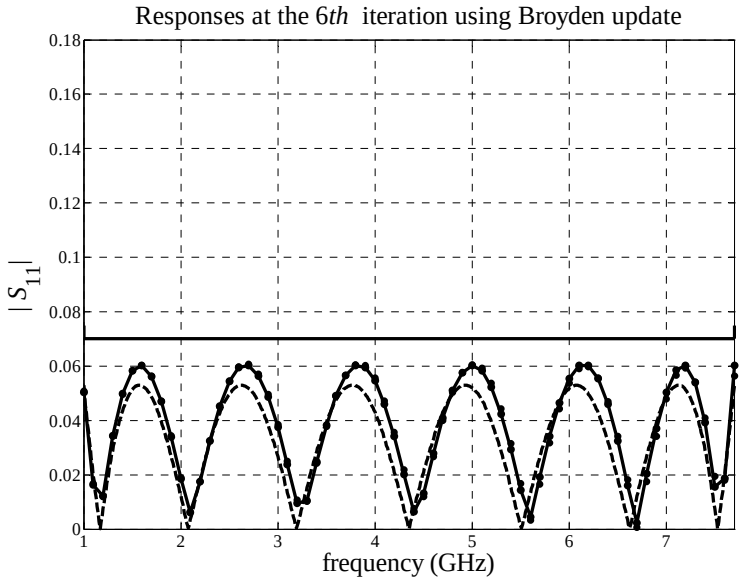

Fig. A.4. Optimal coarse model response (--), optimal fine model response (–•–) and the fine model response (•) at the final iteration for the seven-section transmission line capacitively loaded impedance transformer using the Broyden update.

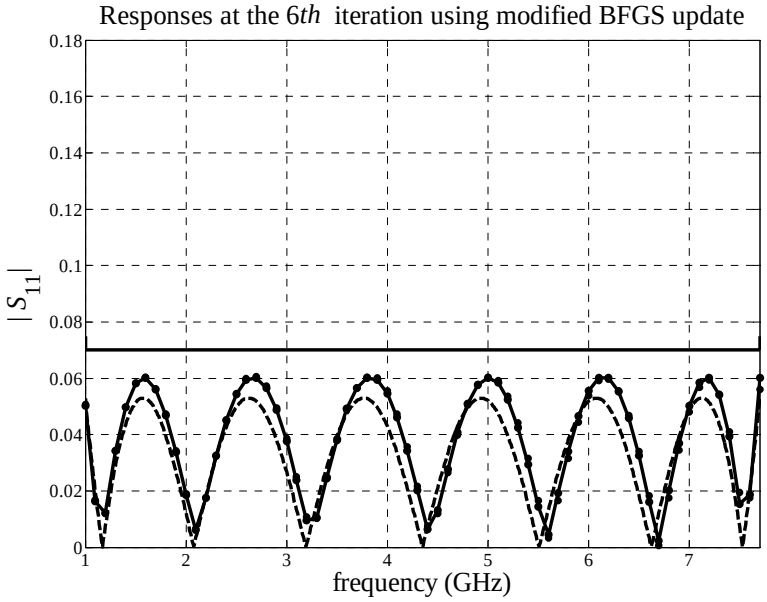

Fig. A.5. Optimal coarse model response (--), optimal fine model response (–•–) and the fine model response (•) at the final iteration for the seven-section transmission line capacitively loaded impedance transformer using the modified BFGS update.

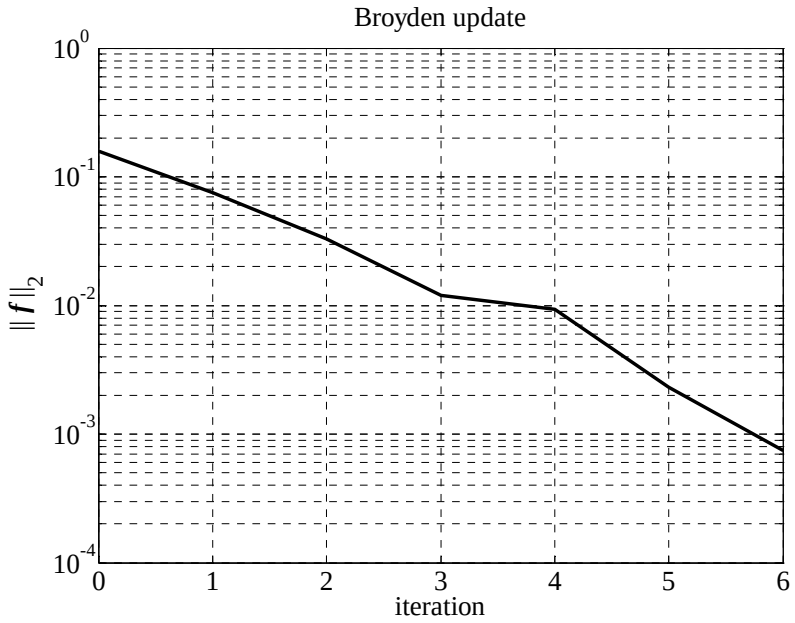

Fig. A.6. $\|\boldsymbol{f}\|_2$ versus iteration for the seven-section transmission line capacitively loaded impedance transformer using the Broyden update.

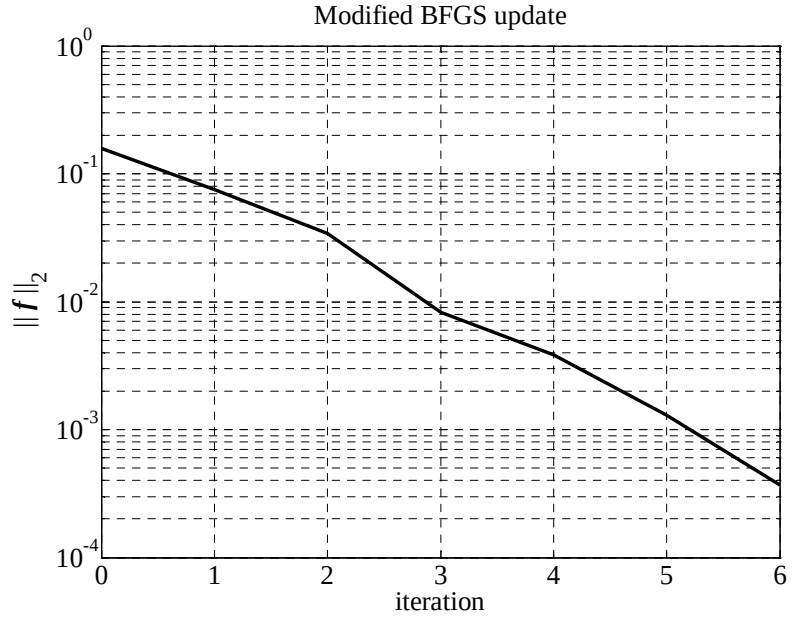

Fig. A.7. $\|\boldsymbol{f}\|_2$ versus iteration for the seven-section transmission line capacitively loaded impedance transformer using the modified BFGS update.

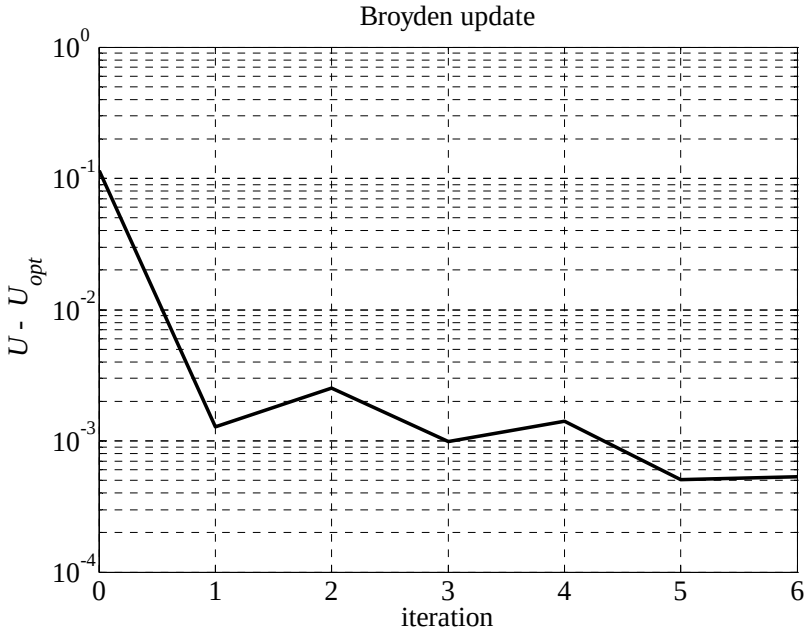

Fig. A.8. $U - U_{opt}$ versus iteration for the seven-section transmission line capacitively loaded impedance transformer using the Broyden update.

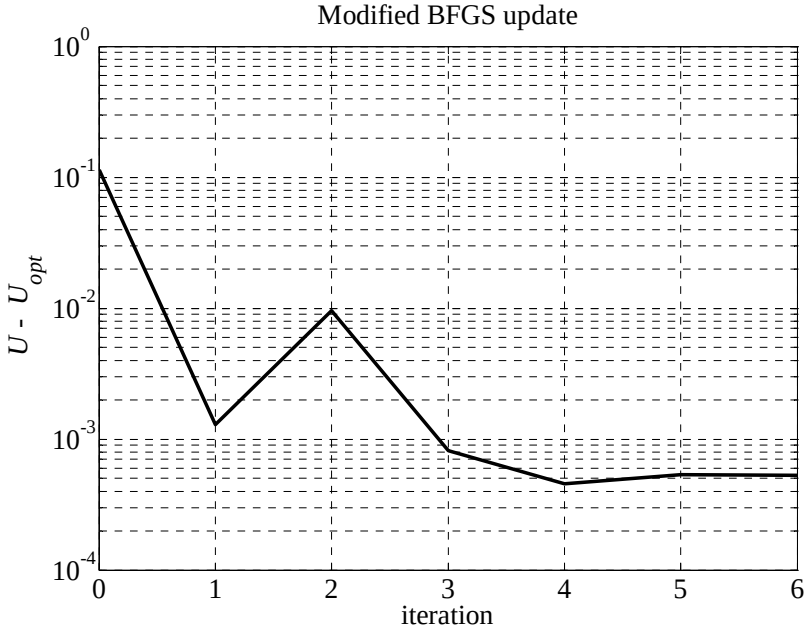

Fig. A.9. $U - U_{opt}$ versus iteration for the seven-section transmission line capacitively loaded impedance transformer using the modified BFGS update.

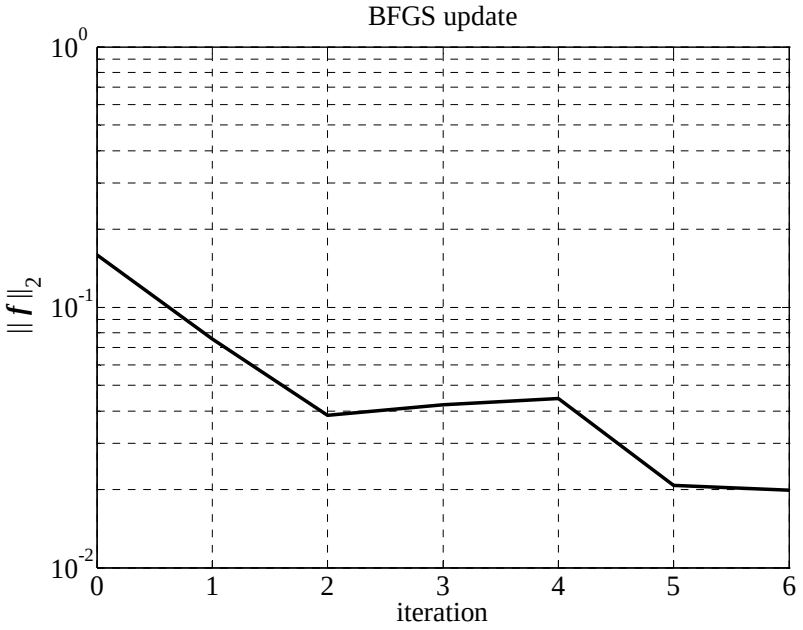

Fig. A.10. $\|\boldsymbol{f}\|_2$ versus iteration for the seven-section transmission line capacitively loaded impedance transformer using the original BFGS update.

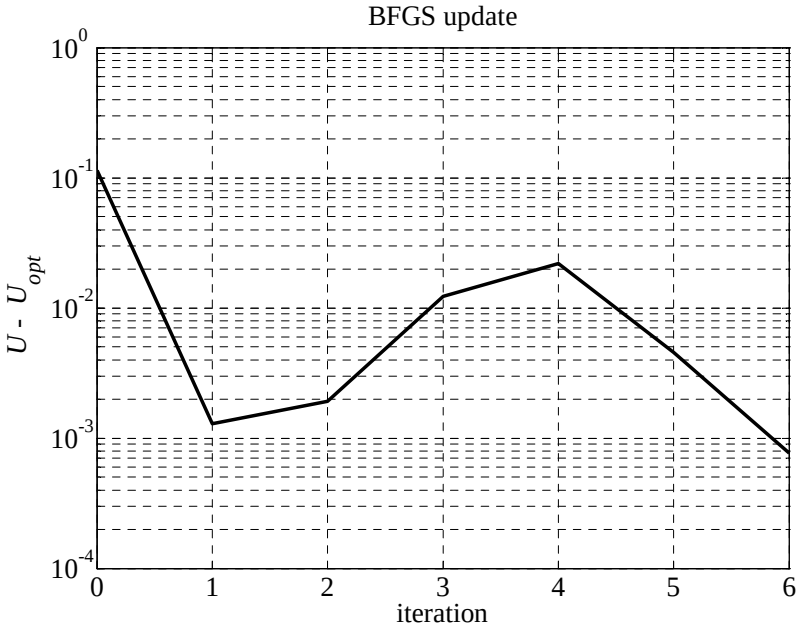

Fig. A.11. $U - U_{\text{opt}}$ versus iteration for the seven-section transmission line capacitively loaded impedance transformer using the original BFGS update.

A.3 CONCLUDING REMARKS

The usage of the original BFGS rank-2 formula to update the Jacobian matrix in the context of solving a system of nonlinear equations is not appropriate. The Jacobian matrix is not symmetric and it is not necessarily a positive definite matrix. The BFGS rank-2 formula is primarily designed to update the Hessian matrix in the context of solving nonlinear optimization problems. Utilizing the Broyden rank-1 formula to update the Jacobian matrix within the aggressive SM algorithm provides better convergence versus the BFGS rank-2.

We propose a modified rank-2 BFGS updating formula for the non-symmetric case. The proposed formula is successfully examined with an illustrative example. It provides slightly better convergence for solving the system of nonlinear equation using the aggressive SM algorithm versus the Broyden rank-1 update.

The results presented are promising. We expect that the proposed formula will outperform the Broyden formula if the coarse model is badly chosen. Employing the trust region methodology with the proposed formula to improve the convergence properties of the algorithm needs further investigation. Using higher ranks of our proposed formula, e.g., rank-3, in the case of complicated problems and an inaccurate coarse model, is another research topic to be addressed in future.

REFERENCES

[1] J.W. Bandler, R.M. Biernacki, S.H. Chen, P.A. Grobelny and R.H. Hemmers, "Space mapping technique for electromagnetic optimization," *IEEE Trans. Microwave Theory Tech.*, vol. 42, pp. 2536–2544, Dec. 1994.

[2] J.W. Bandler, R.M. Biernacki, S.H. Chen, R.H. Hemmers and K. Madsen, "Electromagnetic optimization exploiting aggressive space mapping," *IEEE Trans. Microwave Theory Tech*., vol. 43, pp. 2874–2882, Dec. 1995.

[3] C.G. Broyden, "A class of methods for solving nonlinear simultaneous equations," *Math. Comp.*, vol. 19, pp. 577–593, 1965.

[4] J. Nocedal and S.J. Wright, *Numerical Optimization*. New York, NY: Springer-Verlag, 1999.

[5] R. Fletcher, *Practical Methods of Optimization*, 2nd ed. New York, NY: Wiley, 1987.

[6] P.E. Frandsen, K. Jonasson and O. Tingleff, *Unconstrained Optimization*. Lecture Notes, Informatics and Mathematical Modelling (IMM), Technical University of Denmark (DTU), Lyngby, Denmark, Aug. 1997.

[7] J.E. Dennis, Jr. and R.B. Schnabel, *Numerical Methods for Unconstrained Optimization and Nonlinear Equations*. Englewood Cliffs, NJ: Prentice-Hall, 1983. Reprinted by SIAM Publications, 1996.

[8] W. C. Davidon, "Variable metric method for minimization," *SIAM Journal on Optimization*, vol. 1, pp. 1–17, Feb. 1991.

[9] M.H. Bakr, J. W. Bandler, K. Madsen and J. Søndergaard, "An introduction to the space mapping technique," *Optimization and Engineering*, vol. 2, pp. 369–384, 2001.

[10] J.W. Bandler, D.M. Hailu, K. Madsen, and F. Pedersen, "A space-mapping interpolating surrogate algorithm for highly optimized EM-based design of microwave devices," *IEEE Trans. Microwave Theory and Tech.*, vol. 52, pp. 2593–2600, Nov. 2004.

[11] J.W. Bandler and R. E. Seviora, "Computation of sensitivities for noncommensurate networks," *IEEE Trans. Circuit Theory*, vol. CT-18, pp. 174–178, Jan. 1971.

[12] Matlab, The MathWorks, Inc., 3 Apple Hill Drive, Natick MA 01760-2098, USA.

[13] K. Madsen, "An algorithm for minimax solution of overdetermined systems of non-linear equations," *J. Inst. Math. Applicat.*, vol. 16, pp. 321–328, 1975.

[14] J. Hald and K. Madsen, "Combined LP and quasi-Newton methods for minimax optimization," *Math. Programming*, vol. 20, pp. 49–62, 1981.

APPENDIX B

CONSTRAINED UPDATE FOR B

B could be better conditioned, in the PE process, if it is constrained to be close to the identity matrix ***I*** by

$$\boldsymbol{B} = \arg\min_{\boldsymbol{B}} \left\| [\boldsymbol{e}_1^T \cdots \boldsymbol{e}_n^T \; \eta\Delta\boldsymbol{b}_1^T \cdots \eta\Delta\boldsymbol{b}_n^T]^T \right\|_2^2 \tag{B.1}$$

where η is a weighting factor, $\boldsymbol{e}_i$ and $\Delta\boldsymbol{b}_i$ are the ith columns of ***E*** and $\Delta\boldsymbol{B}$, respectively, defined as

$$\begin{aligned} \boldsymbol{E} &= \boldsymbol{J}_f - \boldsymbol{J}_c \boldsymbol{B} \\ \Delta\boldsymbol{B} &= \boldsymbol{B} - \boldsymbol{I} \end{aligned} \tag{B.2}$$

Solving (B.1) as follows

$$\begin{aligned} \boldsymbol{B} &= \arg\min_{\boldsymbol{B}} \left\{ \left\| [\boldsymbol{e}_1^T \cdots \boldsymbol{e}_n^T]^T \right\|_2^2 + \eta^2 \left\| [\Delta\boldsymbol{b}_1^T \cdots \Delta\boldsymbol{b}_n^T]^T \right\|_2^2 \right\} \\ \boldsymbol{B} &= \arg\min_{\boldsymbol{B}} \left\{ \|\boldsymbol{E}\|_F^2 + \eta^2 \|\Delta\boldsymbol{B}\|_F^2 \right\} \end{aligned} \tag{B.3}$$

where $\|.\|_F$ stands for the Frobenius matrix norm. Generally, $\|\boldsymbol{A}\|_F$ for any matrix ***A*** can be described as

$$\|\boldsymbol{A}\|_F^2 = Tr(\boldsymbol{A}^T \boldsymbol{A}) \tag{B.4}$$

Thus (B.3) can be rewritten as

$$\boldsymbol{B} = \arg\min_{\boldsymbol{B}} \left\{ Tr(\boldsymbol{E}^T\boldsymbol{E}) + \eta^2 Tr(\Delta\boldsymbol{B}^T\Delta\boldsymbol{B}) \right\} \tag{B.5}$$

To determine the optimal solution for matrix $\boldsymbol{B}$ we differentiate the argument of (B.5) w.r.t. matrix $\boldsymbol{B}$ and equate the result to zero, knowing that $\boldsymbol{E}$ and $\Delta\boldsymbol{B}$ are given by (B.2).

$$\begin{gathered}\frac{\partial}{\partial \boldsymbol{B}} \left\{ Tr(\boldsymbol{E}^T\boldsymbol{E}) + \eta^2 Tr(\Delta\boldsymbol{B}^T\Delta\boldsymbol{B}) \right\} = \boldsymbol{0} \\ \left[\frac{\partial \boldsymbol{E}}{\partial \boldsymbol{B}}\right]\left[\frac{\partial(\boldsymbol{E}^T\boldsymbol{E})}{\partial \boldsymbol{E}}\right]\left[\frac{\partial Tr(\boldsymbol{E}^T\boldsymbol{E})}{\partial(\boldsymbol{E}^T\boldsymbol{E})}\right] + \eta^2\left[\frac{\partial(\Delta\boldsymbol{B})}{\partial \boldsymbol{B}}\right]\left[\frac{\partial(\Delta\boldsymbol{B}^T\Delta\boldsymbol{B})}{\partial(\Delta\boldsymbol{B})}\right]\left[\frac{\partial Tr(\Delta\boldsymbol{B}^T\Delta\boldsymbol{B})}{\partial(\Delta\boldsymbol{B}^T\Delta\boldsymbol{B})}\right] = \boldsymbol{0}\end{gathered} \tag{B.6}$$

However, for any matrix $\boldsymbol{A}$ that has independent elements, the following is true.

$$\left[\frac{\partial Tr(\boldsymbol{A})}{\partial(\boldsymbol{A})}\right] = \boldsymbol{I} \tag{B.7}$$

Therefore, we can simplify (B.6) as follows

$$\begin{aligned}&(-\boldsymbol{J}_c{}^T)(2\boldsymbol{E})(\boldsymbol{I}) + \eta^2(\boldsymbol{I})(2\Delta\boldsymbol{B})(\boldsymbol{I}) = \boldsymbol{0} \\ &(-\boldsymbol{J}_c{}^T)(\boldsymbol{J}_f - \boldsymbol{J}_c\,\boldsymbol{B}) + \eta^2(\boldsymbol{B} - \boldsymbol{I}) = \boldsymbol{0} \\ &(\boldsymbol{J}_c^T\boldsymbol{J}_c + \eta^2\boldsymbol{I})\boldsymbol{B} = (\boldsymbol{J}_c^T\boldsymbol{J}_f + \eta^2\boldsymbol{I})\end{aligned} \tag{B.8}$$

The analytical solution of (B.1) is given by

$$\boldsymbol{B} = (\boldsymbol{J}_c^T\boldsymbol{J}_c + \eta^2\boldsymbol{I})^{-1}(\boldsymbol{J}_c^T\boldsymbol{J}_f + \eta^2\boldsymbol{I}) \tag{B.9}$$

APPENDIX C

L-MODEL AND *Q*-MODEL

A linear (quadratic) interpolation scheme [1]–[2], [3]–[4] is essential for optimizing the surrogate in both the calibration (PE) and prediction (surrogate optimization) steps.

We assume a vector $\boldsymbol{\phi}$ contains all the design (optimizable) parameters of a microwave structure. $\boldsymbol{\phi}$ can be represented as a point in the *n*-dimensional parameter space

$$\boldsymbol{\phi} = \begin{bmatrix} \phi_1 & \phi_2 & \ldots & \phi_n \end{bmatrix}^T \tag{C.1}$$

Numerical EM simulation is performed at discretized values of the geometrical design parameters [1]

$$\phi_i = k_i d_i; i = 1, 2, ..., n \tag{C.2}$$

where d_i is a discretization step (modeling grid size), i.e., the distance between adjacent modeling grid points, for the *i*th parameter. It is a positive floating-point number. It has the same units as the corresponding parameter. k_i is an integer, typically positive [1].

L-Model. The *L*-model is a multi-dimensional linear polynomial. To evaluate the response at an off-grid point $\boldsymbol{\phi}$, a set $\boldsymbol{S}$ of $n + 1$ base on-grid points should be created [2].

The first base (reference) point $\boldsymbol{\phi}^1$ is selected by snapping the considered point $\boldsymbol{\phi}$ to the closest (in the l_2 sense) modeling grid point (see Fig. 4.2(a) for n = 2). The following n base points are generated by perturbing one parameter at a time around the reference point $\boldsymbol{\phi}^1$ [2].

$$\begin{aligned} \boldsymbol{\phi}^{i+1} &= \boldsymbol{\phi}^1 + \begin{bmatrix} 0 & \cdots & 0 & sign(\theta_i)d_i & 0 & \cdots & 0 \end{bmatrix}^T \\ \theta_i &= \frac{\left(\phi_i - \phi_i^{\,1}\right)}{d_i}, i = 1, 2, \ldots n \end{aligned} \tag{C.3}$$

where ϕ_i and $\phi_i^{\,1}$ are the ith component of the considered point $\boldsymbol{\phi}$ and the reference point $\boldsymbol{\phi}^1$, respectively.

The *L*-model formula used to evaluate the response function at the considered point $\boldsymbol{\phi}$ could be given by

$$\boldsymbol{R}_L(\boldsymbol{\phi}) = \boldsymbol{R}_{EM}(\boldsymbol{\phi}^1) + \sum_{i=1}^{n} |\theta_i| \left[\boldsymbol{R}_{EM}(\boldsymbol{\phi}^{i+1}) - \boldsymbol{R}_{EM}(\boldsymbol{\phi}^1) \right] \tag{C.4}$$

where $\boldsymbol{R}_L(\boldsymbol{\phi})$ is the linearly interpolated response function and $\boldsymbol{R}_{EM}(.)$ is the EM response function at the on-grid point. In [1], [4], (C.3) and (C.4)are given in a compact matrix form.

Q-model. The *Q*-model is build based on 2*n*+1 base points around the point of interest $\boldsymbol{\phi}$. To build a *Q*-model, we use the maximally flat quadratic

interpolation (MFQI) modeling technique introduced in [1], [5] with a fixed and symmetrical pattern of base points [1]–[2]. The first base (reference) point $\boldsymbol{\phi}^1$ is selected as in the *L*-model case. The other $2n$ base points are chosen by perturbing one parameter at a time with value $\pm d_i$ (see Fig. 4.2(b) for $n = 2$) as follows.

$$\begin{aligned} \boldsymbol{\phi}^{i+1} &= \boldsymbol{\phi}^1 + \begin{bmatrix} 0 & \cdots & 0 & +d_i & 0 & \cdots & 0 \end{bmatrix}^T \\ \boldsymbol{\phi}^{n+1+i} &= \boldsymbol{\phi}^1 + \begin{bmatrix} 0 & \cdots & 0 & -d_i & 0 & \cdots & 0 \end{bmatrix}^T \end{aligned} \tag{C.5}$$

The *Q*-model formula used to evaluate the MFQI response function $\boldsymbol{R}_Q(\boldsymbol{\phi})$ at the considered point $\boldsymbol{\phi}$ is given by [2]

$$\boldsymbol{R}_Q(\boldsymbol{\phi}) = \boldsymbol{R}_{EM}(\boldsymbol{\phi}^1) + \sum_{i=1}^{n} \left\{ \begin{bmatrix} \boldsymbol{R}_{EM}(\boldsymbol{\phi}^{i+1}) - \boldsymbol{R}_{EM}(\boldsymbol{\phi}^{n+1+i}) + \\ \left(\boldsymbol{R}_{EM}(\boldsymbol{\phi}^{i+1}) + \boldsymbol{R}_{EM}(\boldsymbol{\phi}^{n+1+i}) - 2\boldsymbol{R}_{EM}(\boldsymbol{\phi}^1) \right) \theta_i \end{bmatrix} \frac{\theta_i}{2} \right\} \tag{C.6}$$

where θ_i is given in (C.3).

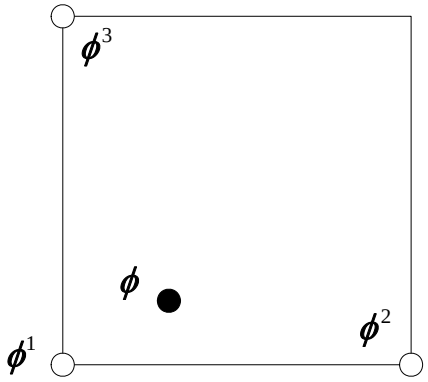

(a)

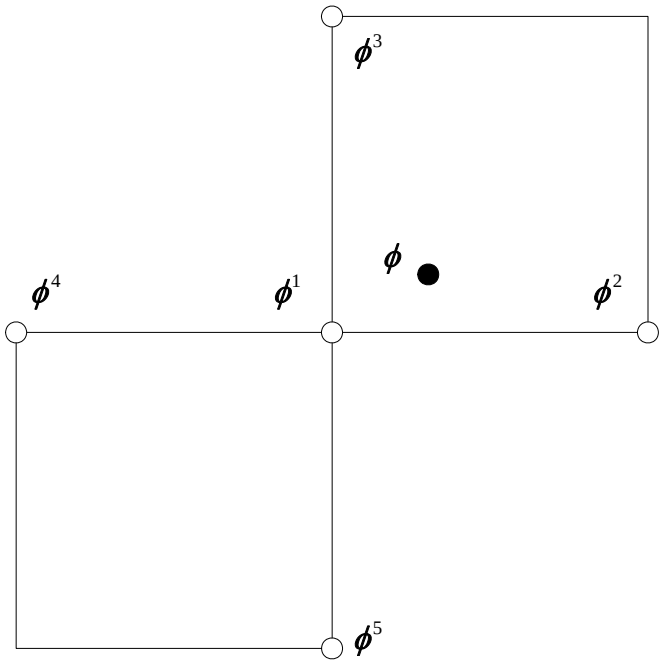

(b)

Fig. C.1 Selection of base points in the $n = 2$ case: (a) for the *L*-model and (b) for the *Q*-model.

REFERENCES

[1] J.W. Bandler, R.M. Biernacki, S.H. Chen, L.W. Hendrick and D. Omeragic, "Electromagnetic optimization of 3D structures," *IEEE Trans. Microwave Theory and Tech.*, vol. 45, pp. 770–779, May 1997.

[2] P.A. Grobelny, *Integrated Numerical Modeling Techniques for Nominal and Statistical Circuit Design*, Ph.D. Thesis, Department of Electrical and Computer Engineering, McMaster University, Hamilton, ON, Canada, 1995.

[3] R.M. Biernacki, J.W. Bandler, J. Song and Q.J. Zhang, "Efficient quadratic approximation for statistical design," *IEEE Trans. Circuits Syst*., vol. 36, pp. 1449–1454, Nov. 1989.

[4] J. W. Bandler, R. M. Biernacki, S. H. Chen, D. G. Swanson, Jr., and S. Ye, "Microstrip filter design using direct EM field simulation," *IEEE Trans. Microwave Theory Tech*., vol. 42, pp. 1353–1359, July 1994.

[5] R. M. Biernacki and M. A. Styblinski, "Efficient performance function interpolation scheme and its application to statistical circuit design," *Int. J. Circuit Theory Appl.*, vol. 19, pp. 403–422, July–Aug. 1991.

BIBLIOGRAPHY

Agilent ADS, Agilent Technologies, 1400 Fountaingrove Parkway, Santa Rosa, CA 95403-1799, USA.

Agilent HFSS, Agilent Technologies, 1400 Fountaingrove Parkway, Santa Rosa, CA 95403-1799, USA.

Agilent Momentum, Agilent Technologies, 1400 Fountaingrove Parkway, Santa Rosa, CA 95403-1799, USA.

F. Alessandri, M. Mongiardo and R. Sorrentino, "New efficient full wave optimization of microwave circuits by the adjoint network method," *IEEE Microwave and Guided Wave Letts.*, vol. 3, pp. 414–416, Nov. 1993.

N. Alexandrov, J.E. Dennis, Jr., R.M. Lewis and V. Torczon, "A trust-region framework for managing the use of approximation models in optimization," *Structural Optimization*, vol. 15, pp. 16–23, 1998.

Ansoft HFSS, Ansoft Corporation, 225 West Station Square Drive, Suite 200, Pittsburgh, PA 15219, USA.

M.H. Bakr, *Advances in Space Mapping Optimization of Microwave Circuits*, Ph.D. Thesis, Department of Electrical and Computer Engineering, McMaster University, Hamilton, ON, Canada, 2000.

M.H. Bakr, *2D-TLM Matlab Implementation*, Department of Electrical and Computer Engineering, McMaster University, Hamilton, ON, Canada, 2004.

M.H. Bakr, J.W. Bandler, R.M. Biernacki, S.H. Chen and K. Madsen, "A trust region aggressive space mapping algorithm for EM optimization," *IEEE Trans. Microwave Theory Tech.*, vol. 46, pp. 2412–2425, Dec. 1998.

M.H. Bakr, J.W. Bandler, Q.S. Cheng, M.A. Ismail and J.E. Rayas-Sánchez, "SMX–A novel object-oriented optimization system," in *IEEE MTT-S Int. Microwave Symp. Dig.*, Phoenix, AZ, 2001, pp. 2083–2086.

M.H. Bakr, J.W. Bandler and N. Georgieva, “Modeling of microwave circuits exploiting space derivative mapping,” in *IEEE MTT-S Int. Microwave Symp. Dig.*, Anaheim, CA, 1999, pp. 715–718.

M.H. Bakr, J.W. Bandler and N. Georgieva, “An aggressive approach to parameter extraction,” *IEEE Trans. Microwave Theory Tech.*, vol. 47, pp. 2428–2439, Dec. 1999.

M.H. Bakr, J.W. Bandler, N.K. Georgieva and K. Madsen, “A hybrid aggressive space-mapping algorithm for EM optimization,” *IEEE Trans. Microwave Theory Tech.*, vol. 47, pp. 2440–2449, Dec. 1999.

M.H. Bakr, J.W. Bandler, M.A. Ismail, J.E. Rayas-Sánchez and Q.J. Zhang, “Neural space-mapping optimization for EM-based design,” *IEEE Trans. Microwave Theory Tech.*, vol. 48, pp. 2307–2315, Dec. 2000.

M.H. Bakr, J.W. Bandler, K. Madsen and J. Søndergaard, “Review of the space mapping approach to engineering optimization and modeling,” *Optimization and Engineering*, vol. 1, pp. 241–276, 2000.

M.H. Bakr, J.W. Bandler, K. Madsen and J. Søndergaard, “An introduction to the space mapping technique,” *Optimization and Engineering*, vol. 2, pp. 369–384, 2001.

M.H. Bakr, J.W. Bandler, K. Madsen, J.E. Rayas-Sánchez and J. Søndergaard, “Space mapping optimization of microwave circuits exploiting surrogate models,” *IEEE Trans. Microwave Theory Tech.*, vol. 48, pp. 2297–2306, Dec. 2000.

M.H. Bakr, P.P.M. So and W.J.R. Hoefer, “The generation of optimal microwave topologies using time-domain field synthesis,” *IEEE Trans. Microwave Theory and Tech.*, vol. 50, pp. 2537–2544, Nov. 2002.

J.W. Bandler, “Computer-aided circuit optimization,” in *Modern Filter Theory and Design*, G.C. Temes and S.K. Mitra, Eds. New York, NY: Wiley, 1973, pp. 211–271.

J.W. Bandler and H.L. Abdel-Malek, “Optimal centering, tolerancing and yield determination via updated approximations and cuts,” *IEEE Trans. Circuits Syst.*, vol. CAS-25, pp. 853–871, Oct. 1978.

J.W. Bandler, R.M. Biernacki, S.H. Chen, W.J. Getsinger, P.A. Grobelny, C. Moskowitz and S.H. Talisa, “Electromagnetic design of high-temperature superconducting microwave filters,” *Int. J. RF and Microwave CAE*, vol. 5, pp. 331–343, 1995.

J.W. Bandler, R.M. Biernacki, S.H. Chen, P.A. Grobelny and S. Ye, "Yield-driven electromagnetic optimization via multilevel multidimensional models," *IEEE Trans. Microwave Theory Tech.*, vol. 41, pp. 2269–2278, Dec. 1993.

J.W. Bandler, R.M. Biernacki, S.H. Chen, P.A. Grobelny and R.H. Hemmers, "Space mapping technique for electromagnetic optimization," *IEEE Trans. Microwave Theory Tech.*, vol. 42, pp. 2536–2544, Dec. 1994.

J.W. Bandler, R.M. Biernacki, S.H. Chen, R.H. Hemmers and K. Madsen, "Electromagnetic optimization exploiting aggressive space mapping," *IEEE Trans. Microwave Theory Tech.*, vol. 43, pp. 2874–2882, Dec. 1995.

J.W. Bandler, R.M. Biernacki, S.H. Chen, L.W. Hendrick and D. Omeragic, "Electromagnetic optimization of 3D structures," *IEEE Trans. Microwave Theory and Tech.*, vol. 45, pp. 770–779, May 1997.

J.W. Bandler, R.M. Biernacki, S.H. Chen and D. Omeragic, "Space mapping optimization of waveguide filters using finite element and mode-matching electromagnetic simulators," *Int. J. RF and Microwave CAE*, vol. 9, pp. 54–70, 1999.

J.W. Bandler, R.M. Biernacki, S.H. Chen, D.G. Swanson, Jr. and S. Ye, "Microstrip filter design using direct EM field simulation," *IEEE Trans. Microwave Theory Tech.*, vol. 42, pp. 1353–1359, July 1994.

J.W. Bandler, R.M. Biernacki and S.H. Chen, "Fully automated space mapping optimization of 3D structures," in *IEEE MTT-S Int. Microwave Symp. Dig.*, San Francisco, CA, 1996, pp. 753–756.

J.W. Bandler, R.M. Biernacki and S.H. Chen, "Parameterization of arbitrary geometrical structures for automated electromagnetic optimization," in *IEEE MTT-S Int. Microwave Symp. Dig.*, San Francisco, CA, 1996, pp. 1059–1062.

J.W. Bandler, R.M. Biernacki and S.H. Chen, "Parameterization of arbitrary geometrical structures for automated electromagnetic optimization," *Int. J. RF and Microwave CAE*, vol. 9, pp. 73–85, 1999.

J.W. Bandler, R.M. Biernacki, S.H. Chen and Y.F. Huang, "Design optimization of interdigital filters using aggressive space mapping and decomposition," *IEEE Trans. Microwave Theory Tech.*, vol. 45, pp. 761–769, May 1997.

J.W. Bandler, R.M. Biernacki, S.H. Chen and Q.H. Wang, "Multiple space mapping EM optimization of signal integrity in high-speed digital circuits," *Proc. 5th Int. Workshop on Integrated Nonlinear Microwave and Millimeter wave Circuits*, Duisburg, Germany, 1998, pp. 138–140.

J.W. Bandler and S.H. Chen, "Circuit optimization: the state of the art," *IEEE Trans. Microwave Theory Tech.*, vol. 36, pp. 424–443, Feb. 1988.

J.W. Bandler, S.H. Chen, R.M. Biernacki, L. Gao, K. Madsen and H. Yu, "Huber optimization of circuits: a robust approach," *IEEE Trans. Microwave Theory Tech.*, vol. 41, pp. 2279–2287, Dec. 1993.

J.W. Bandler, S.H. Chen, S. Daijavad and K. Madsen, "Efficient optimization with integrated gradient approximations," *IEEE Trans. Microwave Theory Tech.*, vol. 36, pp. 444–455, Feb. 1988.

J.W. Bandler, Q.S. Cheng, S.A. Dakroury, A.S. Mohamed, M.H. Bakr, K. Madsen and J. Søndergaard, "Trends in space mapping technology for engineering optimization," *3rd Annual McMaster Optimization Conference: Theory and Applications, MOPTA03,* Hamilton, ON, Aug. 2003.

J.W. Bandler, Q. Cheng, S.A. Dakroury, A.S. Mohamed, M.H. Bakr, K. Madsen and J. Søndergaard, "Space mapping: the state of the art," in *SBMO/IEEE MTT-S International Microwave and Optoelectronics Conference* (IMOC 2003), Parana, Brazil, 2003, vol. 2, pp. 951–956.

J.W. Bandler, Q. Cheng, S.A. Dakroury, A.S. Mohamed, M.H. Bakr, K. Madsen and J. Søndergaard, "Space mapping: the state of the art," *IEEE Trans. Microwave Theory and Tech.*, vol. 52, pp. 337–361, Jan. 2004.

J.W. Bandler, Q.S. Cheng, D. Gebre-Mariam, K. Madsen, F. Pedersen and J. Søndergaard, "EM-based surrogate modeling and design exploiting implicit, frequency and output space mappings," in *IEEE MTT-S Int. Microwave Symp. Dig.*, Philadelphia, PA, 2003, pp. 1003–1006.

J.W. Bandler, Q.S. Cheng, D.M. Hailu, A.S. Mohamed, M.H. Bakr, K. Madsen and F. Pedersen, "Recent trends in space mapping technology," in *Proc. 2004 Asia-Pacific Microwave Conf.* (APMC'04), New Delhi, India, Dec. 2004.

J.W. Bandler, Q.S. Cheng, D.M. Hailu and N.K. Nikolova, "A space-mapping design framework," *IEEE Trans. Microwave Theory and Tech.*, vol. 52, pp. 2601–2610, Nov. 2004.

J.W. Bandler, Q.S. Cheng, N.K. Nikolova and M.A. Ismail, "Implicit space mapping optimization exploiting preassigned parameters," *IEEE Trans. Microwave Theory Tech.*, vol. 52, pp. 378–385, Jan. 2004.

J.W. Bandler, Q.S. Cheng and S. Koziel, "Implementable space mapping approach to enhancement of microwave device models," in *IEEE MTT-S Int. Microwave Symp. Dig.*, Long Beach, CA, 2005, (accepted).

J.W. Bandler, N. Georgieva, M.A. Ismail, J.E. Rayas-Sánchez and Q. J. Zhang, "A generalized space mapping tableau approach to device modeling," *IEEE Trans. Microwave Theory Tech*., vol. 49, pp. 67–79, Jan. 2001.

J.W. Bandler, D.M. Hailu, K. Madsen, and F. Pedersen, "A space-mapping interpolating surrogate algorithm for highly optimized EM-based design of microwave devices," *IEEE Trans. Microwave Theory and Tech.*, vol. 52, pp. 2593–2600, Nov. 2004.

J.W. Bandler, M.A. Ismail, J.E. Rayas-Sánchez and Q.J. Zhang, "Neuromodeling of microwave circuits exploiting space mapping technology," *IEEE Trans. Microwave Theory Tech.*, vol. 47, pp. 2417–2427, Dec. 1999.

J.W. Bandler, M.A. Ismail and J.E. Rayas-Sánchez, "Broadband physics-based modeling of microwave passive devices through frequency mapping," *Int. J. RF and Microwave CAE*, vol. 11, pp. 156–170, 2001.

J.W. Bandler, M.A. Ismail and J.E. Rayas-Sánchez, "Expanded space mapping EM-based design framework exploiting preassigned parameters," *IEEE Trans. Circuits Syst.—I*, vol. 49, pp. 1833–1838, Dec. 2002.

J.W. Bandler, M.A. Ismail, J.E. Rayas-Sánchez and Q.J. Zhang, "Neural inverse space mapping (NISM) optimization for EM-based microwave design," *Int. J. RF and Microwave CAE*, vol. 13, pp. 136–147, 2003.

J.W. Bandler, W. Kellermann and K. Madsen, "A superlinearly convergent minimax algorithm for microwave circuit design," *IEEE Trans. Microwave Theory Tech.*, vol. MTT-33, pp. 1519–1530, Dec. 1985.

J.W. Bandler, P.C. Liu and J.H.K. Chen, "Worst case network tolerance optimization," *IEEE Trans. Microwave Theory Tech.*, vol. MTT-23, pp. 630–641, Aug. 1975.

J.W. Bandler, P.C. Liu and H. Tromp, "A nonlinear programming approach to optimal design centering, tolerancing and tuning," *IEEE Trans. Circuits Syst*., vol. CAS-23 pp. 155-165, Mar. 1976.

J.W. Bandler, P.C. Liu and H. Tromp, "Integrated approach to microwave design," *IEEE Trans. Microwave Theory Tech.*, vol. MTT-24, pp. 584–591, Sep. 1976.

J.W. Bandler and A.S. Mohamed, "Space mapping optimization exploiting adjoint sensitivities," *Micronet Annual Workshop*, Ottawa, ON, Apr. 2002, pp. 61–62.

J.W. Bandler and A.S. Mohamed, "Engineering Space mapping optimization exploiting exact sensitivities," *2nd Annual McMaster Optimization Conference: Theory and Applications, MOPTA02,* Hamilton, ON, Aug. 2002.

J.W. Bandler, A.S. Mohamed, M.H. Bakr, K. Madsen and J. Søndergaard, "EM–based optimization exploiting partial space mapping and exact sensitivities," in *IEEE MTT–S Int. Microwave Symp. Dig.*, Seattle, WA, 2002, pp. 2101–2104.

J.W. Bandler, A.S. Mohamed, M.H. Bakr, K. Madsen and J. Søndergaard, "EM-based optimization exploiting partial space mapping and exact sensitivities," *IEEE Trans. Microwave Theory Tech.*, vol. 50, pp. 2741–2750, Dec. 2002.

J.W. Bandler, A.S. Mohamed and M.H. Bakr, "TLM modeling and design exploiting space mapping," *IEEE Trans. Microwave Theory Tech*., vol. 53, 2005.

J.W. Bandler, J.E. Rayas-Sánchez and Q.J. Zhang, "Yield-driven electromagnetic optimization via space mapping-based neuromodels," *Int. J. RF and Microwave CAE*, vol. 12, pp. 79–89, 2002.

J.W. Bandler and M.R.M. Rizk, "Optimization of electrical circuits," *Math. Program. Study*, vol. 11, pp. 1–64, 1979.

J.W. Bandler and R.E. Seviora, "Computation of sensitivities for noncommensurate networks," *IEEE Trans. Circuit Theory*, vol. CT-18, pp. 174–178, Jan. 1971.

J.W. Bandler, Q. J. Zhang and R.M. Biernacki, "A unified theory for frequency-domain simulation and sensitivity analysis of linear and nonlinear circuits," *IEEE Trans. Microwave Theory Tech.*, vol. 36, pp. 1661–1669, Dec. 1988.

J.W. Bandler, Q.J. Zhang, J. Song and R.M. Biernacki, "FAST gradient based yield optimization of nonlinear circuits," *IEEE Trans. Microwave Theory Tech.*, vol. 38, pp. 1701–1710, Nov. 1990.

R.M. Barrett, "Microwave printed circuits—A historical survey," *IEEE Trans. Microwave Theory Tech.*, vol. MTT-3, pp. 1–9, Mar. 1955.

R.M. Biernacki, J.W. Bandler, J. Song and Q.J. Zhang, "Efficient quadratic approximation for statistical design," *IEEE Trans. Circuits Syst.*, vol. 36, pp. 1449–1454, Nov. 1989.

R.M. Biernacki and M.A. Styblinski, "Efficient performance function interpolation scheme and its application to statistical circuit design," *Int. J. Circuit Theory Appl.*, vol. 19, pp. 403–422, July–Aug. 1991.

S. Bila, D. Baillargeat, S. Verdeyme and P. Guillon, "Automated design of microwave devices using full EM optimization method," in *IEEE MTT-S Int. Microwave Symp. Dig.*, Baltimore, MD, 1998, pp. 1771–1774.

A.J. Booker, J.E. Dennis, Jr., P.D. Frank, D.B. Serafini, V. Torczon and M.W. Trosset, "A rigorous framework for optimization of expensive functions by surrogates," *Structural Optimization*, vol.17, pp.1–13, 1999.

R.K. Brayton, G.D. Hachtel and A.L. Sangiovanni-Vincentelli, "A survey of optimization techniques for integrated-circuit design," *Proc. IEEE*, vol. 69, pp. 1334–1362, 1981.

C.G. Broyden, "A class of methods for solving nonlinear simultaneous equations," *Math. Comp.*, vol. 19, pp. 577–593, 1965.

D.A. Calahan, *Computer-Aided Network Design*, rev. ed. New York, NY: McGraw Hill, 1972.

Q. Cheng, *Advances in Space Mapping Technology Exploiting Implicit Space Mapping and Output Space Mapping*, Ph.D. Thesis, Department of Electrical and Computer Engineering, McMaster University, Hamilton, ON, Canada, 2004.

H.-S. Choi, D.H. Kim, I.H. Park and S.Y. Hahn, "A new design technique of magnetic systems using space mapping algorithm," *IEEE Trans. Magnetics*, vol. 37, pp. 3627–3630, Sep. 2001.

R.E. Collin, *Foundations for Microwave Engineering*. New York, NY: McGraw Hill, 1966.

A.R. Conn, N.I.M. Gould and P.L. Toint, *Trust-Region Methods*. Philadelphia, PA: SIAM and MPS, 2000, pp. 11.

W.C. Davidon, "Variable metric method for minimization," *SIAM Journal on Optimization*, vol. 1, pp. 1–17, Feb. 1991.

J.E. Dennis, Jr., “A summary of the Danish Technical University November 2000 workshop,” Dept. Computational and Applied Mathematics, Rice University, Houston, Texas, 77005-1892, USA.

J.E. Dennis, Jr., “Optimization using surrogates for engineering design,” *IMA short course: Industrial Strength Optimization*, Institute for Mathematics and its Applications (IMA), University of Minnesota, Minneapolis, MN, Jan. 2003.

J.E. Dennis, Jr., and R.B. Schnabel, *Numerical Methods for Unconstrained Optimization and Nonlinear Equations*. Englewood Cliffs, NJ: Prentice-Hall, 1983. Reprinted by SIAM Publications, 1996.

V. Devabhaktuni, B. Chattaraj, M.C.E. Yagoub and Q.J. Zhang, “Advanced microwave modeling framework exploiting automatic model generation, knowledge neural networks and space mapping,” *IEEE Trans. Microwave Theory Tech.*, vol. 51, pp. 1822–1833, July 2003.

S.W. Director and G.D. Hachtel, “The simplicial approximation approach to design centering,” *IEEE Trans. Circuits Syst.*, vol. CAS-24, pp.363–372, July 1977.

P. Draxler, “CAD of integrated passives on printed circuit boards through utilization of multiple material domains,” in *IEEE MTT-S Int. Microwave Symp. Dig.*, Seattle, WA, 2002, pp. 2097–2100.

R.L. Eisenhart and P.J. Khan, “Theoretical and experimental analysis of a waveguide mounting structure,” *IEEE Trans. Microwave Theory Tech.*, vol. MTT-19, pp. 706–19, Aug. 1971.

em, Sonnet Software, Inc., 100 Elwood Davis Road, North Syracuse, NY 13212, USA.

Empipe and Empipe3D Version 4.0, formerly Optimization Systems Associates Inc., P.O. Box 8083, Dundas, Ontario, Canada L9H 5E7, 1997, now Agilent Technologies, 1400 Fountaingrove, Parkway, Santa Rosa, CA 95403-1799, USA.

Eswarappa, G.I. Costache and W.J.R. Hoefer, “Transmission line matrix modeling of dispersive wide-band absorbing boundaries with time-domain diakoptics for S-parameter extraction”, *IEEE Trans. Microwave Theory and Tech.*, vol. 38, pp 379–386, Apr. 1990.

N.-N. Feng and W.-P. Huang, “Modeling and simulation of photonic devices by generalized space mapping technique,” *J. Lightwave Technol.*, vol. 21, pp. 1562–1567, June 2003.

N.-N. Feng, G.-R. Zhou and W.-P. Huang, “Space mapping technique for design optimization of antireflection coatings in photonic devices,” *J. Lightwave Technol.*, vol. 21, pp. 281–285, Jan. 2003.

First International Workshop on Surrogate Modeling and Space Mapping for Engineering Optimization, Informatics and Mathematical Modeling (IMM), Technical University of Denmark (DTU), Lyngby, Denmark, 2000, http://www.imm.dtu.dk/~km/smsmeo/.

R. Fletcher, *Practical Methods of Optimization*, 2nd ed. New York, NY: Wiley, 1987.

G. Gentili, G. Macchiarella and M. Politi, “A space-mapping technique for the design of comb filters,” *33th European Microwave Conference*, Munich, 2003, pp. 171–173.

N.K. Georgieva, S. Glavic, M.H. Bakr and J.W. Bandler, “Feasible adjoint sensitivity technique for EM design optimization,” *IEEE Trans. Microwave Theory Tech.*, vol. 50, pp. 2751–2758, Dec. 2002.

P.A. Grobelny, *Integrated Numerical Modeling Techniques for Nominal and Statistical Circuit Design,* Ph.D. Thesis, Department of Electrical and Computer Engineering, McMaster University, Hamilton, ON, Canada, 1995.

K.C. Gupta, “Emerging trends in millimeter-wave CAD,” *IEEE Trans. Microwave Theory Tech.*, vol. 46, pp. 475–483, Apr. 1998.

J. Hald and K. Madsen, “Combined LP and quasi-Newton methods for minimax optimization,” *Math. Programming*, vol. 20, pp. 49–62, 1981.

R.F. Harrington, “Matrix methods for field problems,” *Proc. IEEE*, vol. 55, pp. 136–149, Feb. 1967.

P. Harscher, E. Ofli, R. Vahldieck and S. Amari, “EM-simulator based parameter extraction and optimization technique for microwave and millimeter wave filters,” in *IEEE MTT-S Int. Microwave Symp. Dig.*, Seattle, WA, 2002, pp. 1113–1116.

M. Hintermüller and L.N. Vicente, “Space mapping for optimal control of partial differential equations,” to appear in *SIAM Journal on Optimization*, 2005.

W.J.R. Hoefer, “The transmission-line matrix method—Theory and applications,” *IEEE Trans. Microwave Theory Tech.*, vol. MTT-33, pp. 882–893, Oct. 1985.

J.-S. Hong and M.J. Lancaster, *Microstrip Filters for RF/Microwave Applications*. New York, NY: Wiley, 2001, pp. 295–299.

M.A. Ismail, *Space Mapping Framework for Modeling and Design of Microwave Circuits*, Ph.D. Thesis, Department of Electrical and Computer Engineering, McMaster University, Hamilton, ON, Canada, 2001.

M.A. Ismail, K. G. Engel and M. Yu," Multiple space mapping for RF T-switch design," in *IEEE MTT-S Int. Microwave Symp. Dig.*, Fort Worth, TX, 2004, pp. 1569–1572.

M.A. Ismail, D. Smith, A. Panariello, Y. Wang and M. Yu, "EM-based design of large-scale dielectric-resonator filters and multiplexers by space mapping," *IEEE Trans. Microwave Theory Tech.*, vol. 52, pp. 386–392, Jan. 2004.

N. Jain and P. Onno, "Methods of using commercial electromagnetic simulators for microwave and millimeter-wave circuit design and optimization," *IEEE Trans. Microwave Theory Tech.*, vol.45, pp. 724–746, May 1997.

T. Jansson, L. Nilsson and M. Redhe, "Using surrogate models and response surfaces in structural optimization—with application to crashworthiness design and sheet metal forming," *Struct. Multidis. Optim.*, vol. 25, pp 129–140, 2003.

P.B. Johns and K. Akhtarzad, "The use of time domain diakoptics in time discrete models of fields," *Int. J. Num. Methods Eng.*, vol. 17, pp. 1–14, 1981.

P.B. Johns and K. Akhtarzad, "Time domain approximations in the solution of fields by time domain diakoptics," *Int. J. Num. Methods Eng.*, vol. 18, pp. 1361–1373, 1982.

S. Koziel, J.W. Bandler and K. Madsen, "Towards a rigorous formulation of the space mapping technique for engineering design," *Proc. Int. Symp. Circuits Syst., ISCAS*, 2005, pp. 5605–5608.

S. Koziel, J.W. Bandler and K. Madsen, "On the convergence of a space mapping optimization algorithm," *SIAM Journal on Optimization*, (submitted).

S. Koziel, J.W. Bandler and K. Madsen, "An output space mapping framework for engineering optimization," *Math. Programming*, (submitted).

S. Koziel, J.W. Bandler, A.S. Mohamed and K. Madsen, "Enhanced surrogate models for statistical design exploiting space mapping technology," in *IEEE MTT-S Int. Microwave Symp. Dig.*, Long Beach, CA, 2005, (accepted).

L.S. Lasdon, D.F. Suchman and A.D. Waren, “Nonlinear programming applied to linear array design,” *J. Acoust. Soc. Amer.*, vol. 40, pp. 1197–1200, Nov. 1966.

L.S. Lasdon and A.D. Waren, “Optimal design of filters with bounded, lossy elements,” *IEEE Trans. Circuit Theory*, vol. CT-13, pp. 175–187, June 1966.

S.J. Leary, A. Bhaskar and A.J. Keane, “A constraint mapping approach to the structural optimization of an expensive model using surrogates,” *Optimization and Engineering*, vol. 2, pp. 385–398, 2001.

J.-W. Lobeek, “Space mapping in the design of cellular PA output matching circuits,” *Workshop on Microwave Component Design Using Space Mapping Methodologies, IEEE MTT-S Int. Microwave Symp. Dig.*, Seattle, WA, 2002.

K. Madsen, “An algorithm for minimax solution of overdetermined systems of non-linear equations,” *J. Inst. Math. Applicat.*, vol. 16, pp. 321–328, 1975.

K. Madsen, H.B. Nielsen and J. Søndergaard, “Robust subroutines for non-linear optimization,” DTU, Lyngby, Denmark, *Technical Report IMM-REP-2002-02*, 2002.

K. Madsen and J. Søndergaard, “Convergence of hybrid space mapping algorithms,” *Optimization and Engineering*, vol. 5, pp. 145–156, 2004.

N. Marcuvitz, *Waveguide Handbook*, 1st ed. New York, NY: McGraw Hill, 1951.

Matlab, The MathWorks, Inc., 3 Apple Hill Drive, Natick MA 01760–2098, USA.

G.L. Matthaei, “Interdigital band-pass filters,” *IEEE Trans. Microwave Theory Tech.*, vol. MTT-10, pp. 479–491, Nov. 1962.

G.L. Matthaei, L. Young and E.M.T. Jones, *Microwave Filters, Impedance-Matching Networks, and Coupling Structures*, 1st ed. New York, NY: McGraw-Hill, 1964.

MEFiSTo-3D, Faustus Scientific Corporation, 1256 Beach Drive, Victoria, BC, V8S 2N3, Canada.

J.J. Moré and D.C. Sorenson, “Computing a trust region step,” *SIAM J. Sci. Stat. Comp.*, vol. 4, pp. 553–572, 1983.

J.V. Morro, H. Esteban, P. Soto, V.E. Boria, C. Bachiller, S. Cogollos and B. Gimeno, "Automated design of waveguide filters using aggressive space mapping with a segmentation strategy and hybrid optimization techniques," in *IEEE MTT-S Int. Microwave Symp. Dig.*, Philadelphia, PA, 2003, pp. 1215–1218.

J.V. Morro Ros, P. Soto Pacheco, H. Esteban Gonzalez, V.E. Boria Esbert, C. Bachiller Martin, M. Taroncher Calduch, S. Cogollos Borras and B. Gimeno Martinez, "Fast automated design of waveguide filters using aggressive space mapping with a new segmentation strategy and a hybrid optimization algorithm," *IEEE Trans. Microwave Theory Tech.*, vol. 53, pp.1130–1142, Apr. 2005.

N.K. Nikolova, J.W. Bandler and M.H. Bakr, "Adjoint techniques for sensitivity analysis in high-frequency structure CAD," *IEEE Trans. Microwave Theory Tech.*, vol. 52, pp. 403–419, Jan. 2004.

J. Nocedal and S.J. Wright, *Numerical Optimization*. New York, NY: Springer-Verlag, 1999.

OSA90/hope Version 4.0, formerly Optimization Systems Associates Inc., P.O. Box 8083, Dundas, ON, Canada, L9H 5E7, 1997, now Agilent Technologies, 1400 Fountaingrove Parkway, Santa Rosa, CA 95403-1799, USA.

A.M. Pavio, J. Estes and L. Zhao, "The optimization of complex multi-layer microwave circuits using companion models and space mapping techniques," *Workshop on Microwave Component Design Using Space Mapping Methodologies, IEEE MTT-S Int. Microwave Symp. Dig.,* Seattle, WA, 2002.

A.M. Pavio, "The electromagnetic optimization of microwave circuits using companion models," *Workshop on Novel Methodologies for Device Modeling and Circuit CAD, IEEE MTT-S Int. Microwave Symp. Dig.*, Anaheim, CA, 1999.

F. Pedersen, *Advances on the Space Mapping Optimization Method*, Masters Thesis, Informatics and Mathematical Modelling (IMM), Technical University of Denmark (DTU), Lyngby, Denmark, 2001.

D. Pelz, "Coupled resonator filter realization by 3D-EM analysis and space mapping," *Workshop on Microwave Component Design Using Space Mapping Methodologies, IEEE MTT-S Int. Microwave Symp. Dig.,* Seattle, WA, 2002.

M. Pozar, *Microwave Engineering*, 2nd ed. New York, NY: Wiley, 1998.

J.C. Rautio and R. F. Harrington, "An electromagnetic time-harmonic analysis of shielded microstrip circuits," *IEEE Trans. Microwave Theory Tech.*, vol. MTT-35, pp. 726–730, Aug. 1987.

J.E. Rayas-Sánchez, *Neural Space Mapping Methods for Modeling and Design of Microwave Circuits*, Ph.D. Thesis, Department of Electrical and Computer Engineering, McMaster University, Hamilton, ON, Canada, 2001.

J.E. Rayas-Sánchez, "EM-Based optimization of microwave circuits using artificial neural networks: the state-of-the-art," *IEEE Trans. Microwave Theory Tech.*, vol. 52, pp. 420–435, Jan. 2004.

J.E. Rayas-Sánchez, F. Lara-Rojo and E. Martínez-Guerrero, "A linear inverse space mapping algorithm for microwave design in the frequency and transient domains," in *IEEE MTT-S Int. Microwave Symp. Dig.*, Fort Worth, TX, 2004, pp. 1847–1850.

M. Redhe and L. Nilsson, "Optimization of the new Saab 9-3 exposed to impact load using a space mapping technique," *Struct. Multidis. Optim.*, vol. 27, pp 411–420, 2004.

S. Safavi-Naeini, S.K. Chaudhuri, N. Damavandi and A. Borji, "A multi-level design optimization strategy for complex RF/microwave structures," *Workshop on Microwave Component Design Using Space Mapping Methodologies, IEEE MTT-S Int. Microwave Symp. Dig.*, Seattle, WA, 2002.

P. Silvester, "A general high-order finite-element waveguide analysis program," *IEEE Trans. Microwave Theory Tech.*, vol. MTT-17, pp. 204–210, Apr. 1969.

J. Snel, "Space mapping models for RF components," *Workshop on Statistical Design and Modeling Techniques For Microwave CAD, IEEE MTT-S Int. Microwave Symp. Dig.*, Phoenix, AZ, 2001.

P.P.M. So and W.J.R. Hoefer, "Locally conformal cell for two-dimensional TLM," in *IEEE MTT-S Int. Microwave Symp. Dig.*, Philadelphia, PA, 2003, pp. 977–980.

R.S. Soin and R. Spence, "Statistical exploration approach to design centering," *Proc. Inst. Elec. Eng.*, vol. 127, pt. G., pp. 260–269, 1980.

J. Søndergaard, *Non-linear Optimization Using Space Mapping*, Masters Thesis, Informatics and Mathematical Modelling (IMM), Technical University of Denmark (DTU), Lyngby, Denmark, 1999.

J. Søndergaard, *Optimization Using Surrogate Models—by the Space Mapping Technique*, Ph.D. Thesis, Informatics and Mathematical Modelling (IMM), Technical University of Denmark (DTU), Lyngby, Denmark, 2003.

Space Mapping: A Knowledge-Based Engineering Modeling and Optimization Methodology Exploiting Surrogates, Minisymposia, SIAM Conference on Optimization, Stockholm, Sweden, May 2005.

M.B. Steer, J.W. Bandler and C.M. Snowden, "Computer-aided design of RF and microwave circuits and systems," *IEEE Trans. Microwave Theory Tech.*, vol. 50, pp. 996–1005, Mar. 2002.

W. Steyn, R. Lehmensiek and P. Meyer, "Integrated CAD procedure for IRIS design in a multi-mode waveguide environment," in *IEEE MTT-S Int. Microwave Symp. Dig.*, Phoenix, AZ, 2001, pp. 1163–1166.

D.G. Swanson, Jr., "Optimizing a microstrip bandpass filter using electromagnetics," *Int. J. Microwave and Millimeter-wave CAE*, vol. 5, pp. 344–351, 1995.

D.G. Swanson, Jr., and R. J. Wenzel, "Fast analysis and optimization of combline filters using FEM," in *IEEE MTT-S Int. Microwave Symp. Dig.*, Phoenix, AZ, 2001, pp. 1159–1162.

G.C. Temes and D.A. Calahan, "Computer-aided network optimization the state-of-the-art," *Proc. IEEE*, vol. 55, pp.1832–1863, 1967.

L.N. Vicente, "Space mapping: models, sensitivities, and trust-regions methods," *Optimization and Engineering*, vol. 4, pp. 159–175, 2003.

A.D. Waren, L.S. Lasdon and D.F. Suchman, "Optimization in engineering design," *Proc. IEEE*, vol. 55, pp. 1885–1897, 1967.

R.J. Wenzel, "Exact theory of interdigital band–pass filters and related coupled structures," *IEEE Trans. Microwave Theory Tech.*, vol. MTT-13, pp. 559–575, Sep. 1965.

A. Wexler, "Solution of waveguide discontinuities by modal analysis," *IEEE Trans. Microwave Theory Tech*, vol. MTT-15, pp. 508–517, Sep. 1967.

A. Wexler, "Computation of electromagnetic fields," *IEEE Trans. Microwave Theory Tech.*, vol. MTT-17, pp. 416–439, Aug. 1969.

Workshop on Microwave Component Design Using Space Mapping Methodologies, IEEE MTT-S Int. Microwave Symp., Seattle, WA, 2002.

K.-L. Wu, R. Zhang, M. Ehlert and D.-G. Fang, “An explicit knowledge-embedded space mapping technique and its application to optimization of LTCC RF passive circuits,” *IEEE Components and Packaging Technologies*, vol. 26, pp. 399–406, June 2003.

K.-L. Wu, Y.-J. Zhao, J. Wang and M.K.K. Cheng, ”An effective dynamic coarse model for optimization design of LTCC RF circuits with aggressive space mapping,” *IEEE Trans. Microwave Theory Tech.*, vol. 52, pp. 393–402, Jan. 2004.

XFDTD, Remcom Inc., 315 South Allen Street, Suite 222, State College, PA 16801, USA.

S. Ye and R.R. Mansour, “An innovative CAD technique for microstrip filter design,” *IEEE Trans. Microwave Theory Tech.*, vol. 45, pp. 780–786, May 1997.

K.S. Yee, “Numerical solution of initial boundary value problems involving Maxwell’s equations in isotropic media,” *IEEE Trans. Antennas Propagat.*, vol. AP-14, pp. 302–307, May 1966.

Q.J. Zhang and K.C. Gupta, *Neural Networks for RF and Microwave Design*. Norwood, MA: Artech House Publishers, 2000, Chapter 9.

L. Zhang, J.J. Xu, M.C.E. Yagoub, R.T. Ding and Q.J. Zhang, “Neuro-space mapping technique for nonlinear device modeling and large signal simulation,” in *IEEE MTT-S Int. Microwave Symp. Dig.*, Philadelphia, PA, 2003, pp. 173–176.